Synthesis and Characterization of Ultralow Thermal Expansion NZP-type Compounds

by

Jinmin Kim

Dissertation submitted to the Faculty of the

Virginia Polytechnic Institute and State University

in partial fulfillment of the requirements for the degree of

Doctor of Philosophy

in

Materials Engineering Science

APPROVED:

Robert E. Swanson, Chairman

Jesse J. Brown, Jr.

Diana Farkas

Jack L. Lytton

Richard Zallen

December, 1988

Blacksburg, Virginia

Synthesis and Characterization of Ultralow Thermal Expansion NZP-type Compounds

by

Jinmin Kim

Robert E. Swanson, Chairman

Materials Engineering Science

(ABSTRACT)

New ultra-low thermal expansion materials, based on the NZP structure, have been developed and evaluated for future application in ceramic diesel engines which require exceptional thermal shock resistance. Twenty-four cation substitutions, with electron valence ranging from +1 to +5, were used to replace Na^+ in the NZP skeletal framework. The linear thermal expansion measurements were conducted for ternary systems up to 1000°C. Quarternary & quinternary compounds were processed using combinations of alkali-alkali, alkali-alkaline earth, and alkaline earth-alkaline earth instead of Na^+. These were evaluated for solid solubility. Linear thermal expansion values were obtained for those compositions having single phase composition. Axial thermal expansion measurements were conducted using high temperature XRD for compounds having low linear thermal expansion value from room temperature to 1400°C. Several ultra-low expansion materials(less than $10x10^{-7}$/°C in absolute value) were found, which also had axial thermal expansion anisotropy. The effects of ionic size and valence of the substitution elements are discussed to explain the linear thermal expansion behavior and thermal expansion anisotropy investigated in these compounds. The effect of crystallinity is discussed, and the unit-cell equilibrium is suggested to interpret the general thermal expansion behavior occurring in crystalline solids. Secondary material properties for the com-

pounds $Rb_{0.5}Cs_{0.5}Zr_2(PO_4)_3$ & $Ca_{0.5}Mg_{0.5}Zr_4(PO_4)_6$ with linear thermal expansion values of -0.3×10^{-7}/°C & -5×10^{-7}/°C, respectively, have also been characterized.

Acknowledgements

The author feels indebted to numerous individuals who contributed in a variety of ways to the successful completion of this dissertation project.

First I would like to thank Dr. R.E.Swanson, who started me on a research project and then provided encouragement, understanding, and patience.

Thanks are extended to Dr. J.J.Brown, Jr. who gave me helpful suggestions to get through the dissertation project. Thanks are also extended to the members of the graduate committee, Dr. J.L.Lytton, Dr. D.Farkas, and Dr. R.Zallen for serving on my committee.

This work has been supported by the Department of Energy. Some of experimental works were conducted in High Temperature Materials Laboratory at Oak Ridge National Lab.

My deepest thanks go to my wife who married me despite the fact that I was a student, stayed with me and loved me enough to provide the continuing inspiration needed to finish.

It is with great pleasure that I dedicate this thesis to my beloved wife and two children who sacrificed throughout my academic career.

Table of Contents

List of Illustrations

List of Tables

Chapter I

Introduction

According to F.A.Hummel's classification[1], low thermal expansion materials may be grouped as materials having a thermal expansion coefficient(α) less than 20×10^{-7}/°C in absolute value. Only three low expansion oxide materials were known before World War II , i.e., fused silica glass($\alpha = 5.0\times10^{-7}$/°C)[2], vycor glass($\alpha = 8.0\times10^{-7}$/°C)[2], and cordierite($\alpha = 14\times10^{-7}$/°C)[3,4]. Since then, much research has been done to develop other low thermal expansion materials and to analyze their behavior based on phase relations, stability, crystallization, and crystal chemistry. Many new materials having low α over different temperature ranges have been reported[5-22]; however, correlations between low thermal expansion behavior and other material characteristics remain incomplete.

Low thermal expansion materials can be classified into three groups. The first group consists of systems having strong covalent molecular bonding characteristics. An example of this group is the diamond[23]. Strong bond strength correlates with low thermal expansion. The second group consists of glasses with exceptionally low

α compared to other glasses, these include the glasses containing 85-100% SiO_2[2](except those such as alkali-containing systems), copper aluminosilicate glasses[7,8], and some glass-ceramics[9,10]. The low thermal expansion exhibited by these systems compared to other glasses may be due to the bond angle bending and stretching during heating and to the high bond strength between Si-O. Most of the low thermal expansion materials are categorized into the third group in which low α results from anisotropy due to crystal structure. This includes crystal systems such as the hexagonal[5,6,19,21,22,24], orthorhombic[13], monoclinic[11], and tetragonal[15].

Among the third group, compounds such as sodium dizirconium triphosphate, $NaZr_2(PO_4)_3$ [the NZP[21] structure which can be said to be a structural derivative of zircon $ZrZr_2(SiO_4)_3$], have attracted much attention since the work by Alamo and Roy[21]. Additional research studies have been published on the effects of other elemental substitutions for chemically modified systems[19,22,25]. In the current study, efforts have been made to substitute other cations with electron valence from +1 to +5 for Na^+ in the NZP structure without changing its skeletal framework. Solid-solubility studies between alkali(Na~Cs) - alkali, alkaline earth(Mg~Ba) - alkaline earth and alkali - alkaline earth elements were conducted for the substitution of the first part of NZP structure. A novel processing method, which directly uses P_2O_5 instead of using $NH_4H_2PO_4$ or $(NH_4)_2HPO_4$ to get P_2O_5, was considered to increase the reactivity of ZrO_2. The linear aggregate thermal expansion of the NZP type systems was studied using fused silica and automated dilatometry. For systems showing low thermal expansion, axial thermal expansion measurements were conducted using high temperature X-ray diffractometry(XRD). Secondary material properties, including thermal shock resistance and mechanical strength, have been

characterized for the compounds $Rb_{0.5}Cs_{0.5}Zr_2(PO_4)_3$ & $Ca_{0.5}Mg_{0.5}Zr_4(PO_4)_6$ with the linear α values of -0.3×10^{-7}/°C & -5×10^{-7}/°C, respectively.

Chapter II

Literature Review

2.1 History of development of NZP-type systems

Since the initial development of sodium zirconium phosphate $NaZr_2P_3O_{12}$(NZP) by Hagman and Kierkegaard[25] in 1968, it has attracted much attention, and many studies have been conducted to understand about NZP structure in detail in the last 20 years[26-33].

Until the seventies, this particular system was known as a fast ion conductor because of its open structure[21]. Structure and ionic conductivity studies for the NZP structure, especially in nasicon($Na_3Zr_2SiPO_{12}$) which is the chemical elemental substitutional form of NZP, were published in many articles. They deal with the crystal structure[34-38], ionic conductivity[39-43], the effect of cation substitutions[44], chemical durability[45], phase transition[46-48], ionic conductivity enhancement along

domain and grain boundaries[49], and the mechanism of ion exchange[50] in the crystalline nasicon structure.

In the early eighties, Alamo and Roy[21], at the Pennsylvania State University, found that the system Na_2O-ZrO_2-P_2O_5-SiO_2 showed promise of low thermal expansion. They and other researchers continued work on crystal chemistry[21,51-53], synthesis and sintering[54-56] and chemical elemental substitution[4,19,57-59]. Meanwhile Oota and Yamai, at the Nagoya Institute of Technology in Japan, published several papers concerning low thermal expansion behavior[18,22,60], solid solubility and microcracking[61].

Recently the NZP structure has been considered as a candidate for immobilization of certain types of nuclear waste[62], due to its enormously varied ionic substitution. The NZP-type structure has emerged as a new family of materials, which has extraordinary technical utility in three fields[55] : fast-ion conductors, radwaste solidification and zero expansion ceramics.

2.2 Thermal expansion behavior of NZP-type structure

2.2.1 General expansion theory and factors affecting thermal expansion

It has been generally accepted that thermal expansion is related to the presence of anharmonic vibrations of atoms about their equilibrium positions in the solid lattice[63,64]. Materials expand when heated because the repulsive forces produced when two atoms come closer than their equilibrium distance are greater than the at-

tractive forces produced when the two atoms vibrate apart by the same distance in excess of their equilibrium distance.

The basic principles governing the thermal dilation of solids have been interpreted from several different viewpoints. These include atomistics, thermodynamics, and crystal chemistry. One can be called the kinetic approach, that is, a consideration of the atomic mechanism of expansion[64]. Another is the thermodynamic approach based on general consideration of the energy changes[64]. A third is based on crystal chemistry and is concerned with the size of the atoms or ions, with their arrangement in the crystalline structure, and with the bond characteristics[64,65]. However, none of these approaches has provided a complete and satisfactory explanations for all the observations, although each has led to significant contributions.

The empirical, structural approach to thermal expansion[66], in which thermal expansion is the sum of a bond-length change and a bond angle effect appears to be one of the better qualitative interpretations. To explain the thermal contraction with heating, Hazen and Finger[67] described bond compression and bond angle bending as two important compression mechanisms in ceramic-type materials.

Kirby[65] classified the many parameters affecting the thermal expansion of ceramics into two different categories, one category has a significant effect on thermal expansion, one does not. Even though there are exceptions to the classification, according to his review, the following factors are found to affect thermal expansion: chemical composition($>1\%$ level), crystalline and amorphous phase[68-70], quantity and size of phases[71-73], orientation of grains[74-77], residual stress[78-79], fictive temperature of glassy phase[80-82], formation of cracks[83], formation of point defects, and surface chemistry[84-86]. Factors which usually do not have a significant effect include: density[81], grain size[75,87-88], porosity[75,89-90], stoichiometry of

individual grains[91], impurities(< 1% level), dislocations, grain boundaries and surface topography[92].

2.2.2 Correlation between thermal expansion and other thermal behavior

F.A.Hummel[1] emphasized the usefulness of the thermal expansion as a means of classifying thermal shock resistance. The classification was justified by the following observations. Most of the analytical expressions for the thermal shock resistance contain α(linear thermal expansion) in the denominator, indicating that as α approaches zero, the thermal shock resistance would theoretically approach infinity. It is well known that the low porosity materials with low α value have good thermal shock resistance, and the coefficient of expansion is less likely to be affected by processing techniques.

A search for new ceramics having low thermal expansion is now underway to solve the toughness problem at high temperature as well as the other efforts to increase the fracture toughness at room temperature[93].

2.2.3 Anisotropic characteristics

Thermal expansion behavior of NZP-type compounds is characterized by anisotropy of its hexagonal structure, which causes low bulk thermal expansion during heating. High-temperature XRD studies have shown that axial thermal expansions of $NaZr_2(PO_4)_3$ are:$\alpha_a = -64.2 \times 10^{-7}/°C$, $\alpha_c = 255 \times 10^{-7}/°C$ up to 600°C[21].

Another study by Oota and Yamai[22] showed essentially the same thermal expansion trends up to 1000°C for the $NaZr_2(PO_4)_3$ system.

Those Japanese workers continued their work to determine the axial thermal expansion values for various NZP-type based systems. For the $KZr_2(PO_4)_3$ system, the axial thermal expansions are reported as $\alpha_a = -44 \times 10^{-7}/°C$ and $\alpha_c = 76 \times 10^{-7}/°C$ up to 1300°C[60]; for other NZP-type systems, like $CaZr_4(PO_4)_6$ and $NbZr(PO_4)_3$, axial thermal expansion behavior is shown graphically without actual axial thermal expansion data up to 1000°C[22]. Most of the published axial thermal expansion data show that the c-axis expands and a-axis contracts upon heating. However, one report for the $SrZr_4(PO_4)_6$ compound shows the opposite trend[59].

Because of the anisotropic axial thermal expansion characteristic($\Delta\alpha = |\alpha_c - \alpha_a|$), microcracking has been investigated for $NaZr_2(PO_4)_3$[22]. According to that study, the $NaZr_2(PO_4)_3$ samples composed of fine grains show no microcracking and a thermal expansion hysteresis loop. On the other hand, the sample composed of large grains shows evidence of both intergranular and transgranular microcracks and a low thermal expansion curve with a relatively large hysteresis loop.

2.3 Crystal chemical review of NZP-type structure

2.3.1 Structure

From the Weissenberg data[96], the space group of $NaZr_2(PO_4)_3$ was identified as $R\bar{3}C$. In the space group $R\bar{3}C$(hexagonal axes), the following point positions exist[97]:

$$(0,0,0;\ ^1/_3,\ ^2/_3,\ ^2/_3;\ ^2/_3,\ ^1/_3,\ ^1/_3) +$$

6(*a*) $(0,0,¼;0,0,¾)$

6(*b*) $(0,0,0;0,0,½)$

12(c) $\pm(0,0,z;0,0,½ + z)$

18(*d*) $(½,0,0;0,½,0;½,½,0;½,0,½;0,½,½;½,½,½)$

18(*e*) $\pm(x,0,¼;0,x,¼;\bar{x},\bar{x},¼)$

36(*f*) $\pm(x,y,z;y,x-y,z;y-x,\bar{x},z;\bar{y},\bar{x},½+z;x,x-y,½+z;y-x,y,½+z)$

From the calculation of Patterson projection, section and electron density distributions[98], the positions of the twelve zirconium, the eighteen phosphorus, and the six sodium atoms were found to be located in 12(c), 18(e), and 6(b) in the unit cell. Seventy two oxygen atoms were confirmed to be positioned in 2x36(f) points. The structural data and atomic parameters for $NaZr_2(PO_4)_3$ are listed in Tables 1(a)&(b), respectively.

The crystal structure of $NaZr_2(PO_4)_3$ has been described in terms of PO_4 tetrahedra and ZrO_6 octahedra which are linked at the corners forming a three-dimensional network(Figure 1(a)). Each oxygen atom simultaneously belongs to a

Table 1. The structural(a) & atomic(b) data of $NaZr_2(PO_4)_3$ (compiled from Refs.25&37)

a)

Space Group: $R\bar{3}C$

Unit Cell Dimensions: a= 8.8043 ± 2Å

c= 22.7585 ± 9Å

V= 1527.7 $Å^3$

Cell Constant: 6Na in 6(b): (0, 0, 0; 0, 0, 1/2)

12Zr in 12(c): ±(0, 0, z; 0, 0, 1/2+z)

18P in 18(e): ±(x, 0, 1/4; 0, x, 1/4; $\bar{x}$, $\bar{x}$, 1/4)

$36O_1$ and $36O_2$ in 2X36(f): ±(x, y, z; $\bar{y}$, x-y, z; y-x, $\bar{x}$, z; $\bar{y}$, $\bar{x}$, 1/2+z; x, x-y, 1/2+z; y-x, y, 1/2+z)

b)

Atom	x	y	z
Na	0	0	0
Zr	0	0	0.14568 (0.14568±1)
P	0.2916 (0.2909±6)	0	1/4
O(1)	0.1841 (0.1860±15)	-0.0165 (-0.0144±15)	0.1956 (0.1949±5)
O(2)	0.1911 (0.1913±15)	0.1675 (0.1683±15)	0.0876 (0.0866±5)

PO_4 group and to a ZrO_6 group. The sodium atoms are in the octahedra formed by the triangular faces of two ZrO_6 octahedra, as illustrated in Figure 1(b). The $O_3ZrO_3NaO_3ZrO_3$ groups formed may be considered as major structural units of the atomic arrangement. Such groups are mutually linked in the c-direction by PO_4 tetrahedra in such a way that empty trigonal prisms of oxygen atoms are formed. The endless columns resulting from this linking are also connected normal to the c-direction by the PO_4 tetrahedra[25]. Figures 1(a)&(b) show the $NaZr_2(PO_4)_3$ structure.

The group $Zr_2(PO_4)_3^-$ is considered to be a major structural unit in the atomic arrangement. Two crystallographically different sites for oxygen atoms, which are designated as O(1) and O(2), exist in the skeletal framework in the $NaZr_2(PO_4)_3$ structure. Each PO_4 tetrahedron is composed of two O(1) and two O(2) sites, and Na cations are positioned in Na(1) sites surrounded octahedrally by only O(2) atoms. In $NaZr_2(PO_4)_3$, there is a Na(2) site in addition to a Na(1) site, in the interstitial space which can accommodate extra Na^+[43].

2.3.2 Elemental substitution

Because of the remarkable tendency towards ionic substitution in the NZP-type structure, many possible chemical substitutions have been reported[4,19,22,33,43,51,57,58]. The flexibility of its skeleton, the strength of its bonds, and the existence of a variety of holes that can be vacant or occupied[51], make the NZP structure an excellent candidate for ionic substitution. Table 2 lists previously investigated ionic substitutions.

Alkali elements from Li to Cs have been shown to replace Na^+ in the NZP structure[19,58]. Recently, the substitution of NH_4^+ for Na^+ has been reported[57].

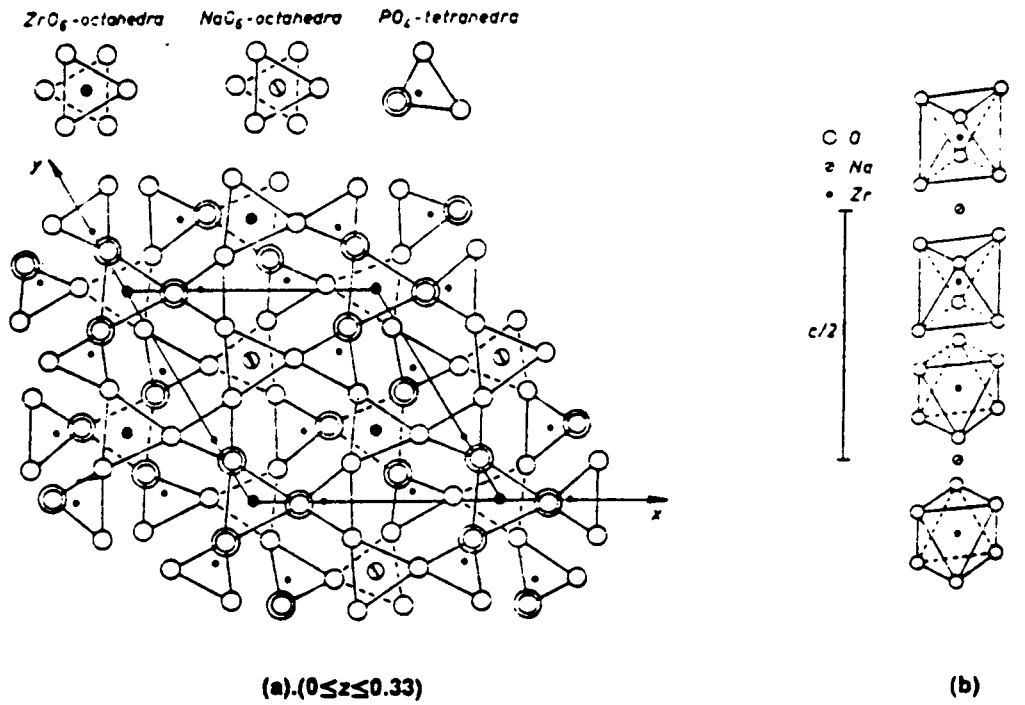

Figure 1. Schematic drawing showing the structure of $NaZr_2(PO_4)_3$ (taken from Ref.25)

Table 2. Chemical elemental substitutions in the NZP structure (compiled from Refs.4,19,22,33,43,51,57,58)

General Formula: $(M_I)(M_{II})_3A_2(BO_4)_3$

M_I	M_{II}	A	B
Li, Na, K, Rb, Cs,	Na, K	Zr	P
NH_4, 1/2Mg, 1/2Ca,		Ge	As
1/2Sr, 1/2Ba,		Ti	Si + Na
1/2Mn, 1/2Co,		Hf	
1/2Zn, 1/4Zr		Nb - Na	
		Y + Na	
		Cr + Na	

In some cases, non-stoichiometric compounds like $Na_{1+x}Zr_2Si_xP_{3-x}O_{12}$(for $0<x<1$)[22,35,37,38], the Na(2) sites(represented by M_{II} in Figure 2) as well as the Na(1) sites(represented by M_I in Figure 2) have been found to accommodate extra Na^+.

The substitutional possibilities for ions with valence of +2 have been reported [4,22,33,43,51]. Alkaline earth elements from Mg to Ba have shown good substitution behavior[4,22,43,51], and some of the transition elements like Mn,Co,Cu,Zn with valence of +2 have been substituted for Na^+ in the NZP skeletal structure. Only three reports have apparently been published regarding the replacement of Na^+ by two elements like $Ca_{0.25}Sr_{0.25}$[59], $Ca_{0.25}Na_{0.5}$ [4], and $Cs_{0.5}Sr_{0.25}$[62] in the NZP structure.

Two ions, Zr and Nb, with electron valence greater than +2 can be substituted for Na^+ in the NZP structure. Those compounds are $Zr_{0.25}Zr_2(PO_4)_3$ [99] and $NbZr(PO_4)_3$[22]. The $Zr_{0.25}Zr_2(PO_4)_3$ system with tetravalent ion substitution is reportedly less stable than other compounds with the same chemical skeleton[51]. $NbZr(PO_4)_3$ has been evaluated[22,43], and it was shown that Nb^{+5} substitutes for Zr^{+4} randomly, with vacancies forming in the sites of Na^+[43].

2.3.3 High temperature chemistry

Hazen et al[52] evaluated bond angles and bond lengths at 4 temperatures up to 690°C for $NaZr_2(PO_4)_3$ with a small amount of Si in the tetrahedral position, and those are tabulated in Table 3. The mean P-O bond length was found to be 1.525Å at 25°C. The P-O bond length was found to decrease with increasing temperature. The zirconium octahedra contains three Zr-O(1) bonds & three Zr-O(2) bonds, and the mean bond length of Zr-O is observed as 2.067Å at 25°C. The mean value of bond

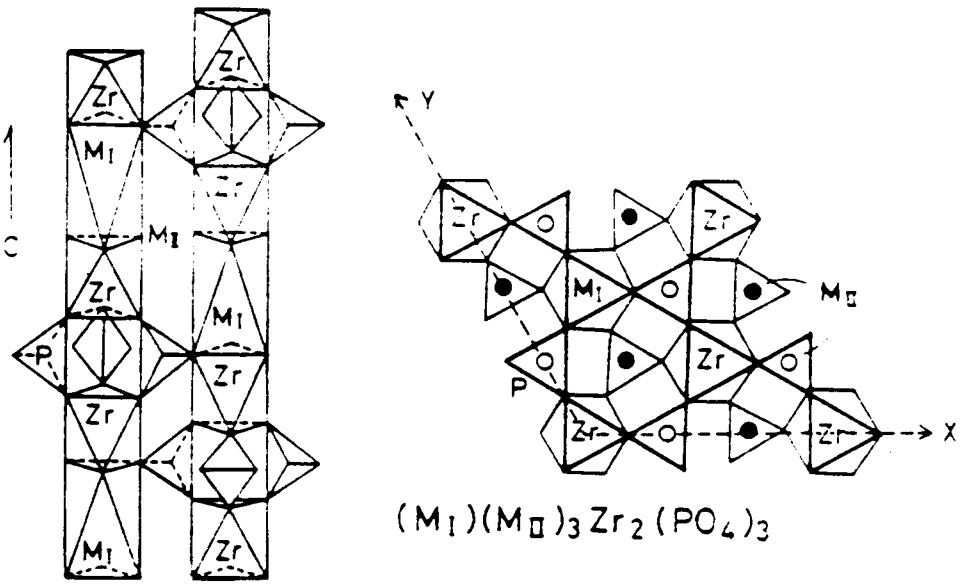

Figure 2. Schematic of alkali sites in $NaZr_2(PO_4)_3$-type structure (taken from Ref.22)

length between zirconium and oxygen at 690°C was essentially the same as the value at 25°C. The adjacent O-Zr-O angles ranged from 84°-93° at room temperature, reflecting the moderate distortion of this cation polyhedron.

Six symmetrically equivalent Na-O(2) pairs increased in bond length from 2.556Å at 25°C to 2.653Å at 690°C. Six adjacent O(2) angles are 66° and six are 114°, compared to the ideal value of 90° for a regular octahedron.

Two angular distortion models have been suggested by Lenain et al[58], and confirmed by observation of polyhedral distortions by Hazen et al[52]. The first model suggested by Lenain allows angular distortions only in the ZrO_6 octahedra. Figure 3(a) exhibits a projection down the three-fold axis of a zirconium octahedron, within which the plane formed by the three O(1) atoms will rotate faster than the O(2) plane, causing the angle O(1)-Zr-O(2) to deviate from 60° (shearing action).

The second model allows both PO_4 tetrahedra and ZrO_6 octahedra to be distorted. Figure 3(b) exhibits a projection of a phosphate tetrahedron in the plane perpendicular to the two fold axis where the line O(1)-P-O(1) can rotate faster than the line O(2)-P-O(2), causing the angle between them to deviate from 90°. For the ZrO_6 octahedron, the distortion process is the same as in the first model[58].

The observed polyhedral distortions are listed in Table 4, and calculated values for rotations are presented in Table 5. The assumption suggested by Lenain[58] (that ZrO_6 octahedra are more distorted in bond angles than that of PO_4 tetrahedra) has been confirmed by the observed polyhedral distortions.

The calculated rotations in a PO_4 tetrahedron and a ZrO_6 octahedron, shown in Table 5, indicate that the rotation is continued in the negative sense as the temperature increases. The angular distortion of the polyhedra also decreased with increasing temperature.

Table 3. Selected bond distances and angles for $NaZr_2(PO_4)_3$ structure (compiled from Ref.52)

Bond/Angle	25°C	270°C	490°C	690°C
P tetrahedron				
P-O1 [2][a]	1.528(1)[b]	1.524(2)	1.519(2)	1.519(3)
P-O2 [2]	1.525(1)	1.522(2)	1.521(2)	1.519(2)
Mean P-O	1.525	1.522	1.520	1.519
O1-P-O1	110.3(1)	110.8(2)	110.8(2)	111.2(2)
O1-P-O2 [2]	107.9(1)	107.7(1)	107.8(1)	107.8(1)
O1-P-O2 [2]	110.6(1)	110.5(1)	110.3(1)	110.4(1)
O2-P-O2	109.5(1)	109.6(2)	109.7(2)	109.4(2)
Zr octahedron				
Zr-O1	2.044(1)	2.047(2)	2.048(2)	2.048(2)
Zr-O2	2.096(1)	2.093(2)	2.088(2)	2.087(2)
Mean Zr-O	2.067	2.070	2.068	2.068
O1-Zr-O1 [3]	92.6(1)	92.2(1)	91.9(1)	91.7(1)
O1-Zr-O2 [3]	90.5(1)	91.0(1)	91.3(1)	91.2(1)
O1-Zr-O2 [3]	92.7(1)	92.2(1)	91.7(1)	91.7(1)
O2-Zr-O2 [3]	83.9(1)	84.4(1)	84.9(1)	85.2(1)
Na1 octahedron				
Na1-O2 [6]	2.566(1)	2.597(2)	2.629(2)	2.653(2)
O2-Na1-O2[6]	66.4(1)	65.5(1)	64.8(1)	64.3(1)
O2-Na1-O2[6]	113.6(1)	114.5(1)	115.2(1)	115.7(1)

a.Figures in brackets represent bond or angle multiplicities.

b.Figures in parentheses represent estimated standard deviation.

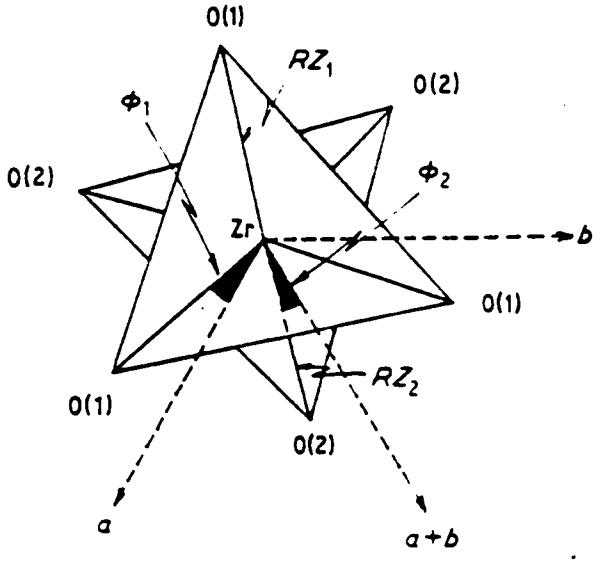

(a)

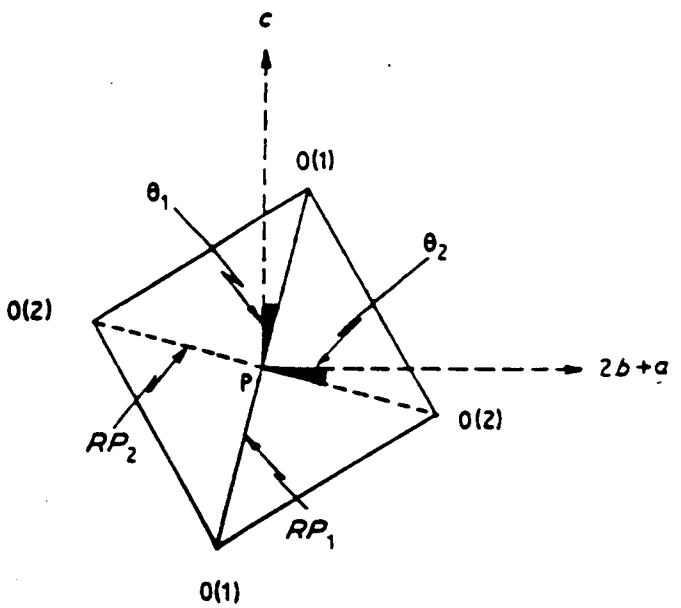

(b)

Figure 3. Projections of ZrO_6 and PO_4: (a).Projection of a ZrO_6 octahedron in the plane perpendicular to the three-fold axis (c-axis); (b).Projection of PO_4 tetrahedron in the plane perpendicular to the two-fold axis (a-axis) (both taken from Ref.58)

Table 4. Polyhedral volumes and distortion indices (taken from Ref.52)

Atom	25°C	270°C	490°C	690°C
P vol(Å^3)	1.824(1)	1.812(3)	1.807(4)	1.796(5)
QE[a]	1.000(2)	1.001(2)	1.000(2)	1.001(3)
AV[b]	1.93	2.22	1.97	2.32
Zr vol(Å^3)	11.76(1)	11.78(1)	11.74(2)	11.76(2)
QE	1.0041(5)	1.0034(7)	1.0027(8)	1.0024(10)
AV	14.1	11.6	9.5	8.3
Na1 vol(Å^3)	18.00(1)	18.53(2)	18.92(3)	19.29(4)
QE	1.1566(4)	1.1685(5)	1.1793(6)	1.1859(7)
AV	610	655	694	719

a.QE= Quadratic elongation= $\sum_{i=1}^{n}[(l_i/l_o)^2/n]$

b.AV= Angle variance= $\sum_{i=1}^{n}[(\theta_i - \theta_o)^2/(n-1)]$ [65, 100]

Table 5. Rotations of polyhedra of [NZP] structure (taken from Ref.52)

	Bond distances				Tetrahedron			Octahedron		
Temp.	P–O1	P–O2	Zr–O1	Zr–O2	θ_1 [a]	θ_2 [a]	$(\theta_2-\theta_1)$	ϕ_1 [b]	ϕ_2 [b]	$(\phi_2-\phi_1)$
25°C	1.528	1.525	2.044	2.096	-6.0	-4.0	1.9	-4.4	-6.31	-1.9
270°C	1.524	1.522	2.047	2.094	-7.4	-5.5	1.9	-5.4	-6.52	-0.9
490°C	1.519	1.521	2.048	2.088	-8.6	-6.8	1.8	-6.2	-6.67	-0.5
690°C	1.519	1.519	2.049	2.087	-9.5	-7.7	1.8	-6.9	-6.62	-0.3

(a,b: defined in Figures 3(a) and (b))

2.4 Processing methods applied in making NZP-type compounds

2.4.1 Solid state reaction

Several different processing methods for synthesis of NZP-type compounds have been described. Hagman and Kierkegaard[25], who first determined the structure of $NaZr_2(PO_4)_3$, heated ZrO_2 and sodium meta-phosphate at 1100°C for several weeks. Sljukic[26,27] reported that stoichiometric phases of NZP-type can be obtained by heating together alkali phosphate and zirconium dioxide, with B_2O_3 added as a flux, at a temperature of 1200°C. The products were washed with boiling H_2O and then with HCl(1:1). Most reports[4,21,37,39,43,48,52,55,56,60] state that Na_2CO_3,ZrO_2 and $NH_4H_2PO_4$/$(NH_4)_2HPO_4$[22,42] were used as raw materials to get the $NaZr_2(PO_4)_3$ compound.

Many workers have noted that unreacted ZrO_2 is often presented when the solid state reaction method is used[21,48]. To overcome the problem of unreacted raw materials, sol-gel processing has been used to make NZP-type compounds. Many reports based on sol-gel processing will be summarized in following section.

2.4.2 Sol-gel method

It has been found that the sol-gel process provides many benefits to the solid state reaction method for synthesizing most of the [NZP]-family

members[4,19,21,54,62]. Furthermore, the traditional sol-gel technique[101] is modified by introducing a seeding step which has improved considerably the sinterability and the microstructure of the material[59], where seeding means the intentional introduction of particles that will act as nuclei. In some cases[22], precipitation from aqueous solutions is used to get homogeneous NZP-type compounds.

The starting components for the sol-gel method include $ZrO(NO_3)_2 \cdot xH_2O$, $NH_4H_2PO_4$ and MNO_3(M:cation), which are made up into solutions which can be mixed in order to form a homogeneous gel. The gel is dried at 60°C. This is followed by calcination at 600°C overnight to decompose the nitrates. The calcines are then ground, pelletized, and sintered at 1000°-1200°C for 24 to 48 hrs.

Even though the sol-gel method has several advantages such as better homogeneity, better stoichiometry of the sample, lower firing temperature and higher reactivity[54,102-104], the sol-gel method for the complex compositions is difficult to use, because in certain cases, it requires very specific control of pH concentration or sequencing of additions[105,106]. Other disadvantages include calcination after gelation, expensive raw materials and cracking difficulties during sintering due to surface adsorbed H_2O and OH groups[107].

2.5 Summary

In section 2.1, the history of the development of NZP-type structures has been presented. General thermal expansion theory and several factors affecting the thermal expansion have been described in section 2.2. Anisotropy in NZP structures has been summarized with the anisotropic expansion data in this section. Initial

studies on axial thermal expansion of the NZP structure were completed up to 600°C, but some studies evaluated axial thermal expansion in modified NZP systems up to 1000°C. Only one axial thermal expansion measurement was conducted up to 1300°C for $KZr_2(PO_4)_3$.

Crystal chemistry reviews have been presented in section 2.3, and the structural studies, elemental substitutions, and high temperature crystal chemistry of NZP structures are summarized in various sub-sections. As introduced in section 2.3.2 for the substitution of first part of $NaZr_2(PO_4)_3$ structure, studies of elemental substitution with valences of +1 & +2 have been conducted, but only two substitutions have been considered for elements having valence greater than +2 to replace the Na^+ in $NaZr_2(PO_4)_3$ structure. Furthermore, few studies have been conducted to determine the solubility of two or three elements to substitute for Na^+ in the NZP structure.

A review of the processing methods to synthesize the NZP-type compounds has been presented in section 2.4. Because of the low reactivity of ZrO_2 in solid-state processing, sol-gel processing was used to promote homogeneity, although several disadvantages still must be overcome in applying the sol-gel process.

Chapter III

Experimental Procedure

3.1 Introduction

The principal purpose of this study is to develop new low thermal expansion materials based on NZP-type structure. To determine the effects of cation substitution for the first part of the NZP structure, twenty-five chemical elements, with the electron valence ranging from +1 to +5, were selected. These are listed in Table 6. Those elements include: Li, Na, K, Rb, and, Cs(from the alkali-metal Group); Mg, Ca, Sr, and Ba(from the alkaline-earth Group); Mn, Ni, Cu, and Zn(with electron valence of +2 from transition elements); Y, La, Al, and Cr(with electron valence of +3); Ti, Zr, Hf, Si, and Ce(with electron valence of +4); and V, Nb, and Ta(from Group VA).

Based on a quarternary system, solid solubility studies between alkali(Na ~ Cs)-alkali, alkaline earth(Mg ~ Ba)-alkaline earth, and alkali-alkaline earth elements,

Table 6. Elements selected to substitute for the Na^+ in the NZP structure

Alkali metal group	Alkaline earth group	Transition elements with +2	Elements with +3	Elements with +4	Transition elements with +5
Li	Mg	Mn	Y	Ti	V
Na	Ca	Ni	La	Zr	Nb
K	Sr	Cu	Al	Hf	Ta
Rb	Ba	Zn	Cr	Si	
Cs				Ce	

substituting for Na cation in the NZP structure, were considered. Several quinternary systems based on CaO-MgO-Na_2O-ZrO_2-P_2O_5 were also included in this study.

All of the systems considered were prepared by a novel method, which was found to be helpful to increase the reactivity of ZrO_2. Details of this processing method will be described in subsequent sections, although it generally involves the use of P_2O_5 instead of $NH_4H_2PO_4$ and $(NH_4)_2HPO_4$. Linear thermal expansion measurements were conducted for systems showing single phase after compound synthesis. For some systems, axial thermal expansions were investigated by high-temperature XRD up to 1400°C.

Secondary material properties including thermal shock resistance, and mechanical strength were evaluated for the compounds $Rb_{0.5}Cs_{0.5}Zr_2(PO_4)_3$ & $Ca_{0.5}Mg_{0.5}Zr_4(PO_4)_6$ with the linear α values of -0.3×10^{-7}/°C & -5×10^{-7}/°C, respectively. Structural attributes, microstructure, and fractography were also characterized for these two compounds.

3.2 Synthesis

3.2.1 Raw materials

The raw materials ZrO_2 and P_2O_5 are included in all of systems considered. Purities of ZrO_2 and P_2O_5, which were obtained from suppliers Fisher Scientific and Aldrich, are shown in Table 7. The purities of other ceramic raw materials selected to modify the NZP structure are also listed in Table 7.

Table 7. Purity of raw materials

Raw material	Purity
ZrO_2	99%
P_2O_5	99% P_2O_5, 0.002% Insoluble matter, Trace amounts of P_2O_3
Li_2CO_3	99%
Na_2CO_3	99.97%
K_2CO_3	99.95%
Rb_2O	99%
Cs_2O	99%
MgO	99%
CaO	98%
SrO	N.A.
BaO	N.A.
MnO	99.5%
NiO	99.8%
CuO	99.5%
ZnO	99.97%
Y_2O_3	99.9%
La_2O_3	99.99%
Al_2O_3	99.4%
Cr_2O_3	99.8%
TiO_2	99.7%
HfO_2	98%
SiO_2	99.9%
CeO_2	99.9%
V_2O_5	99.6%
Nb_2O_5	99.9%
Ta_2O_5	99%

3.2.2 Processing

Sample constituents were weighed to an accuracy of 0.001g, and the raw materials were mechanically mixed with acetone, and were left in air at room temperature for one to two days to allow for reaction between P_2O_5 and acetone. The sticky product from the reaction of P_2O_5 and acetone was heat treated at 1100°C for 24h, and at 1300°C for 4h, followed by furnace cooling to room temperature. Acetone served as the mineralizer as well as the aid to make homogeneous mixtures. After compound synthesis, XRD patterns were obtained to determine the phases present. The following X-ray conditions were used: accelerating potential: 40KV; filament current: 15mA and scan rate: 1°/min.

3.3 Thermal expansion measurements

3.3.1 Linear thermal expansion

The samples synthesized by heat treatment were reground and cold pressed at a pressure of about 14kgf/mm^2 into bar specimens, having dimensions of 10cm(length)x1cm(width)x0.6-0.8cm(thickness). Two to four wt% of methycellulose or methocel(from Dow Chemical Co.) and 1 to 3 wt% ZnO was added to the reground powder to aid sintering. Sintering treatments were performed at 1300°C for 8h.

Thermal expansion was measured from room temperature to 1000°C using a dilatometer with a fused silica pushrod. Length changes were measured by dial in-

dicator and recorded, at temperature intervals of 50°C, up to 1000°C. Mean coefficients of linear thermal expansion were calculated using equation 3.1.

$$\alpha = \frac{\Delta L}{L_0 \Delta T} \quad (3.1)$$

where:

α :*mean coefficient of linear thermal expansion*

L_0 :*initial length of specimen*

ΔL:*observed change in length*

ΔT:*temperature change*

For the systems showing linear thermal expansion less than 20×10^{-7}/°C in absolute value, average values from 2 or more runs were taken. Data were corrected by adding the thermal expansion of fused silica(5×10^{-7}/°C)[2]. The heating rate of 5° to 6°C/min was used to give sufficient time for the specimen to be at a relatively uniform temperature.

A Netzsch-Differential-Dilatometer 402 ED with computerized automatic control was used for the systems having expansion less than 10×10^{-7}/°C in absolute value. The samples had dimensions of 0.55mm(diameter)x25mm(length). Single crystal alumina was used as reference material, and the heating rate was 10°C/min. For the systems showing a difference between the automatic dilatometer and the manual dilatometer, data from automatic dilatometer were reported.

3.3.2 Axial thermal expansion

Lattice parameters of -325 mesh powders were measured at the High Temperature Materials Laboratory(HTML) at Oak Ridge National Lab. High temperature XRD was performed up to 1400°C with intervals of 200°C using a Scintag θ-θ goniometer equipped with a Buehler furnace. Diffraction patterns were obtained using Cu Kα radiation with a wavelength of 1.54059Å[108] in the 2θ range of 18° to 42°. The following conditions were used: accelerating potential: 45KV; filament current: 40mA and scan rate: 2°C/min.

Five or six major peaks were selected to calculate the lattice parameter, typically, (110), (113), (024), (116), (214), and (300). The peak positions were calibrated by the position of the Pt powder(99.99% purity) mixed with the sample powder. The positions of Pt peaks at high temperatures were calculated from an equation for the linear thermal expansion of Pt by Hahn et al[109]. The peak positions were then determined within the 2θ error of $\pm$0.02°, which corresponded to a maximum accuracy of 0.0005 nm[22] in the lattice constant. The lattice parameters at each elevated temperature were calculated by a least-squares computer program. Axial thermal expansions were determined up to 1400°C from the slopes of the curves $a = f(T)$ and $c = f(T)$.

3.4 Secondary material property characterization

3.4.1 Structural attributes

Because the compounds $Rb_{0.5}Cs_{0.5}Zr_2(PO_4)_3$ & $Ca_{0.5}Mg_{0.5}Zr_4(PO_4)_6$ showed the linear CTE values of -0.3×10^{-7}/°C & -5×10^{-7}/°C, respectively, several structural attributes were measured; they include bulk density, %shrinkage, %water absorption, %open porosity, and %theoretical density(%TD). These measurements were based on ASTM standards and test methods suggested in other references. Test references are summarized in Table 8.

3.4.2 Thermal shock resistance

Thermal shock resistance was characterized using the maximum temperature water quench test and the repeated water quench test[113]. Muliple samples were quenched into ice water from successively higher temperatures until surface cracks were detected by visual observation. Rectangular bars with the dimensions of 4.5cm(length)x1cm(width)x0.6cm-0.8cm(height) were used, and the furnace temperature was increased using intervals of 100°C. After finding cracks on the surface, the furnace temperature was increased using intervals of 25°C to determine the more accurate temperature differential.

Repeated quenching from 1200°C to ice water was performed for specimens with the same dimensions as for the maximum temperature difference quench test. Before each quench, specimens were kept at 1200°C for 30 minutes.

Table 8. Standard methods applied to measure structural attributes

	Bulk Density	%Shrinkage	%Water Absorption	%Open Porosity	%TD
Reference	ASTM C20-83 [110]	[111]	ASTM C20-83 [110]	ASTM C20-83 [110]	ASTM C135-66 [112] &[111]
Brief Description	Dry Weight divided by the exterior volume, including pores	%Length change by firing	%Weight of water absorbed, by boiling & soaking, to the dry specimen's weight	%volume of the open pores, from boiling &soaking in water, to its exterior volume	%bulk density to the true density obtained by pycnometer

3.4.3 MOR test and fractography

Room temperature MOR data were obtained from 3-point and 4-point bend tests using an MTS universal testing machine. In both cases, the crosshead displacement speed was 0.0058mm/sec. The span for the 3-point fixture was 69.2mm, while the spans for the 4-point fixture were 25.2mm between outer loading points and 12.7mm between inner loading points. The ratio of width and height was controlled close to 2:1 according to recommended practice[114]. The width ranged from 0.8-0.9cm, and the specimen height ranged from 0.4-0.45cm. The trueness[115] for the specimens used for 4-point bend testing was measured using a steel ruler along the height and face.

Fractured surfaces were examined in a SEM operated at 15KV. All of the specimens required coating with vaporized gold or carbon to provide a conducting layer.

3.4.4 Microstructure

Microstructural investigation was conducted for the compounds $Rb_{0.5}Cs_{0.5}Zr_2(PO_4)_3$ and $Ca_{0.5}Mg_{0.5}Zr_4(PO_4)_6$. The specimen $Rb_{0.5}Cs_{0.5}Zr_2(PO_2)_3$ was ground using a 600 grit emery paper, followed by mechanical polishing in aqueous slurries of 0.3μm Al_2O_3. And then it was etched using 1HF-1HCl-1HNO_3 solution. $Ca_{0.5}Mg_{0.5}Zr_4(PO_4)_6$ was ground and polished; etching was not required. SEM was used to characterize the microstructures of both compounds.

3.4.5 DTA analysis & long-term thermal stability

Phase stability of specimens was studied by differential thermal analysis(DTA) with a Perkin-Elmer thermal analysis system 7/4 up to 1500°C with a heating rate of 20°C/min. Long-term thermal stability was evaluated by exposure at 1400°C for 96 h, followed by cooling to room temperature and XRD analysis.

3.4.6 Lot-to-lot & replicate test variability

Statistical analysis of lot-to-lot variability and replicate test variability from 10 batches for each tests was done for the compound $Ca_{0.5}Mg_{0.5}Zr_4(PO_4)_6$, which showed very promising thermal expansion value of $-5X10^{-7}/°C$, using the automatic dilatometer. Mean value, standard deviation, standard error, and coefficient of variation were calculated[117,118].

Chapter IV

Experimental Results

4.1 Ternary system

Twenty-four cation substitutions, with valence values ranging from +1 to +5, were used to replace Na^+ in the NZP skeletal framework. Their linear thermal expansion results are presented in sections 4.1.1.1 through 4.1.1.6. Section 4.1.1.1 summarizes the results for the systems substituted by alkali elements, and the following two sections, 4.1.1.2 and 4.1.1.3, present the experimental results of the compounds replaced by elements with valence of +2, dealing with the alkaline-earth elemental substitution in section 4.1.1.2 and the transition elemental substitution in section 4.1.1.3. Sections 4.1.1.4 and 4.1.1.5 show results for compounds substituted by elements with valence of +3 and +4, respectively. Finally, the results by transition elements with +5 are shown in section 4.1.1.6.

Among the elemental substitution in the ternary systems, twelve substitutions showed linear α values less than $20x10^{-7}/°C$, in absolute value. Axial thermal expansion measurements were conducted for these compounds, and their results are presented in sections 4.1.2.1 through 4.1.2.4. Section 4.1.2.1 summarizes the results substituted by Rb and Cs, and section 4.1.2.2 presents the results for the systems replaced by elements with electron valence of +2. In section 4.1.2.3, the experimental results for the compounds substituted by +3(Y) and +4(Ti,Ce) are included. The axial thermal expansion results for systems substituted by Nb and Ta are shown in section 4.1.2.4.

4.1.1 Linear thermal expansion

4.1.1.1 M^{+1}_2O-ZrO_2-P_2O_5(M^{+1}=Li, Na, K, Rb, Cs; alkali elements)

Five different alkali-modified di-zirconium tri-phosphates were prepared, and linear aggregate α values are shown in Table 9. Thermal expansion behavior from room temperature(R.T.) to 1000°C is shown in Figure 4.

The system with substitution by Li_2O(JK-111) showed a transition, at a temperature of about 150°C, from positive expansion to negative expansion. This transition is apparently related to the phase transition from monoclinic to hexagonal structure, which has been investigated by Lenain et al[19] and Petit et al[34]. The high temperature hexagonal phase has a linear thermal expansion value of $-22x10^{-7}/°C$.

Many studies[4,19,21,22,60] have been conducted to measure the thermal expansion for the $NaZr_2(PO_4)_3$ and $KZr_2(PO_4)_3$ compounds. $NaZr_2(PO_4)_3$ has been reported to have values between $-40x10^{-7}/°C$[4,21] and $-30x10^{-7}/°C$[19]. $KZr_2(PO_4)_3$

Table 9. Linear thermal expansion results for the alkali-modified systems

Sample No	Composition (Moles)	Phase	Linear CTE	
			$\alpha(x10^{-7}/^{\circ}C)$	Temp.Range($^{\circ}C$)
JK-111	$1Li_2O-4ZrO_2-3P_2O_5$	$LiZr_2(PO_4)_3$	-22	150-1000
JK-112	$1Na_2O-4ZrO_2-3P_2O_5$	$NaZr_2(PO_4)_3$	-33	R.T.-1000
JK-113	$1K_2O-4ZrO_2-3P_2O_5$	$KZr_2(PO_4)_3$	-22	R.T.-1000
JK-114	$1Rb_2O-4ZrO_2-3P_2O_5$	$RbZr_2(PO_4)_3$	2	R.T.-1000
JK-115	$1Cs_2O-4ZrO_2-3P_2O_5$	$CsZr_2(PO_4)_3$	5	R.T.-1000

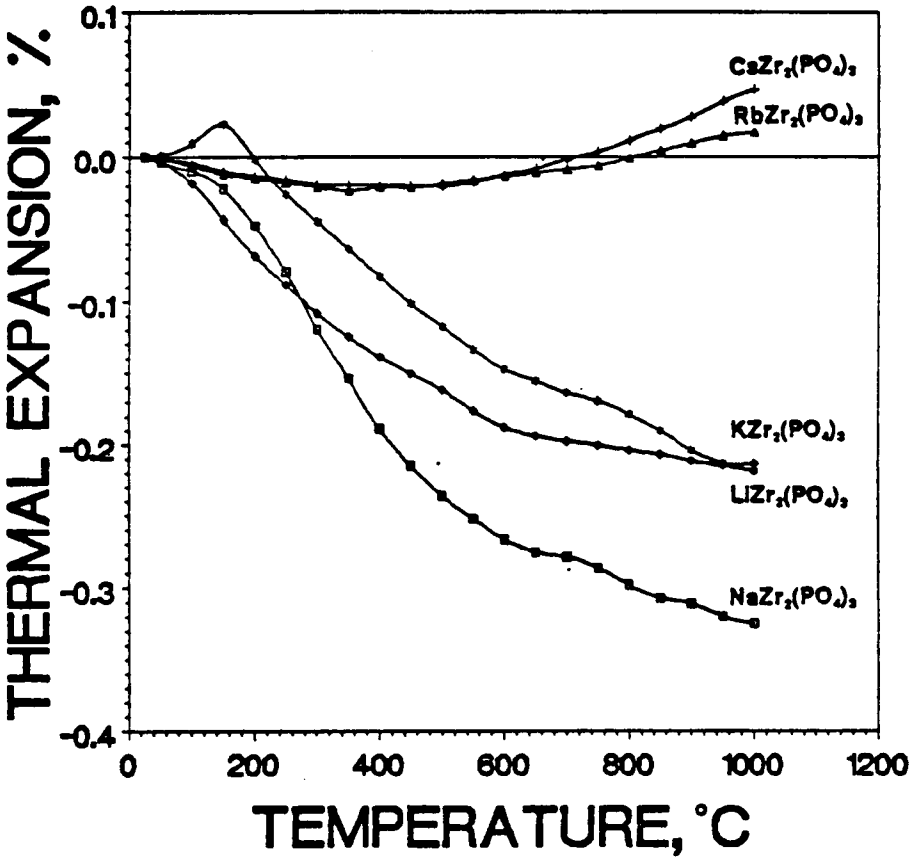

Figure 4. Linear thermal expansion behavior of the alkali-modified systems

reportedly has α values between $-75x10^{-7}$/°C[19] and $4x10^{-7}$/°C[22,60]. In the present study, the following average linear aggregate thermal expansion values have been obtained: $-33x10^{-7}$/°C for $NaZr_2(PO_4)_3$ and $-22x10^{-7}$/°C for $KZr_2(PO_4)_3$, from R.T. to 1000°C. Thus, our values fall within the reported ranges.

Low expansion coefficients for $RbZr_2(PO_4)_3$ and $CsZr_2(PO_4)_3$ were measured by Lenain et al[19]. The values reported are $-15x10^{-7}$/°C for $RbZr_2(PO_4)_3$ and $-5x10^{-7}$/°C for $CsZr_2(PO_4)_3$, but those data are available only up to 500°C. Our linear thermal expansion results for JK-114($RbZr_2(PO_4)_3$) and JK-115($CsZr_2(PO_4)_3$), shown in Figure 4, show that linear aggregate expansion decreases up to 500°C, but begin to increase above 500°C. The mean linear thermal expansion values, up to 1000°C, are $2x10^{-7}$/°C for $RbZr_2(PO_4)_3$ and $5x10^{-7}$/°C for $CsZr_2(PO_4)_3$.

Linear thermal expansion trends observed in these alkali modified systems, such as negative($LiZr_2(PO_4)_3$,$NaZr_2(PO_4)_3$, $KZr_2(PO_4)_3$) and transition from negative to positive ($RbZr_2(PO_4)_3$,$CsZr_2(PO_4)_3$), will be discussed later.

4.1.1.2 $M^{+2}O$-ZrO_2-P_2O_5(M^{+2}=Mg, Ca, Sr, Ba; alkaline earth elements)

Substitution of alkaline earth elements(with +2 valence) for Na^+, the first part of NZP, creates vacancies of half-position of Na ion, because of the need to maintain charge neutrality. Therefore, the general form of the systems substituted by elements with the electron valence of +2 can be written as $[M^{II}_{0.5}, \square^{II}_{0.5}]Zr_2(PO_4)_3$ or $M^{II}Zr_4(PO_4)_6$, where the superscript 'II' means the electron valence of +2. Linear thermal expansion was measured for sintered bars, and results are summarized in Table 10. Thermal expansion behavior from R.T. to 1000°C for the systems modified by alkaline-earth elements are shown in Figure 5.

Table 10. Linear thermal expansion results for the alkaline earth-modified systems

Sample No	Composition (Moles)	Phase	Linear CTE	
			$\alpha(x10^{-7}/^{\circ}C)$	Temp.Range($^{\circ}C$)
JK-121	$1MgO-4ZrO_2-3P_2O_5$	$MgZr_4(PO_4)_6$	16	R.T.-1000
JK-122	$1CaO-4ZrO_2-3P_2O_5$	$CaZr_4(PO_4)_6$	-18	R.T.-1000
JK-123	$1CaO-4ZrO_2-3P_2O_5$	$SrZr_4(PO_4)_6$	22	R.T.-1000
JK-124	$1BaO-4ZrO_2-3P_2O_5$	$BaZr_4(PO_4)_6$	15	R.T.-1000

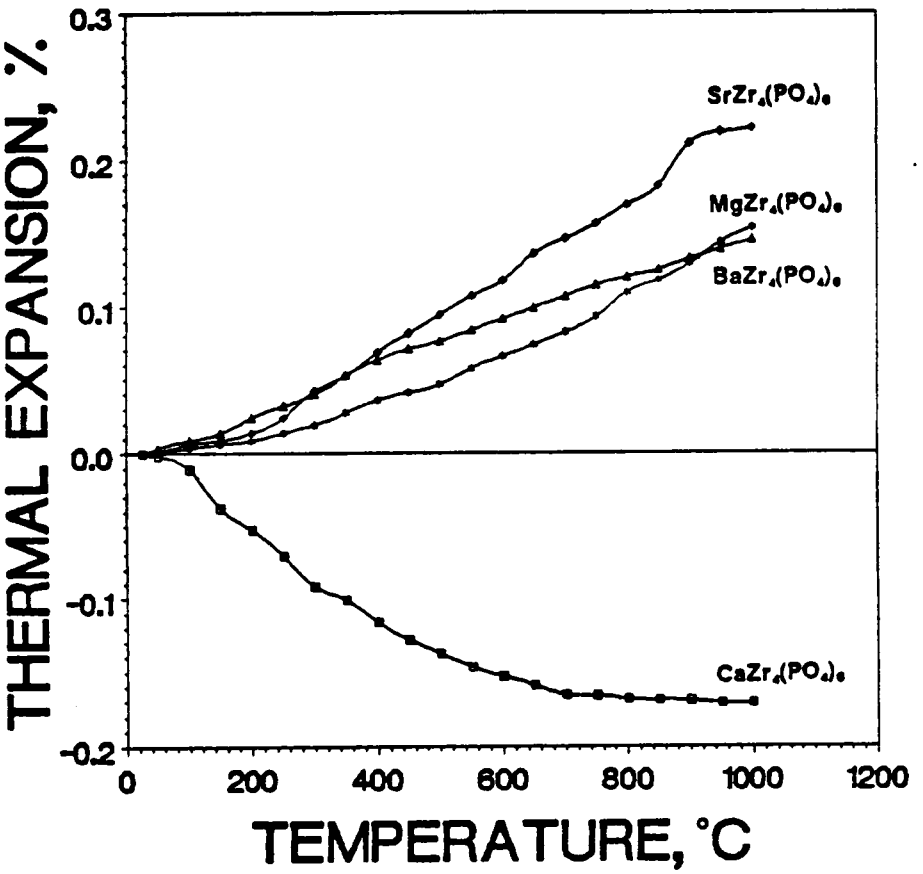

Figure 5. Linear thermal expansion behavior of the alkaline earth-modified systems

From Figure 5, $MgZr_4(PO_4)_6$ compound showed positive thermal expansion with a mean value of $16x10^{-7}/°C$ with increasing temperature up to 1000°C. On the other hand, $CaZr_4(PO_4)_6$ system exhibited negative thermal expansion with the value of $-18x10^{-7}/°C$. Our value for the $CaZr_4(PO_4)_6$ compound is close to the value reported by Roy et al($-16x10^{-7}/°C$[4]).

The thermal expansion behavior of JK-123($SrZr_4(PO_4)_6$) was similar with that previously reported by Oota et al, with a mean thermal expansion value of $22x10^{-7}/°C$. The system modified by BaO showed low thermal expansion behavior of $15x10^{-7}/°C$.

Figure 5 shows that the linear thermal expansion behavior of $BaZr_4(PO_4)_6$ is much more positive than $MgZr_4(PO_4)_6$ and very close to that of $SrZr_4(PO_4)_6$ up to 400°C. Above 400°C, the rate of expansion is decreased, giving a mean expansion value up to 1000°C as $15x10^{-7}/°C$ for $BaZr_4(PO_4)_6$, which is less than the values for $MgZr_4(PO_4)_6$($16x10^{-7}/°C$) & $SrZr_4(PO_4)_6$($22x10^{-7}/°C$). This particular expansion behavior of $BaZr_4(PO_4)_6$ might be related with the decrease of α due to microcrack formation during heating[83].

Except for the system $CaZr_4(PO_4)_6$ which showed negative expansion, the three other systems showed positive expansion. The effect of crystallinity affecting thermal expansion will be more fully described in the Discussion to explain the linear expansion behavior observed in $CaZr_4(PO_4)_6$.

4.1.1.3 $M'^{+2}O$-ZrO_2-P_2O_5(M'^{+2}=Mn, Ni, Cu, Zn; transition elements with +2)

The thermal expansion studies for the modified zirconium phosphates by transition elements with electron valence of +2 were conducted. The transition elements selected in the study include Mn, Ni, Cu, and Zn, and their ionic radii, with coordination number of 6, range from 0.74Å to 0.91Å[116]. Linear thermal expansion

results are listed in Table 11, and linear thermal expansion results are shown in Figure 6.

A formula for the systems with substitution by transition elements having electron valence of +2 can be written in a similar fashion as for the alkaline earth modified systems. An example is $[M'^{II}_{0.5}, \square^{II}_{0.5}]Zr_2(PO_4)_3$ or $M'^{II}Zr_4(PO_4)_6$. From Figure 6, there are two definite linear expansion characteristics such as the continuous increase observed in $MnZr_4(PO_4)_6$ and $CuZr_4(PO_4)_6$, and the expansion transition investigated in $NiZr_4(PO_4)_6$ and $ZnZr_4(PO_4)_6$. Thermal expansion transitions from negative to positive for $NiZr_4(PO_4)_6$ and $ZnZr_4(PO_4)_6$ occurred around 550°C.

The sample JK-125($MnZr_4(PO_4)_6$) showed a thermal expansion of $7x10^{-7}$/°C up to 1000°C. Mean linear thermal expansion of the $NiZr_4(PO_4)_6$ system was measured as $10x10^{-7}$/°C up to 1000°C. The system in which CuO replaced the first part of NZP exhibited a large linear thermal expansion with the value of $40x10^{-7}$/°C.

The specimen JK-128($ZnZr_4(PO_4)_6$) showed a low α value of $5x10^{-7}$/°C up to 900°C, however the thermal expansion suddenly decreased above 900°C. This change might be related with a phase transition or decomposition. Prior to analysis, all of the compounds studied were sintered at 1300°C. This sintering temperature is higher than the temperature where the system $ZnZr_4(PO_4)_6$ showed the sudden decrease in thermal expansion. Phase analysis before and after sintering treatment showed no difference in diffraction peaks. This implies that the phase transformation or decomposition observed in the $ZnZr_4(PO_4)_6$ system which accompanied the sudden decrease in the thermal expansion is considered to be reversible.

Table 11. Linear thermal expansion results for the transition metal substitution with +2 valence

Sample No	Composition (Moles)	Phase	Linear CTE	
			$\alpha(x10^{-7}/^{\circ}C)$	Temp.Range($^{\circ}C$)
JK-125	$1MnO-4ZrO_2-3P_2O_5$	$MnZr_4(PO_4)_6$	7	R.T.-1000
JK-126	$1NiO-4ZrO_2-3P_2O_5$	$NiZr_4(PO_4)_6$	10	R.T.-1000
JK-127	$1CuO-4ZrO_2-3P_2O_5$	$CuZr_4(PO_4)_6$	40	R.T.-1000
JK-128	$1ZnO-4ZrO_2-3P_2O_5$	$ZnZr_4(PO_4)_6$	5	R.T.-900

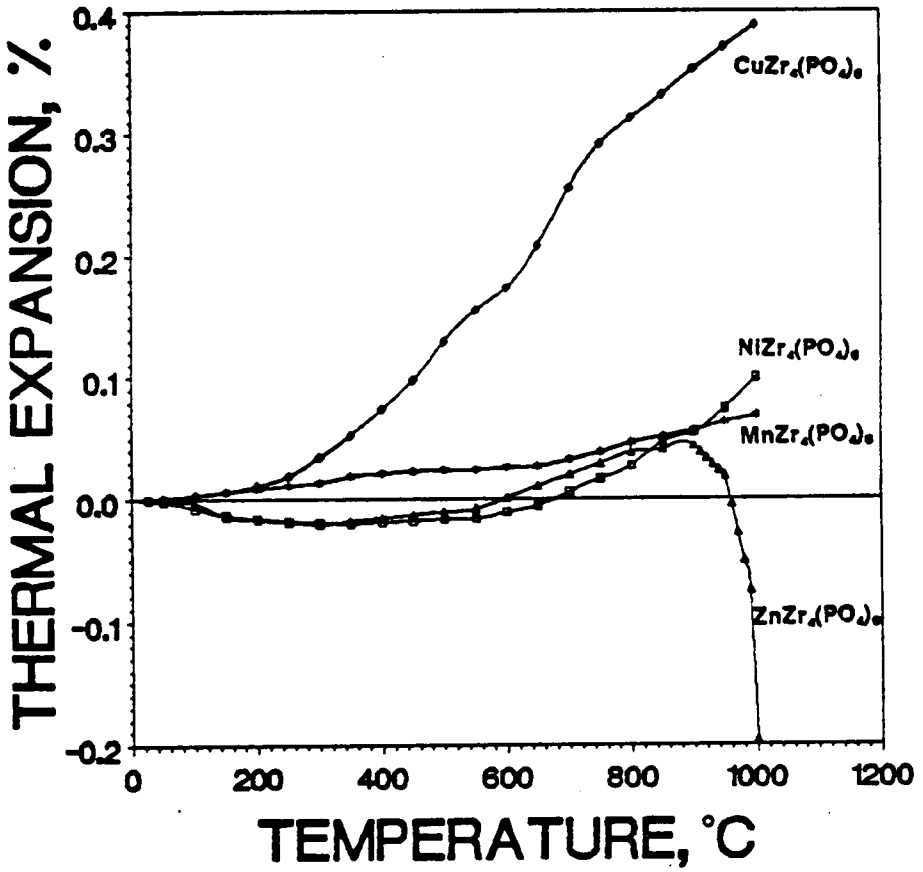

Figure 6. Linear thermal expansion behavior of the transition metal substitution with +2 valence

4.1.1.4 $M^{+3}_2O_3$-ZrO_2-P_2O_5(M^{+3} = Y, La, Cr, Al; elements with +3)

Four oxides containing cations with a +3 charge were selected to investigate the possibility of synthesizing a modified NZP structure. Phases present before and after sintering treatment were analyzed by XRD. All of the resulting compounds studied were isomorphous with $NaZr_2(PO_4)_3$.

The $NaZr_2(PO_4)_3$ crystal structure contains 6 sodium atoms in 6(b) positions based on space group of $R\bar{3}C$ [98], which is the structure of NZP. Because of the large channels within the structure, ions with a valence of +3 can be positioned at the Na sites filling one-third of those sites or at the M_I/M_{II} site shown in Figure 2 randomly, or at vacant sites. Even in any case, the general formula for the systems substituted by elements of +3 electron valence can be written as $[M^{III}_{0.33}, \square^{III}_{0.67}]Zr_2(PO_4)_3$ or $M^{III}Zr_6(PO_4)_9$, where superscript 'III' denotes a valence of +3.

Linear thermal expansion results are listed in Table 12, and detailed expansion behavior is shown in Figure 7. For the +3 cation modified systems, only JK-131($YZr_6(PO_4)_9$), with the value of $14x10^{-7}$/°C, was included in the low thermal expansion group. Thermal expansion data for other systems ranged from $24x10^{-7}$/°C to $29x10^{-7}$/°C.

Two distinct trends can be found in the linear expansion behavior for the systems substituted by cation with +3 electron valence. One trend, illustrated by samples JK-131 and 132 (modified with Y and La, respectively), shows a big increase in α for temperatures above 700°C. The other trend, which can be found in JK-133 and 134, modified by Al and Cr respectively, is that the linear thermal expansion rate is largest in the temperature range from 200°C to 300°C. This maximum in expansion rate might be related to structural instability. These two different trends are probably due to the differences in ionic size and atomic weight of the substituted elements.

Table 12. Linear thermal expansion results for the substituted systems with +3 valence

Sample No	Composition (Moles)	Phase	Linear CTE $\alpha(\times 10^{-7}/^{\circ}C)$	Temp.Range($^{\circ}C$)
JK-131	$1Y_2O_3-12ZrO_2-9P_2O_5$	$YZr_6(PO_4)_9$	14	R.T.-1000
JK-132	$1La_2O_3-12ZrO_2-9P_2O_5$	$LaZr_6(PO_4)_9$	25	R.T.-1000
JK-133	$1Al_2O_3-12ZrO_2-9P_2O_5$	$AlZr_6(PO_4)_9$	24	R.T.-1000
JK-134	$1Cr_2O_3-12ZrO_2-9P_2O_5$	$CrZr_6(PO_4)_9$	29	R.T.-1000

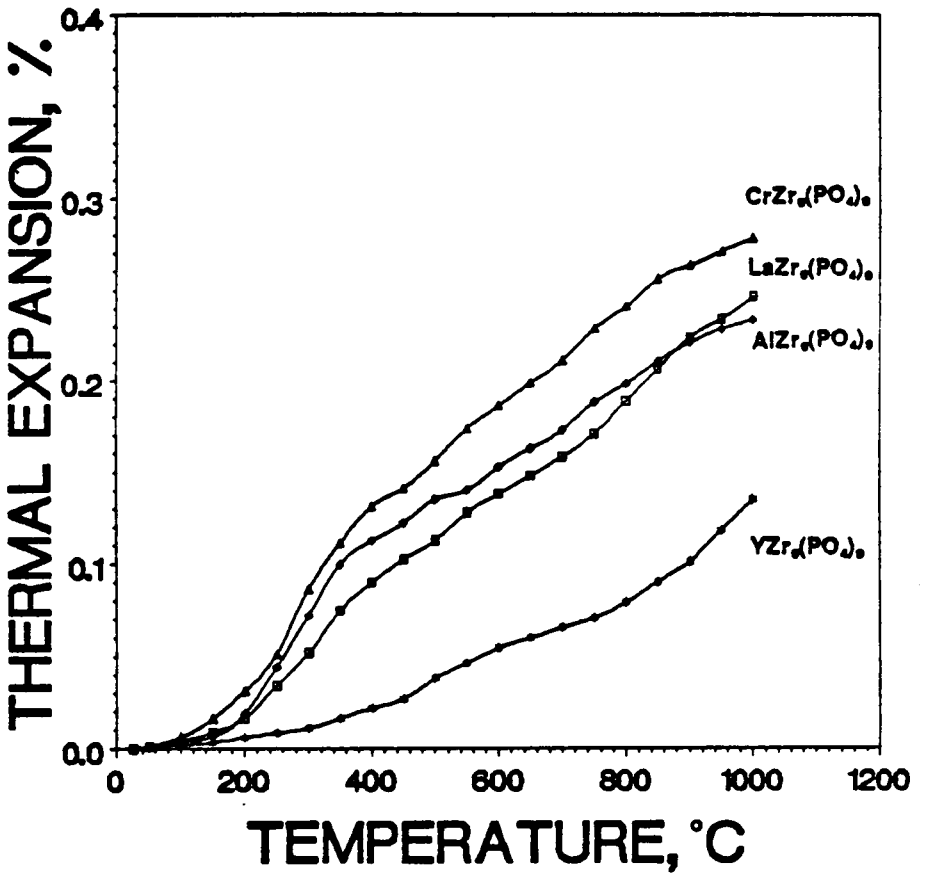

Figure 7. Linear thermal expansion behavior of the substituted systems with +3 valence

4.1.1.5 $M^{+4}O_2$-ZrO_2-P_2O_5(M^{+4}=Ti, Zr, Hf, Si, Ce; elements with +4)

Only one tetravalent ion, Zr[99], had been reported to replace the Na cation in the NZP structure. The structural form of this system with one-quarter mole of Zr replacing one mole of Na was expressed as $Zr_{0.25}Zr_2(PO_4)_3$, or more simply $Zr_3(PO_4)_4$[99]. As explained in the previous section, the NZP crystal structure contains 6 Na atom positions, therefore to substitute one-quarter mole of tetravalent Zr for univalent Na, extra sites are needed. Previous studies[22,36,41,44,45] verified that extra ions can be positioned in the M_{II} site[22] which corresponds to the 18(e) lattice position in space group $R\bar{3}C$[97]. One can write the general formula of NZP systems substituted by cations with +4 valence as $[M^{IV}_{0.25}, \square^{IV}_{0.75}]Zr_2(PO_4)_3$ or $M^{IV}Zr_8(PO_4)_{12}$, where the superscript 'IV' denotes the cation valence of +4.

Linear thermal expansion results are tabulated in Table 13, and expansion behavior is shown graphically in Figure 8. From Figure 8, it can be seen that specimen JK-142[$Zr_3(PO_4)_3$] shows a thermal expansion value of $39x10^{-7}$/°C up to 980°C, but then slightly decreases.

The compound $Zr_3(PO_4)_4$ is known to decompose slowly at 900°C into a mixture of ZrP_2O_7 and α-$Zr_2P_2O_9$[99]. Systems synthesized in this study were heat treated at 1300°C, and later sintered at 1300°C. Diffraction patterns were obtained and analyzed at three different stages: after compound formation, after sintering, and finally after thermal expansion runs up to 1000°C. The results showed no difference in X-ray diffraction pattern. However, the diffraction patterns before and after sintering treatment showed a large difference in intensity, with no difference in position.

Because sintering was conducted above the temperature at which $Zr_3(PO_4)_4$ can be decomposed, other phases were expected from decomposition at the room temperature phase after sintering treatment. However, only a change in the intensity of

Table 13. Linear thermal expansion results for the substituted systems with +4 valence

Sample No	Composition (Moles)	Phase	Linear CTE $\alpha(x10^{-7}/^{\circ}C)$	Temp.Range($^{\circ}C$)
JK-141	$1TiO_2-8ZrO_2-6P_2O_5$	$TiZr_8(PO_4)_{12}$	20	R.T.-980
JK-142	$1ZrO_2-8ZrO_2-6P_2O_5$	$Zr_3(PO_4)_4$	39	R.T.-980
JK-143	$1HfO_2-8ZrO_2-6P_2O_5$	$HfZr_8(PO_4)_{12}$	42	R.T.-950
JK-144	$1SiO_2-8ZrO_2-6P_2O_5$	$SiZr_8(PO_4)_{12}$	23	R.T.-1000
JK-145	$1CeO_2-8ZrO_2-6P_2O_5$	$CeZr_8(PO_4)_{12}$	11	R.T.-1000

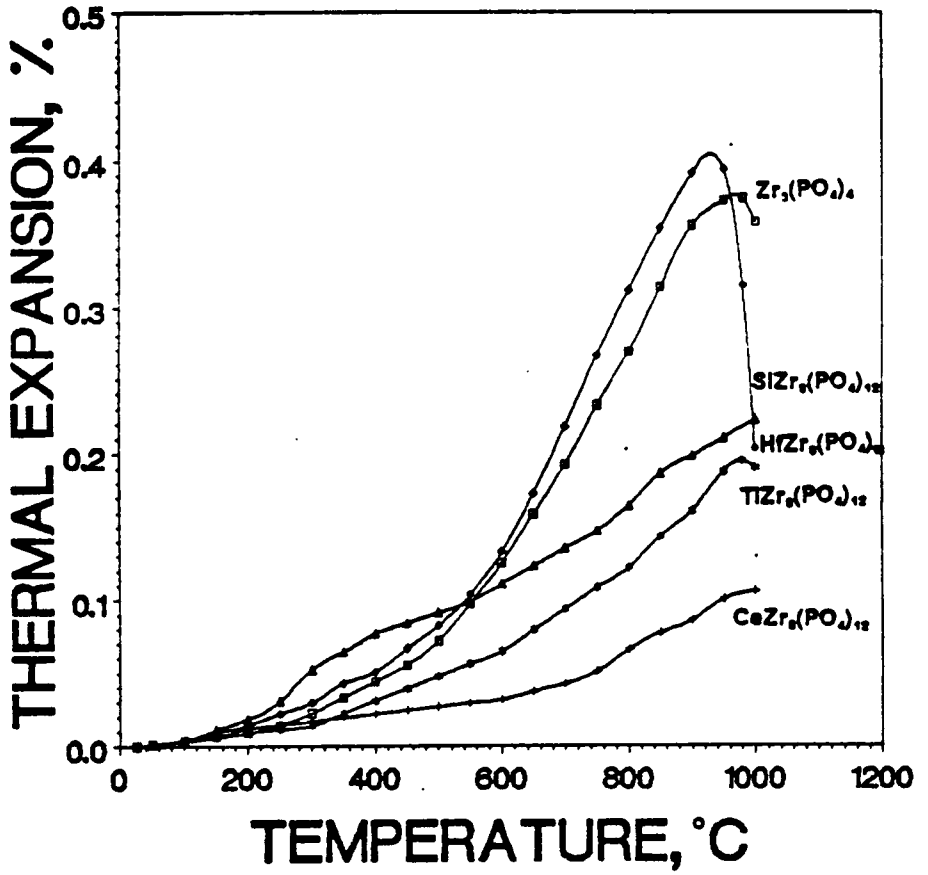

Figure 8. Linear thermal expansion behavior of the substituted systems with +4 valence

the diffraction peaks was observed. The reason that $Zr_3(PO_4)_4$ remained at room temperature after sintering at 1300°C might have resulted from the addition of ZnO which was used as sintering aid. ZnO may inhibit the decomposition of $Zr_3(PO_4)_4$, or slow down reaction kinetics involved in decomposition equilibrium.

The compound $HfZr_8(PO_4)_{12}$, where the substituted element, Hf, has same ionic radius[116] as Zr, showed behavior similar to sample JK-142($Zr_3(PO_4)_4$). It showed a linear thermal expansion of $42x10^{-7}$/°C up to 950°C, followed by a sudden decrease above 950°C. The Ti-substituted compound, $TiZr_8(PO_4)_{12}$, showed low linear expansion behavior of $20x10^{-7}$/°C, again followed by a decrease around 980°C. The transition observed in the linear thermal expansion behavior around 950°C for the compounds substituted with elements from Group IV A(Ti,Zr,Hf) might be related to phase instability or a sudden change in the axial thermal expansion which might arise from the different behavior of several polyhedron comprising the network structure.

The linear thermal expansion of $SiZr_8(PO_4)_{12}$ was measured as $23x10^{-7}$/°C, and showed a large expansion rate from 200°C to 300°C which was also observed in samples JK-133($AlZr_6(PO_4)_9$) and JK-134($CrZr_6(PO_4)_9$). The three systems(JK-133, 134, 144) substituted by Al, Cr, Si, respectively, are similar due to the small ionic radii of the substituted elements: i.e., 0.57Å(Al), 0.64Å(Cr), 0.39Å(Si). This will be covered in the Discussion section in detail with other trends investigated from linear thermal expansion behavior. Among the systems considered for substitution with +4 cation valence, $CeZr_8(PO_4)_{12}$ showed the lowest linear thermal expansion with a mean value of $11x10^{-7}$/°C up to 1000°C.

4.1.1.6 $M^{+5}_2O_5$-ZrO_2-P_2O_5(M^{+5}= V, Nb, Ta; elements with +5)

Nagai et al[43] synthesized the compound $NbZr(PO_4)_3$ [which was discussed as $Na_xNb_{1-x}Zr_{1+x}(PO_4)_3$ $(0 \leq x \leq 1)$], and examined it with powder X-ray diffraction, infrared absorption and Raman scattering. In the $NbZr(PO_4)_3$ structure, it was shown that Nb^{+5} substitutes for Zr^{+4} randomly while vacancies form in the Na^+ sites[43]. Therefore, the general form of NZP systems substituted by elements with +5 electron valence can be written as $M^V(Zr_{0.5}, \square^{IV}_{0.5})_2(PO_4)_3$ or $M^VZr(PO_4)_3$, where the superscripts 'IV' and 'V' mean the cation valence of +4 and +5, respectively. Three elemental substitutions were studied and their results are listed and shown in Table 14 and Figure 9, respectively.

The system substituted with V_2O_5 (which has a low melting temperature of 690°C)[119] showed thermal expansion transitions at around 300°C and 850°C. During cooling from the sintering treatment at 1300°C, the sintered bar passed through a phase transition region which accompanied the thermal expansion transition. The resulting sintered bar, after having cooled down to room temperature, had visible cracks over the whole specimen. However, the phase transition was observed to be a reversible reaction by XRD analysis before and after sintering treatment. A linear thermal expansion value of 20×10^{-7}/°C was measured for this sample in the temperature range from 400°C to 800°C.

Similar linear thermal expansion behavior was observed for samples JK-152($NbZr(PO_4)_3$) and JK-153($TaZr(PO_4)_3$). With increasing temperature, the $NbZr(PO_4)_3$ compound was found to expand less than $TaZr(PO_4)_3$. Their thermal expansion values were 4×10^{-7}/°C for $NbZr(PO_4)_3$ and 11×10^{-7}/°C for $TaZr(PO_4)_3$. The expansion value of 4×10^{-7}/°C for $NbZr(PO_4)_3$ agreed well with the value of 5×10^{-7}/°C reported by Oota et al[22].

Table 14. Linear thermal expansion results for the substituted systems with +5 valence

Sample No	Composition (Moles)	Phase	Linear CTE	
			$\alpha(x10^{-7}/^{o}C)$	Temp.Range(^{o}C)
JK-151	$1V_2O_5$-$2ZrO_2$-$3P_2O_5$	$VZr(PO_4)_3$	20	400-800
JK-152	$1Nb_2O_5$-$2ZrO_2$-$3P_2O_5$	$NbZr(PO_4)_3$	4	R.T.-1000
JK-153	$1Ta_2O_5$-$2ZrO_2$-$3P_2O_5$	$TaZr(PO_4)_3$	11	R.T.-1000

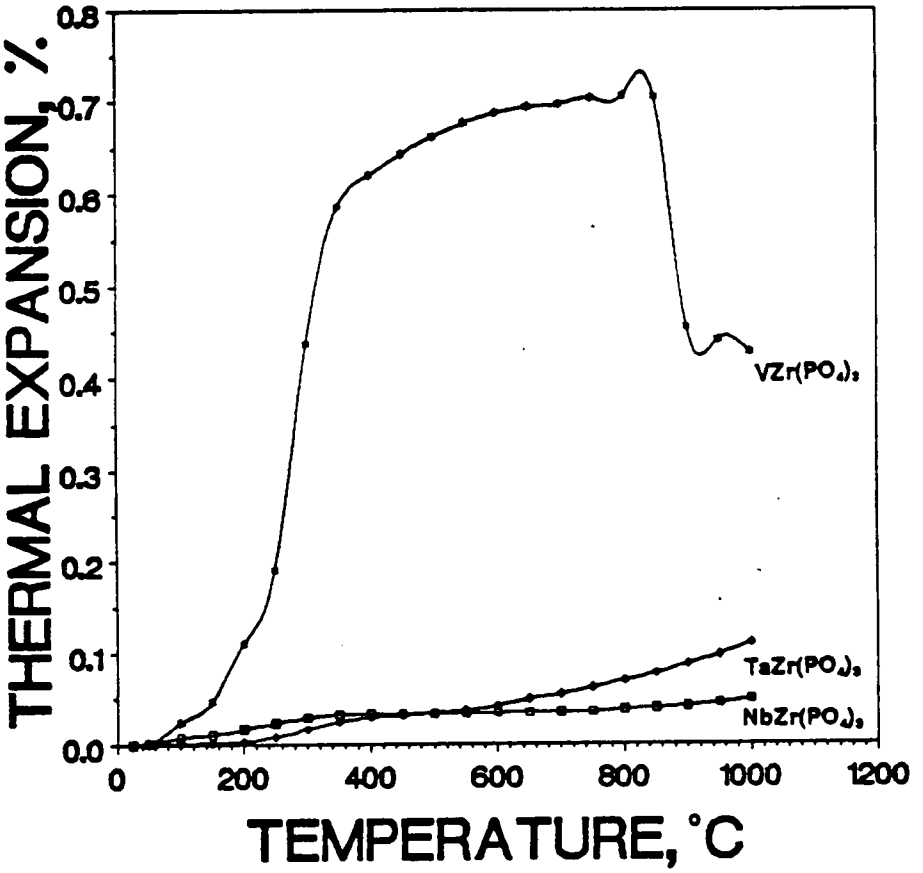

Figure 9. Linear thermal expansion behavior of the substituted systems with +5 valence

4.1.2. Axial thermal expansion

4.1.2.1 $L^{+1}{}_2O$-ZrO_2-P_2O_5(L^{+1}=Rb, Cs)

Axial thermal expansion measurements were conducted for the systems exhibiting α less than 20×10^{-7}/°C in absolute value. Among the alkali-modified systems, two compounds, $RbZr_2(PO_4)_3$ and $CsZr_2(PO_4)_3$, were selected for the investigation into the change of lattice parameters from room temperature to 1400°C. In Table 15, lattice parameters at R.T. and mean axial thermal expansion values up to 1400°C are listed. Also listed in Table 15 is the average linear thermal expansion calculated using the relationship ($\alpha_l = \frac{2}{3}\alpha_a + \frac{1}{3}\alpha_c$)[19] from the axial thermal expansion values. Detailed axial thermal expansion behavior is shown in Figures 10 and 11 along with the axial thermal expansion of $NaZr_2(PO_4)_3$ taken from Alamo & Roy[21].

Axial thermal expansion results for $RbZr_2(PO_4)_3$ and $CsZr_2(PO_4)_3$ showed a linear relationship. The axial α values were 12×10^{-7}/°C for the a-axis and 30×10^{-7}/°C for the c-axis for the compound $RbZr_2(PO_4)_3$. The $CsZr_2(PO_4)_3$ compound had axial α values of -9×10^{-7}/°C for the a-axis and 23×10^{-7}/°C for the c-axis. From these axial thermal expansion values, identical average α values, 2×10^{-7}/°C, were calculated for the two compounds.

The compound $RbZr_2(PO_4)_3$ showed good agreement between the measured linear α and the calculated linear α. Even though some discrepancy between the measured linear α and axial α for the compound $CsZr_2(PO_4)_3$ was found, the difference(3×10^{-7}/°C) is considered to be negligible when experimental condition and error are considered. Detailed discussion about the correlation between the measured linear α and calculated linear α, including anisotropic characteristic of axial ex-

Table 15. Lattice parameters and axial & linear CTE(coefficient of thermal expansion) data for alkali-modified systems

Sample Designation Phase		JK-114 $RbZr_2(PO_4)_3$	JK-115 $CsZr_2(PO_4)_3$
Lattice parameters (Å at R.T.)	a-axis c-axis	8.65 24.43	8.58 24.96
Axial CTE($x10^{-7}/^{o}C$) (R.T.-1400°C)	α_a α_c $\alpha_c-\alpha_a$	-12 30 42	-9 23 32
Calculated α_1($x10^{-7}/^{o}C$) Measured α_1($x10^{-7}/^{o}C$)		2 2	2 5

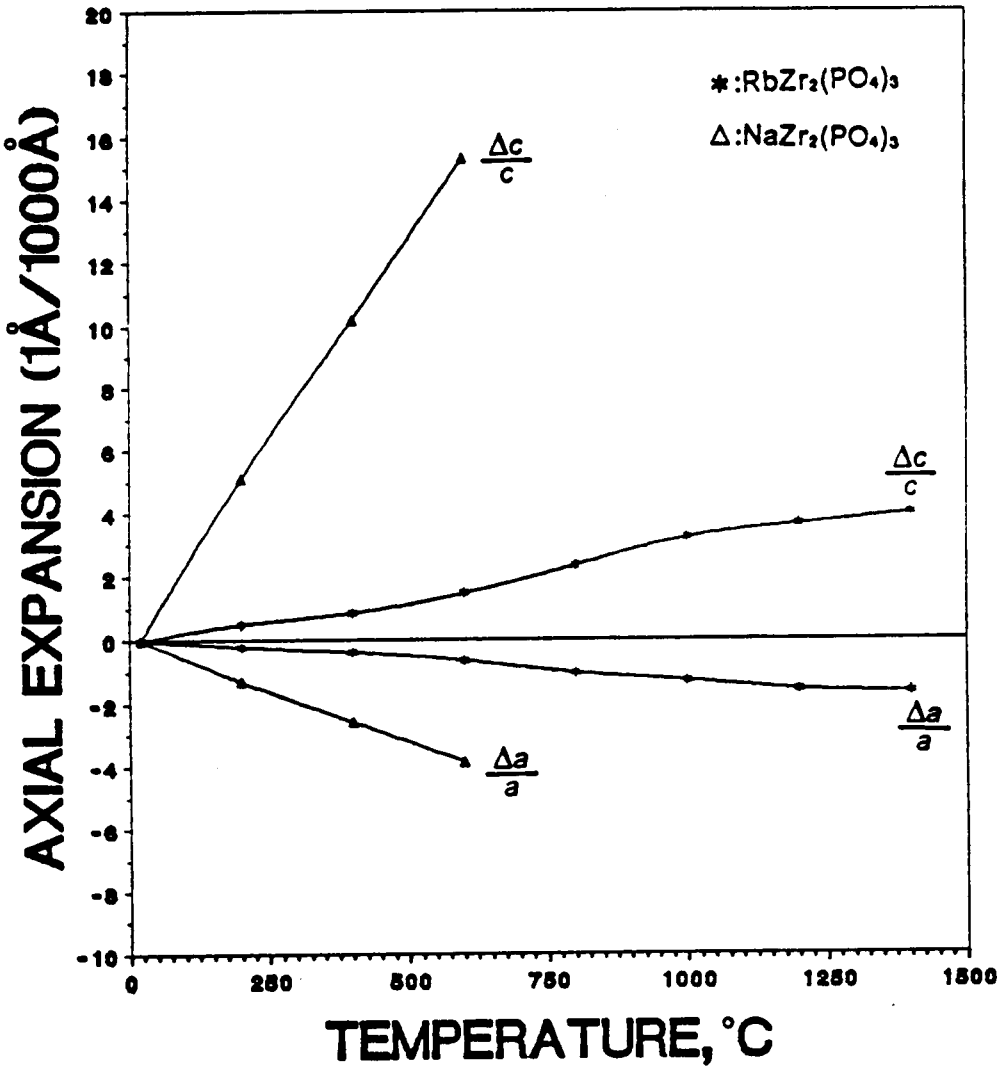

Figure 10. Axial thermal expansion behavior of $RbZr_2(PO_4)_3$ system

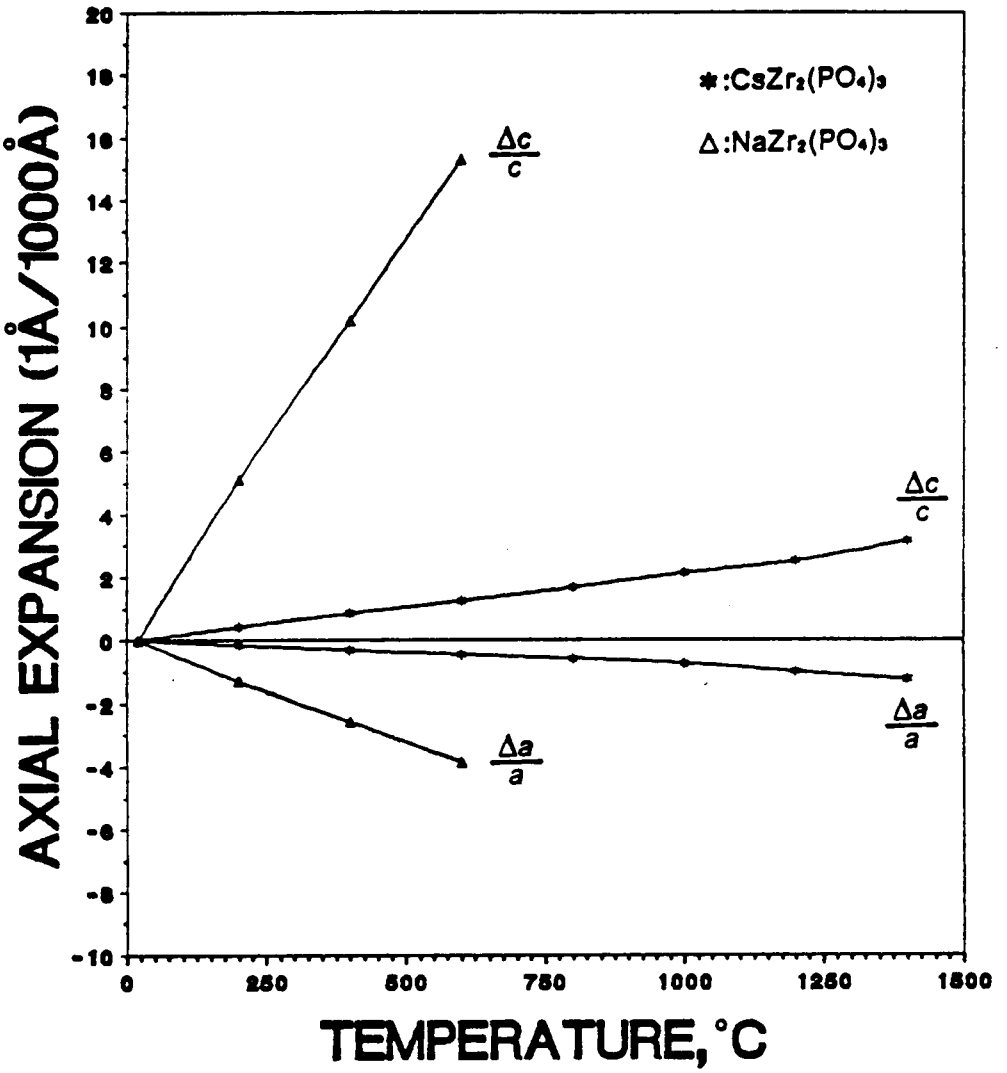

Figure 11. Axial thermal expansion behavior of $CsZr_2(PO_4)_3$ system

pansion behavior, will be presented in the Discussion section. In addition, the relationship between lattice parameters and ionic radii of the elements selected for substitution in the NZP structure will be discussed.

Differences in the axial α values between the a-axis and the c-axis($\alpha_c - \alpha_a$) are also included in Table 15. The compound $CsZr_2(PO_4)_3$, which contained a larger cation(1.65Å)[116] than Rb(1.49Å)[116], showed less anisotropy, $32x10^{-7}$/°C, than that of $RbZr_2(PO_4)_3$, $42x10^{-7}$/°C. Previous average α results up to 600°C for the compounds, $RbZr_2(PO_4)_3$ and $CsZr_2(PO_4)_3$, were published by Lenain et al[19]. Although axial thermal expansion values were not listed, calculated average α values were reported as $2.1x10^{-7}$/°C for $CsZr_2(PO_4)_3$ and $-7.6x10^{-7}$/°C for $RbZr_2(PO_4)_3$. The result for $CsZr_2(PO_4)_3$ is in good agreement with the value obtained in this study.

4.1.2.2 $L^{+2}O$-ZrO_2-P_2O_5(L^{+2} = Mg, Ca, Ba, Mn, Ni)

Room temperature lattice parameters and mean axial thermal expansion data for $MgZr_4(PO_4)_6$, $CaZr_4(PO_4)_6$ and $BaZr_4(PO_4)_6$ are listed in Table 16. High temperature XRD data are summarized in Table 17 for the structures substituted with transition elements(Mn and Ni). Detailed axial thermal expansion behavior is shown in Figures 12 through 14 for the alkaline earth modified systems and in Figures 15 and 16 for the transition element (with +2 valence) modified systems.

Sample JK-121($MgZr_4(PO_4)_6$) had axial α values of $-22x10^{-7}$/°C for the a-axis and $58x10^{-7}$/°C for the c-axis. The calculated average linear α was $5x10^{-7}$/°C, with the linear α measured as $16x10^{-7}$/°C. The axial thermal expansion difference($\alpha_c - \alpha_a$) was $80x10^{-7}$/°C, which was the lowest difference among the systems substituted with elements with cation valence of +2.

Table 16. Lattice parameters and axial & linear CTE data for the alkaline earth-modified systems

Sample Designation / Phase		JK-121 $MgZr_4(PO_4)_6$	JK-122 $CaZr_4(PO_4)_6$	JK-124 $BaZr_4(PO_4)_6$
Lattice parameters (Å at R.T.)	a-axis	8.90	8.78	8.59
	c-axis	21.84	22.69	23.89
Axial CTE($\times 10^{-7}/^{\circ}C$) (R.T.-1400°C)	α_a	-22	-38	-67
	α_c	58	79	279
	$\alpha_c - \alpha_a$	80	117	346
Calculated α_l($\times 10^{-7}/^{\circ}C$)		5	1	45
Measured α_l($\times 10^{-7}/^{\circ}C$)		16	-18	15

Table 17. Lattice parameters and axial & linear CTE data for the transition metal(with +2) substituted systems

Sample Designation / Phase			JK-125 $MnZr_4(PO_4)_6$	JK-126 $NiZr_4(PO_4)_6$
Lattice parameters (Å at R.T.)		a-axis	8.88	8.42
		c-axis	21.81	23.15
Axial CTE ($x10^{-7}/^{\circ}C$)	R.T.-1000°C	α_a	-51	-70
		α_c	112	172
		$\alpha_c-\alpha_a$	163	242
	R.T.-1400°C	α_a	-96	-89
		α_c	250	188
		$\alpha_c-\alpha_a$	346	277
Calculated α_l ($x10^{-7}/^{\circ}C$)	R.T.-1000°C		3	10
	R.T.-1400°C		19	3
Measured α_l ($x10^{-7}/^{\circ}C$) (R.T.-1000°C)			7	10

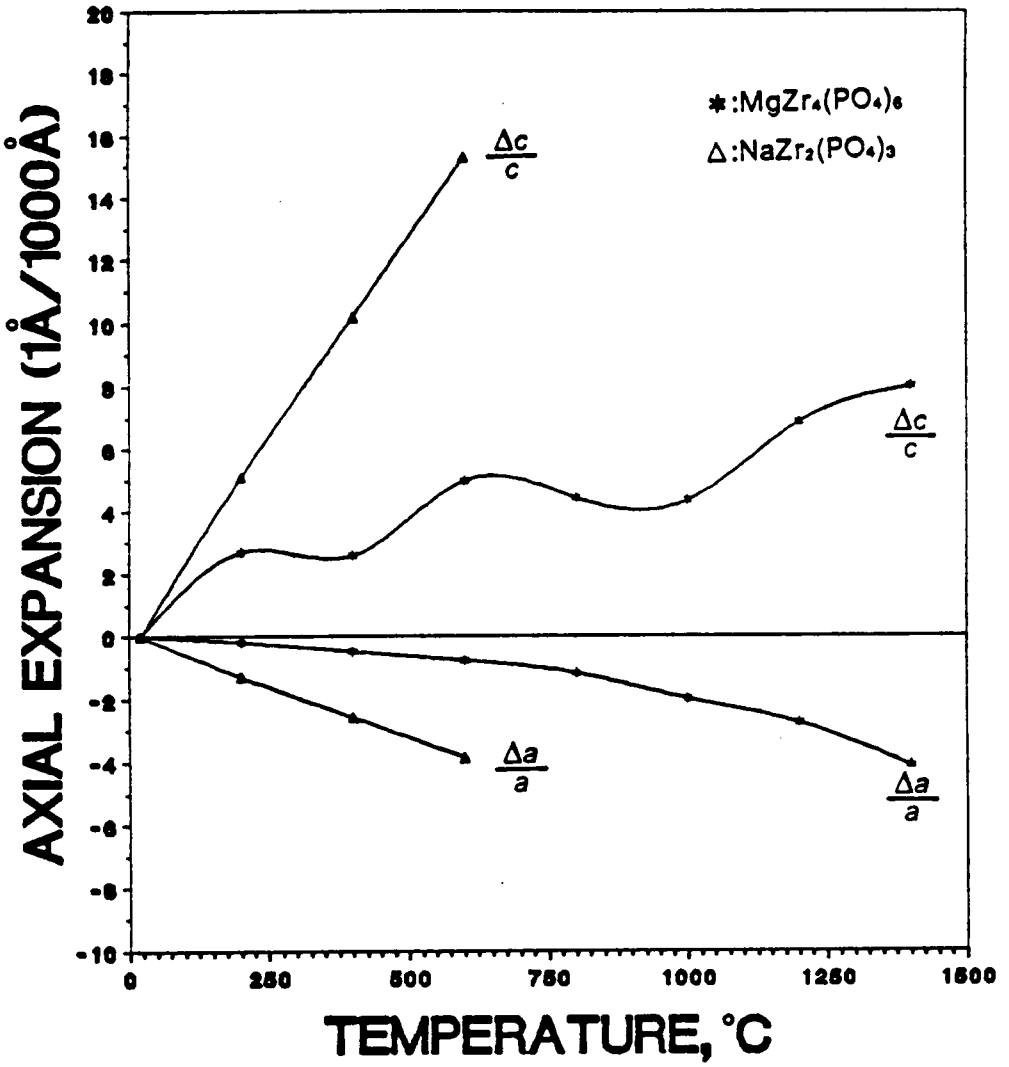

Figure 12. Axial thermal expansion behavior of $MgZr_4(PO_4)_6$ system

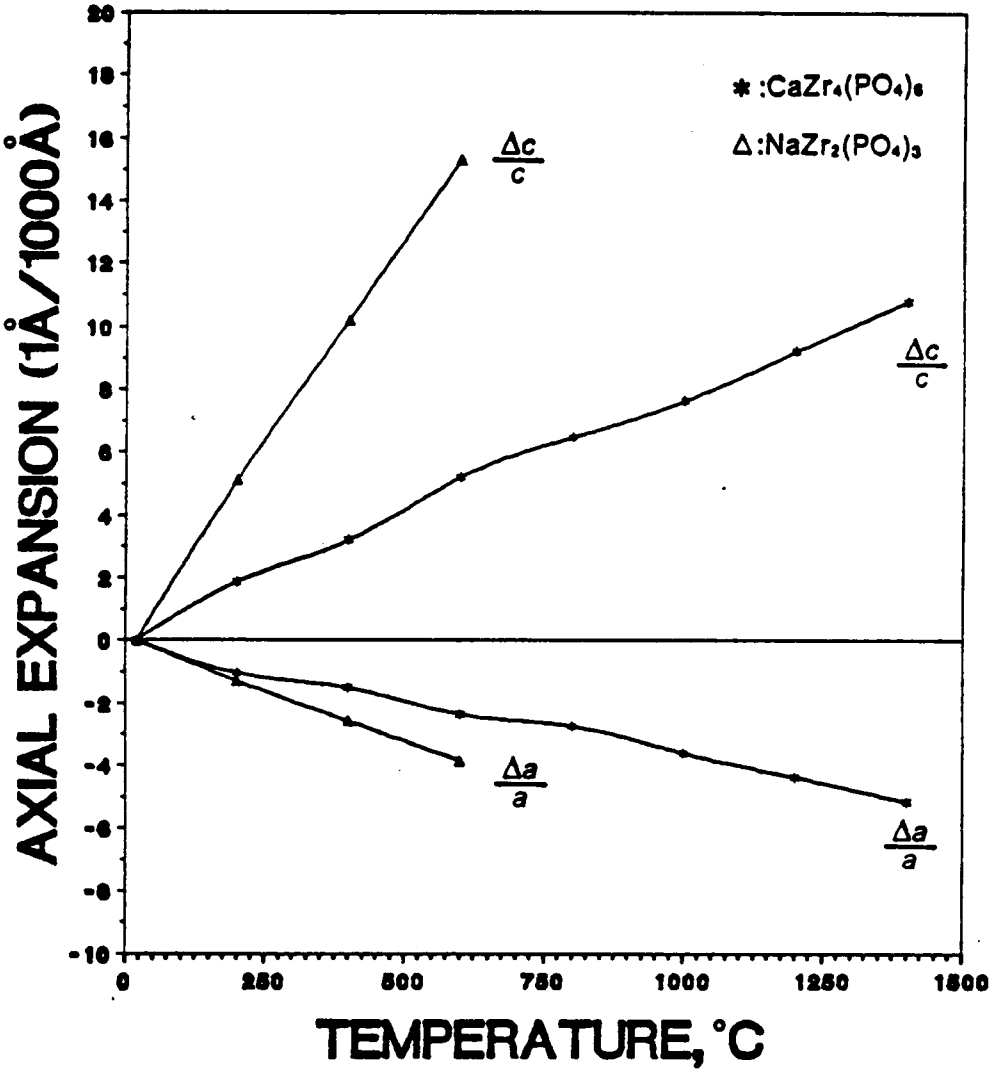

Figure 13. Axial thermal expansion behavior of $CaZr_4(PO_4)_6$ system

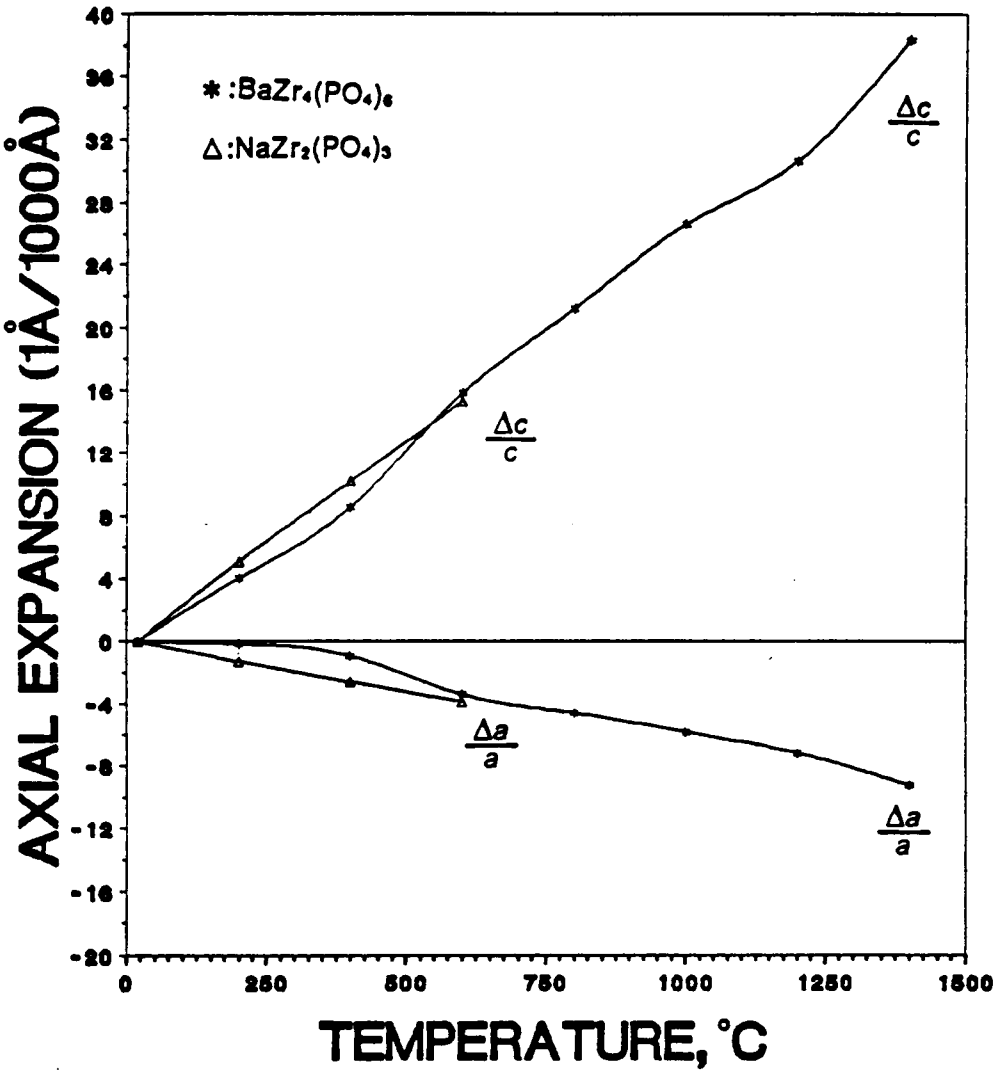

Figure 14. Axial thermal expansion behavior of $BaZr_4(PO_4)_6$ system

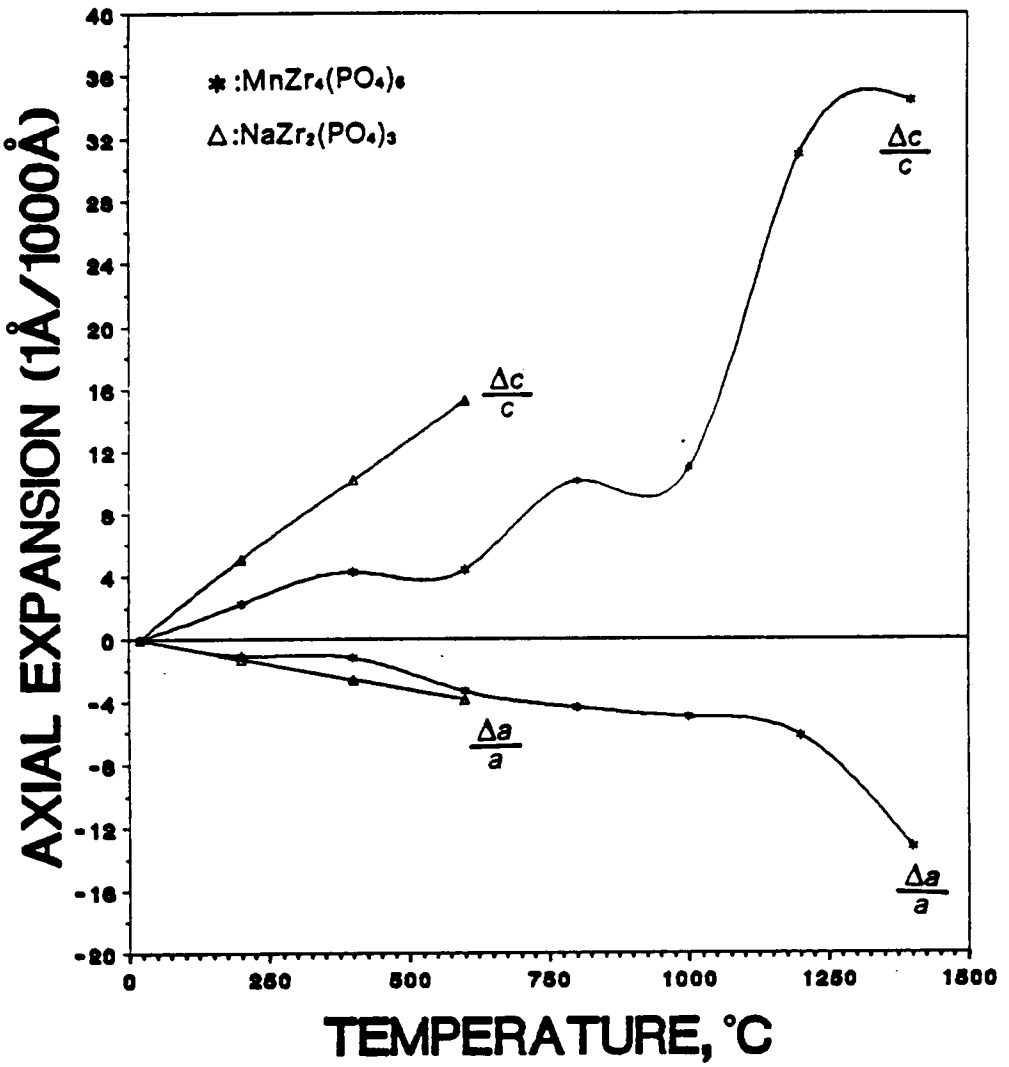

Figure 15. Axial thermal expansion behavior of $MnZr_4(PO_4)_6$ system

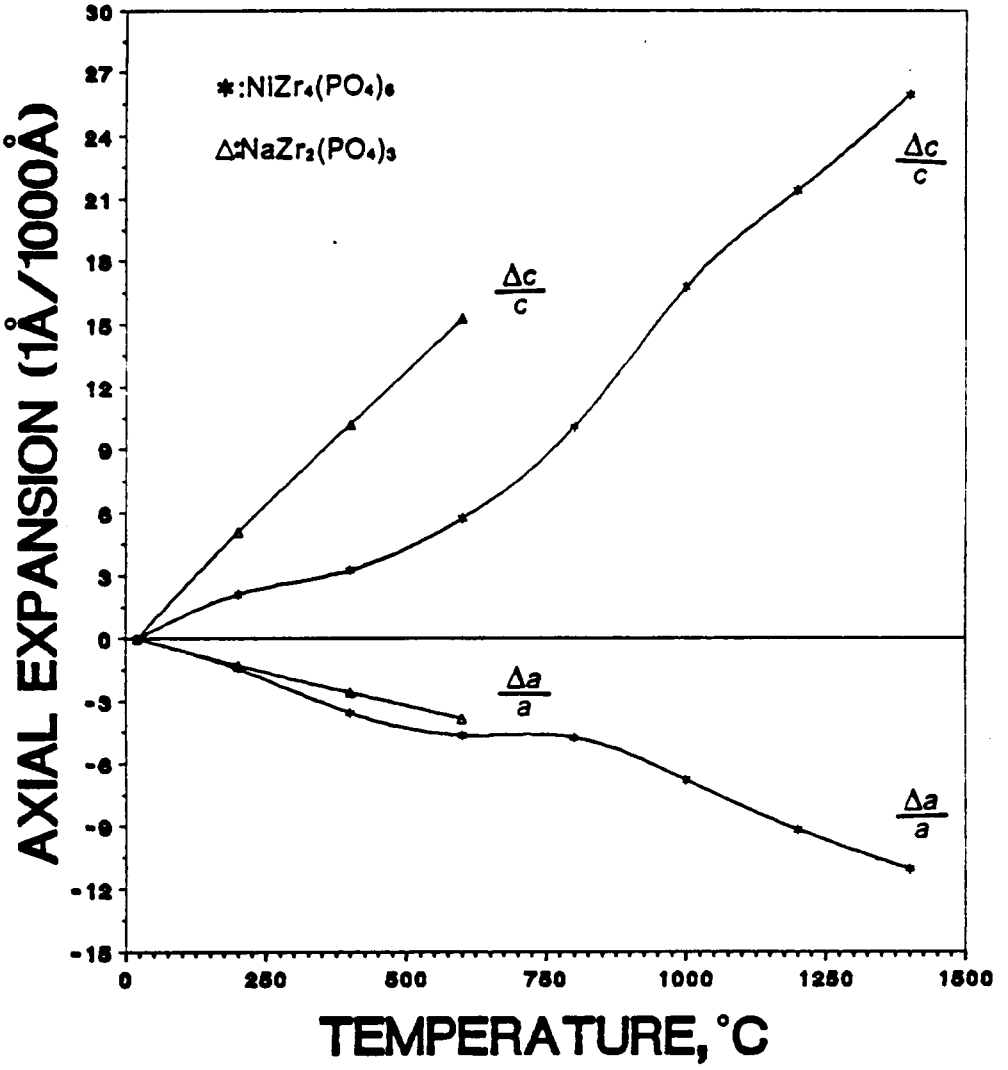

Figure 16. Axial thermal expansion behavior of $NiZr_4(PO_4)_6$ system

The compound substituted with Ca showed axial expansion behavior similar to that for the system modified with Mg, but exhibited a larger anisotropic characteristic (-38×10^{-7}/°C & 79×10^{-7}/°C for the a & c axes, respectively), 117×10^{-7}/°C. Also, a bigger difference(19×10^{-7}/°C) between the measured linear α and calculated linear α was obtained compared to the value for $MgZr_4(PO_4)_6$(11×10^{-7}/°C).

$BaZr_4(PO_4)_6$ had the largest anisotropic characteristic among the alkaline earth modified systems. The axial α values are -67×10^{-7}/°C and 279×10^{-7}/°C for the a- and c-axes, respectively. Furthermore, its difference(30×10^{-7}/°C) between calculated linear α and measured linear α is large.

Two compounds, $MnZr_4(PO_4)_6$ and $NiZr_4(PO_4)_6$, substituted with transition elements having a +2 cation valence, showed large anisotropic axial expansion differences, 346×10^{-7}/°C and 277×10^{-7}/°C, up to 1400°C. Their respective differences between measured and calculated α are 12×10^{-7}/°C and 7×10^{-7}/°C. These values are small compared to the system, $BaZr_4(PO_4)_6$, which showed similar anisotropic behavior. Up to 1000°C, the measured linear α values for $MnZr_4(PO_4)_6$ and $NiZr_4(PO_4)_6$ agree well with the calculated linear α values, differing by 4×10^{-7}/°C for $MnZr_4(PO_4)_6$, and zero for $NiZr_4(PO_4)_6$.

4.1.2.3 $L^{+3}{}_2O_3/L^{+4}O_2$-ZrO_2-P_2O_5(L^{+3} = Y; L^{+4} = Ti, Ce)

Three compounds among the systems substituted with cation valence of +3 or +4, having α values less than 20×10^{-7}/°C, were selected to measure the axial thermal expansion up to 1400°C. These compounds include $YZr_6(PO_4)_9$, $TiZr_8(PO_4)_{12}$, and $CeZr_8(PO_4)_{12}$. Room temperature lattice parameters and axial/linear α data are listed in Table 18, and detailed axial expansion behavior is shown in Figures 17 through 19.

Table 18. Lattice parameters and axial & linear CTE data for the transition metal(with +3 &+4) substituted systems

Sample Designation / Phase			JK-131 $YZr_6(PO_4)_9$	JK-141 $TiZr_8(PO_4)_{12}$	JK-145 $CeZr_8(PO_4)_{12}$
Lattice parameters (Å at R.T.)		a-axis	8.29	8.25	8.31
		c-axis	24.75	24.69	24.75
Axial CTE ($x10^{-7}/^{o}C$)	R.T.-1000°C	α_a	-27	-30	-35
		α_c	62	34	57
		$\alpha_c-\alpha_a$	89	64	92
	R.T.-1400°C	α_a	-31	-30	-29
		α_c	46	44	39
		$\alpha_c-\alpha_a$	77	74	68
Calculated α_1 ($x10^{-7}/^{o}C$)	R.T.-1000°C		3	-9	-4
	R.T.-1400°C		-5	-5	-6
Measured α_1 ($x10^{-7}/^{o}C$) (R.T.-1000°C)			14	20	11

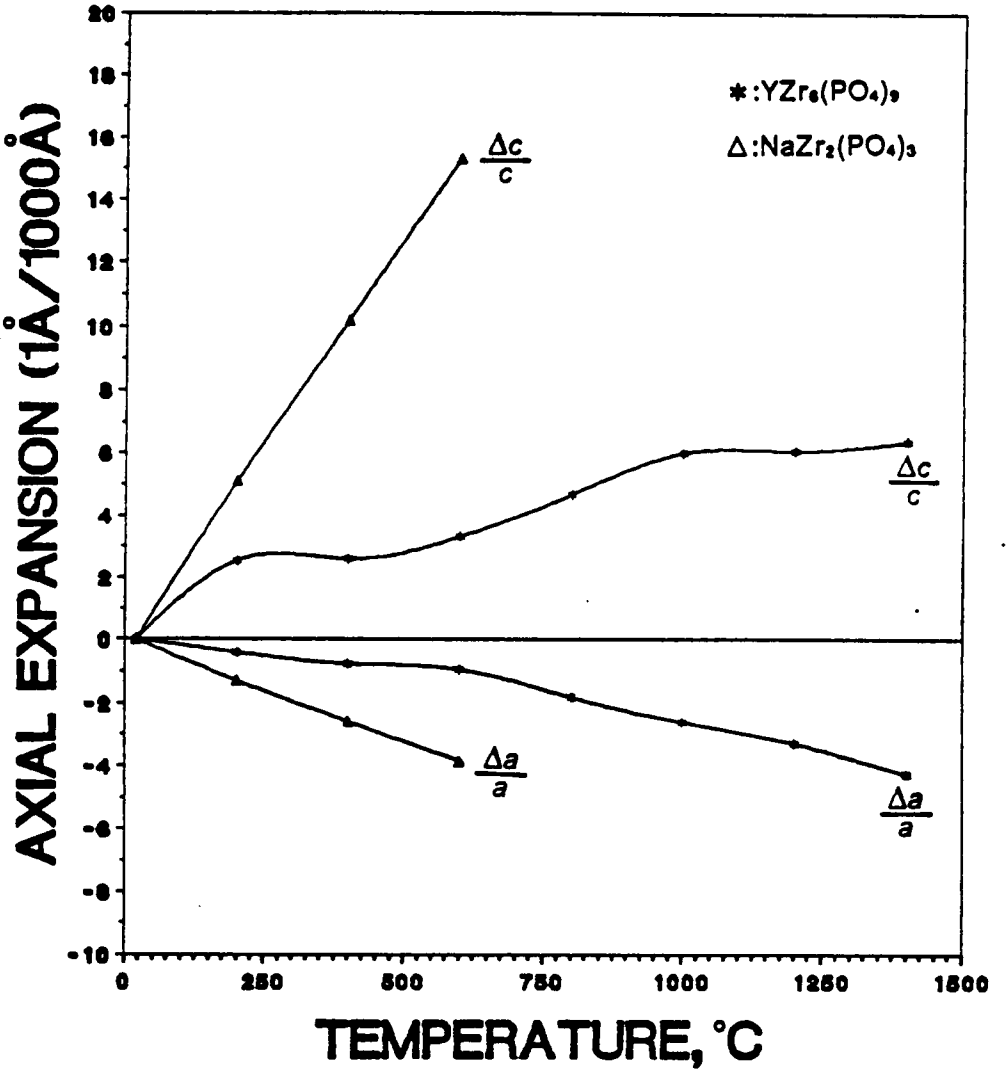

Figure 17. Axial thermal expansion behavior of $YZr_6(PO_4)_9$ system

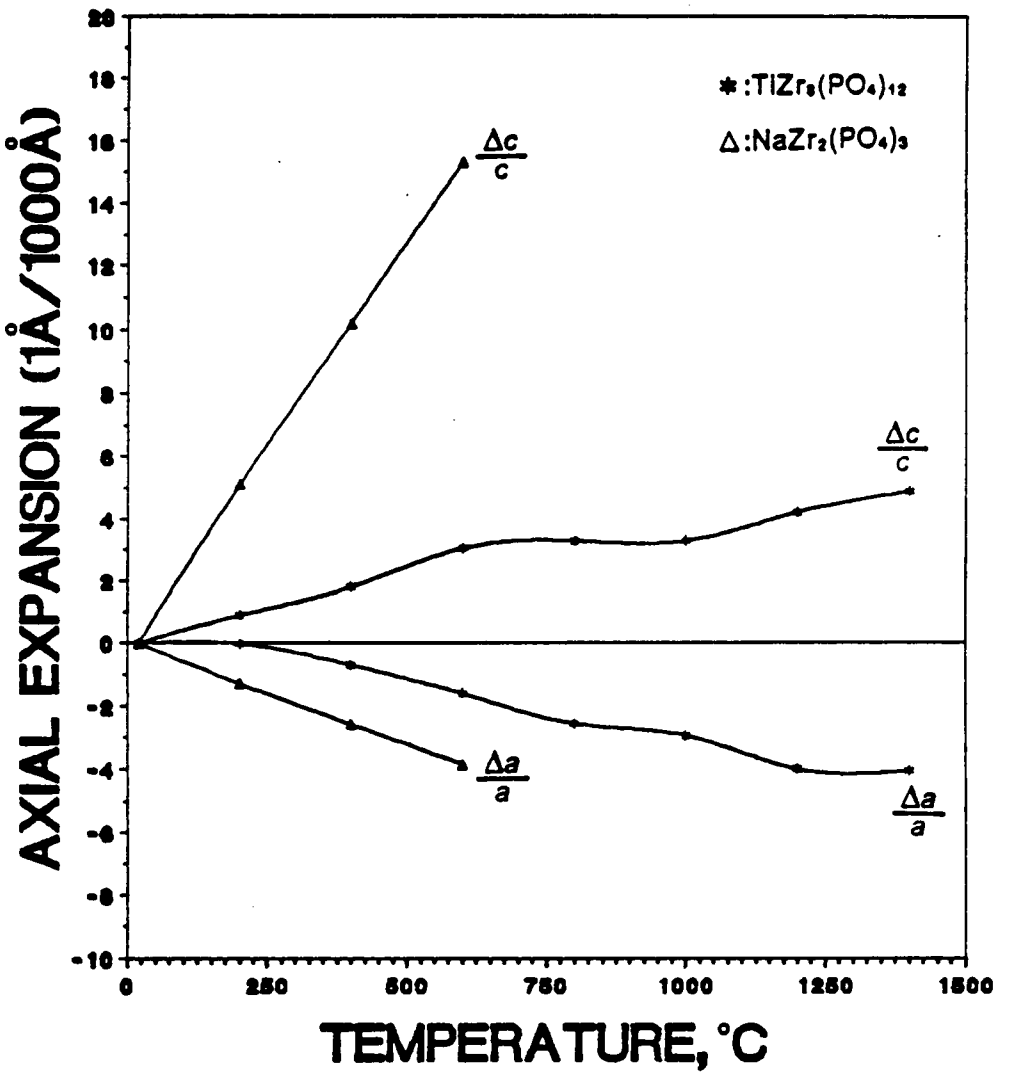

Figure 18. Axial thermal expansion behavior of $TiZr_8(PO_4)_{12}$ system

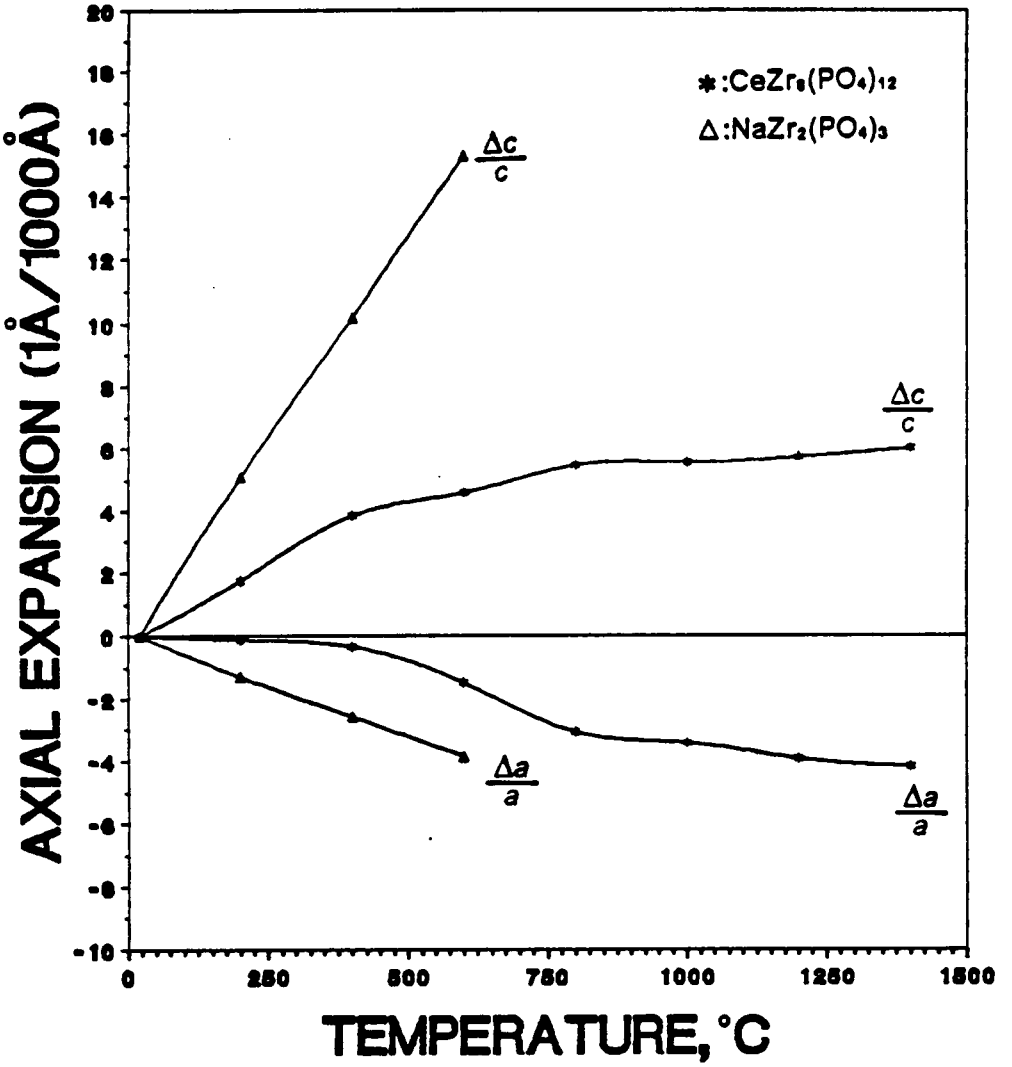

Figure 19. Axial thermal expansion behavior of $CeZr_8(PO_4)_{12}$ system

Average axial α values ranged from -29 to $-31x10^{-7}$/°C for the a-axis, and 39 to $46x10^{-7}$/°C for the c-axis. Their calculated mean linear α values ranged from -6 to $-5x10^{-7}$/°C up to 1400°C. Up to 1000°C, the average axial α values ranged from -9 to $3x10^{-7}$/°C.

Axial expansion behavior of these compounds substituted with Y, Ti, Ce in the NZP structure, are characterized by nonlinear axial expansion compared with other systems studied. For the $YZr_6(PO_4)_9$ system, the change of axial α values for each interval of every 200°C ranged from $-49x10^{-7}$/°C (1200°-1400°C) to $-9x10^{-7}$/°C (400°-600°C) for the a-axis, and from $3x10^{-7}$/°C(200-400°C & 1200-1400°C) to $145x10^{-7}$/°C(R.T.-200°C) for the c-axis. The change in the average calculated linear expansions showed a gradual decrease from $33x10^{-7}$/°C(R.T.-200°C) to $-28x10^{-7}$/°C(1200-1400°C).

Axial expansion behavior for the compounds $TiZr_8(PO_4)_{12}$ and $CeZr_8(PO_4)_{12}$ was similar in that the calculated linear α values of those two systems decreased up to 800°C, but above 800°C their calculated α values increased up to 1400°C. Detailed changes of calculated linear α values for the $TiZr_8(PO_4)_{12}$ and $CeZr_8(PO_4)_{12}$ are tabulated in Table 19 along with the calculated linear α of $YZr_6(PO_4)_9$.

4.1.2.4 $L^{+5}{}_2O_5$-ZrO_2-P_2O_5(L^{+5}=Nb, Ta)

Axial thermal expansion data including lattice parameters and measured linear α values for the systems modified with Nb and Ta with +5 cation valence are summarized in Table 20 and detailed axial thermal expansion behavior is shown in Figures 20 and 21.

The axial α values for the compounds $NbZr(PO_4)_3$ and $TaZr(PO_4)_3$ are characterized by transition in axial α values at 600°C. The a-lattice parameter increases up to

Table 19. The change of calculated linear CTE values at different temperature intervals

Temperature interval(°C)	$YZr_6(PO_4)_9$	$TiZr_8(PO_4)_{12}$	$CeZr_8(PO_4)_{12}$
R.T.-200	33	16	29
200-400	-11	-1	28
400-600	6	-21	-25
600-800	-6	-23	-39
800-1000	-5	-13	-11
1000-1200	-29	-12	-11
1200-1400	-28	10	-4

Table 20. Lattice parameters and axial & linear CTE data for the substituted systems with +5

Sample Designation Phase			JK-152 $NbZr(PO_4)_3$	JK-153 $TaZr(PO_4)_3$
Lattice parameters (Å at R.T.)		a-axis	8.25	8.39
		c-axis	23.92	23.85
Axial CTE ($x10^{-7}/^{\circ}C$)	R.T.-600°C	α_a	24	38
		α_c	-61	-36
		$\alpha_a-\alpha_c$	85	74
	600-1400°C	α_a	-25	-35
		α_c	79	78
		$\alpha_c-\alpha_a$	104	115
Calculated α_l ($x10^{-7}/^{\circ}C$)		R.T.-600°C	-4	13
		600-1400°C	10	1
Measured α_l ($x10^{-7}/^{\circ}C$) (R.T.-1000°C)			4	11

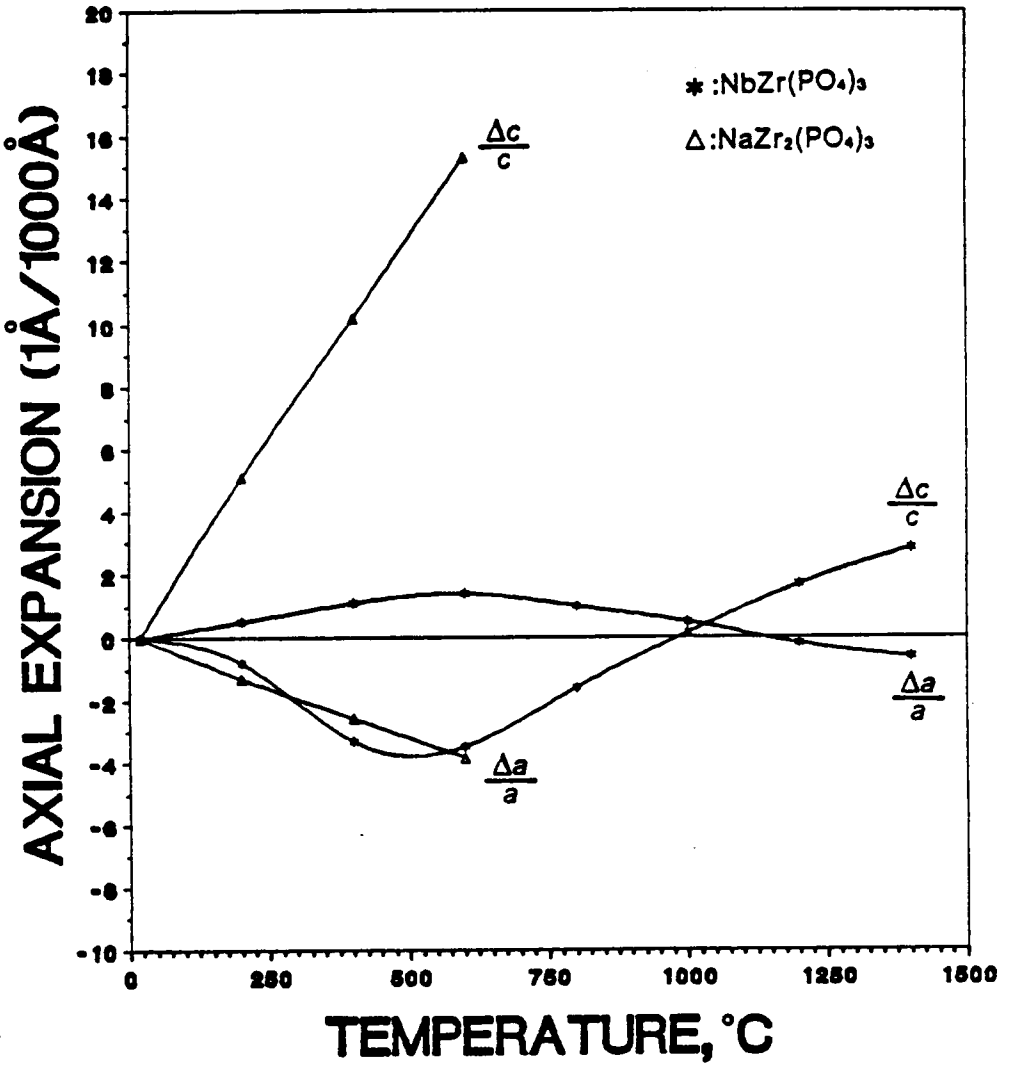

Figure 20. Axial thermal expansion behavior of $NbZr(PO_4)_3$ system

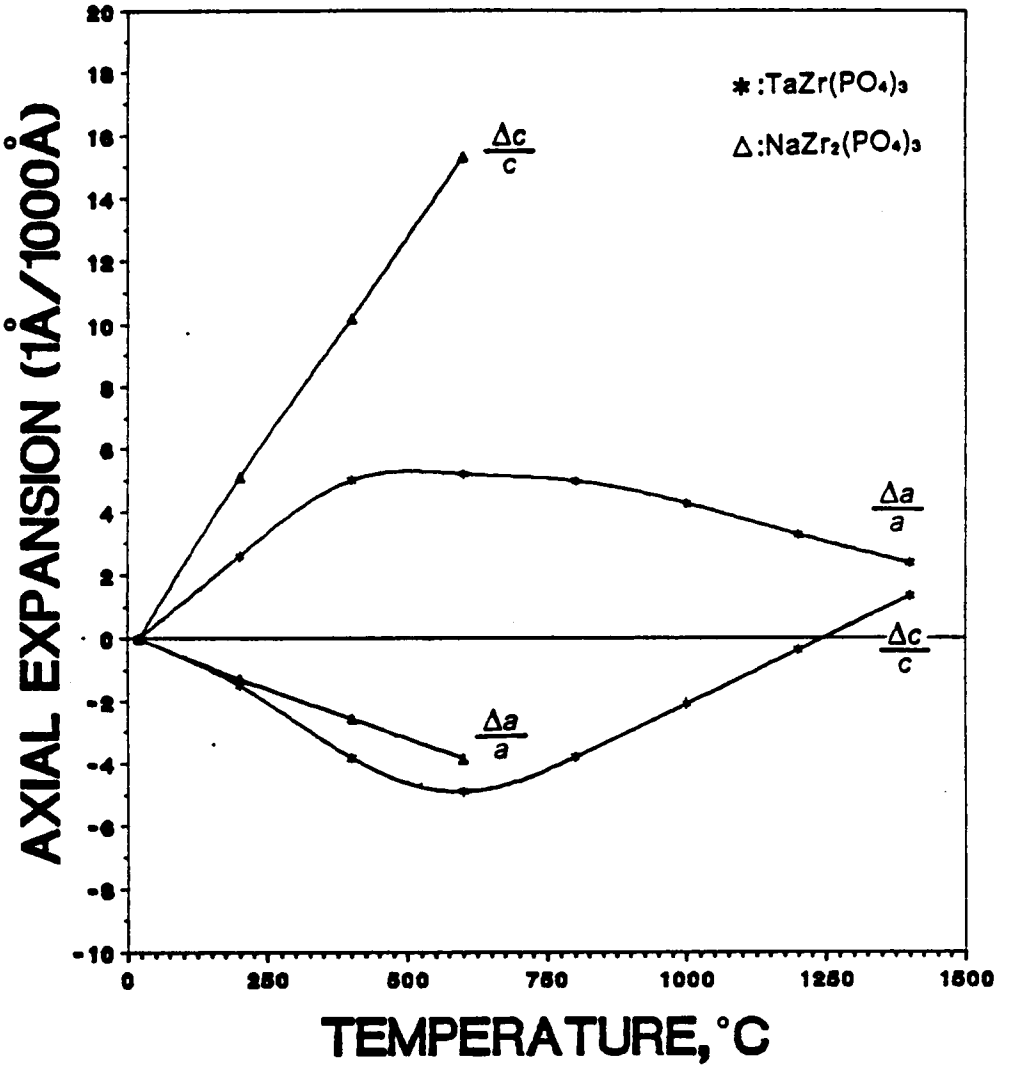

Figure 21. Axial thermal expansion behavior of $TaZr(PO_4)_3$ system

600°C, but above 600°C, the a-axis decreases. Conversely, the c-axis decreases up to 600°C, but increases at temperatures above 600°C. The average calculated linear expansion value is $-4x10^{-7}$/°C up to 600°C and $10x10^{-7}$/°C from 600°C to 1400°C for $NbZr(PO_4)_3$. The average linear expansion value for $TaZr(PO_4)_3$ decreases above 600°C from $13x10^{-7}$/°C below 600°C to $1x10^{-7}$/°C above 600°C.

A previous study[22] which measured axial α values of NZP-type structures reported similar results for the compound $NbZr(PO_4)_3$. According to their results, the c-axis expands from R.T. to 200°C and then contracts up to 600°C. The a-axis showed a decrease up to 600°C, followed by a slight increase above 600°C. This axial expansion transition behavior observed in compounds substituted with +5 valence cations will be covered in the Discussion section.

4.2 Quarternary system

The experimental linear and axial thermal expansion measurements for the ternary NZP systems modified with cations with valences ranging from +1 to +5 were presented in section 4.1. In this section, the experimental results of quarternary compounds modified with combinations of alkali-alkali, alkali-alkaline earth, and alkaline earth-alkaline earth elements will be presented. First, sections 4.2.1.1 through 4.2.1.3 deal with the solid-solubility of the quarternary compounds, followed by sections 4.2.2 and 4.2.3 which include the linear and axial thermal expansion results for the compounds which resulted in single phase formation.

Secondary material properties for the compounds $Rb_{0.5}Cs_{0.5}Zr_2(PO_4)_3$ and $Ca_{0.5}Mg_{0.5}Zr_4(PO_4)_6$ with linear α values of $-0.3x10^{-7}$/°C and $-5x10^{-7}$/°C respectively,

have been characterized and are shown in sections 4.2.4.1 through 4.2.4.5. They include structural attributes, thermal shock resistance, MOR test results, along with fractography, microstructure, DTA analysis, and long-term thermal stability. Statistical analysis of the compound $Ca_{0.5}Mg_{0.5}Zr_4(PO_4)_6$ has been done and is summarized in section 4.2.5.

4.2.1 Solid solubility

4.2.1.1 Y^+_2O-Y'^+_2O-ZrO_2-P_2O_5(Y^+,Y'^+=Na, K, Rb, Cs)

Solid solubility was investigated for systems substituted with several mole combinations of alkali elements replacing Na^+ in the NZP structure. The structural formula for these compounds can be written as $Y'_xY''_{1-x}Zr_2(PO_4)_3$, where x=0.25, 0.5, 0.75 and Y', Y''=Na, K, Rb, Cs, but $Y'\neq Y''$. Phases identified by XRD are tabulated in Table 21.

XRD patterns for systems substituted with Rb^+(1.49Å)-Cs^+(1.69Å) and Na^+(0.98Å)-K^+(1.33Å), showed a single phase independent of the different combinations of moles of cations selected. The difference in ionic radius of elements showing solubility was 9.7%(for Rb^+-Cs^+) and 26.3%(for Na^+-K^+).

In systems substituted with Rb^+-K^+, the combination of ½Rb^+-½K^+ showed solubility in spite of the ionic size difference of 10.7%, whereas the combinations of ¾Rb^+-¼K^+ and ¼Rb^+-¾K^+ did not show solid solubility. Other combinations, Rb^+-Na^+, Cs^+-Na^+, and Cs^+-K^+ never reached solid solubility, probably because the ionic size differences for these combinations are 34.2%, 42.0%, and 21.3%, respectively.

Table 21. Phase analysis of the substituted by several mole combinations of alkali elements

Sample No	Composition(Moles)	Phases
JK-RN1	$Rb_{0.25}Na_{0.25}Zr_2(PO_4)_3$	$RbZr_2(PO_4)_3 + NaZr_2(PO_4)_3$
JK-RN2	$Rb_{0.5}Na_{0.5}Zr_2(PO_4)_3$	$RbZr_2(PO_4)_3 + NaZr_2(PO_4)_3$
JK-RN3	$Rb_{0.75}Na_{0.25}Zr_2(PO_4)_3$	$RbZr_2(PO_4)_3 + NaZr_2(PO_4)_3$
JK-RK1	$Rb_{0.25}K_{0.75}Zr_2(PO_4)_3$	$RbZr_2(PO_4)_3 + KZr_2(PO_4)_3$
JK-RK2	$Rb_{0.5}K_{0.5}Zr_2(PO_4)_3$	$(Rb_{0.5}K_{0.5})Zr_2(PO_4)_3$
JK-RK3	$Rb_{0.75}K_{0.25}Zr_2(PO_4)_3$	$RbZr_2(PO_4)_3 + KZr_2(PO_4)_3$
JK-RC1	$Rb_{0.25}Cs_{0.75}Zr_2(PO_4)_3$	$(Rb_{0.25}Cs_{0.75})Zr_2(PO_4)_3$
JK-RC2	$Rb_{0.5}Cs_{0.5}Zr_2(PO_4)_3$	$(Rb_{0.5}Cs_{0.5})Zr_2(PO_4)_3$
JK-RC3	$Rb_{0.75}Cs_{0.25}Zr_2(PO_4)_3$	$(Rb_{0.75}Cs_{0.25})Zr_2(PO_4)_3$
JK-CN1	$Cs_{0.25}Na_{0.75}Zr_2(PO_4)_3$	$CsZr_2(PO_4)_3 + NaZr_2(PO_4)_3$
JK-CN2	$Cs_{0.5}Na_{0.5}Zr_2(PO_4)_3$	$CsZr_2(PO_4)_3 + NaZr_2(PO_4)_3$
JK-CN3	$Cs_{0.75}Na_{0.25}Zr_2(PO_4)_3$	$CsZr_2(PO_4)_3 + NaZr_2(PO_4)_3$
JK-CK1	$Cs_{0.25}K_{0.75}Zr_2(PO_4)_3$	$CsZr_2(PO_4)_3 + KZr_2(PO_4)_3$
JK-CK2	$Cs_{0.5}K_{0.5}Zr_2(PO_4)_3$	$CsZr_2(PO_4)_3 + KZr_2(PO_4)_3$
JK-CK3	$Cs_{0.75}K_{0.25}Zr_2(PO_4)_3$	$CsZr_2(PO_4)_3 + KZr_2(PO_4)_3$
JK-NK1	$Na_{0.25}K_{0.75}Zr_2(PO_4)_3$	$(Na_{0.25}K_{0.75})Zr_2(PO_4)_3$
JK-NK2	$Na_{0.5}K_{0.5}Zr_2(PO_4)_3$	$(Na_{0.5}K_{0.5})Zr_2(PO_4)_3$
JK-NK3	$Na_{0.75}K_{0.25}Zr_2(PO_4)_3$	$(Na_{0.75}K_{0.25})Zr_2(PO_4)_3$

The tendency for solid-solution formation between alkali-alkali elements in the NZP-type structure is not readily predicted due to the complex structure. Two explanations might be possible to interpret this solid-solubility behavior. The first possible cause is due to the weight difference of the two elements selected. Another possibility is an order-disorder transition. Most of the systems which showed solid-solution had one or two extra diffraction peaks which were not from impurities or raw materials. The tendency to form a more ordered state with the substitution of two elements, for example Rb^{+}-K^{+}, for Na^{+} in the NZP structure is different for different compositions. A more detailed discussion will be presented later.

4.2.1.2 $Y^{+}{}_{2}O$-$Y^{+2}O$-ZrO_2-P_2O_5(Y^{+} = Na, K, Rb, Cs; Y^{+2} = Mg, Ca, Sr, Ba)

Compounds substituted by combining alkali and alkaline earth elements were synthesized, and their phases were identified. The phases identified for the compounds substituted with combinations 0.5:0.25 alkali to alkaline-earth are tabulated in Table 22. The general formula for these combinations can be written as $Y^{I}_{0.5}Y^{II}_{0.25}Zr_2(PO_4)_3$, where Y^{I} = Na,K,Rb,Cs; and Y^{II} = Mg,Ca,Sr,Ba, and superscripts 'I' and 'II' denote +1 and +2 cation valence, respectively. XRD studies for the compounds $Na_{0.75}Ca_{0.125}Zr_2(PO_4)_3$ and $Na_{0.25}Ca_{0.375}Zr_2(PO_4)_3$ were done and identified phases are presented in Table 23 along with the compound $Na_{0.5}Ca_{0.25}Zr_2(PO_4)_3$. Table 24 lists the ionic radius of the alkali and alkaline earth elements used in this study.

Among compounds substituted with 0.5:0.25 alkali to alkaline earth cations, only compounds combining large alkaline earth ions with small alkali ions showed complete solubility. These are Ca^{+2}(1.04Å)-Na^{+}(0.98Å), Ba^{+2}(1.38Å)-Na^{+}(0.98Å), Ba^{+2}(1.38Å)-K^{+}(1.33Å), and Sr^{+2}(1.20Å)-Na^{+}(0.98Å). In compounds JK-CNM4[(⅛Ca¾Na)$Zr_2(PO_4)_3$] and JK-CNMC[(⅜Ca¼Na)$Zr_2(PO_4)_3$] which used dif-

Table 22. Phase analysis of the systems substituted by one-half mole of alkali with one-quarter mole of alkaline earth element

Sample No	Composition(Moles)	Phases
JK-RMM	$Rb_{0.5}Mg_{0.25}Zr_2(PO_4)_3$	$RbZr_2(PO_4)_3 + MgZr_4(PO_4)_6$
JK-RCM	$Rb_{0.5}Ca_{0.25}Zr_2(PO_4)_3$	$RbZr_2(PO_4)_3 + CaZr_4(PO_4)_6$
JK-RSM	$Rb_{0.5}Sr_{0.25}Zr_2(PO_4)_3$	$RbZr_2(PO_4)_3 + SrZr_4(PO_4)_6$
JK-RBM	$Rb_{0.5}Ba_{0.25}Zr_2(PO_4)_3$	$RbZr_2(PO_4)_3 + BaZr_4(PO_4)_6$
JK-CMM	$Cs_{0.5}Mg_{0.25}Zr_2(PO_4)_3$	$CsZr_2(PO_4)_3 + MgZr_4(PO_4)_6$
JK-CCM	$Cs_{0.5}Ca_{0.25}Zr_2(PO_4)_3$	$CsZr_2(PO_4)_3 + CaZr_4(PO_4)_6$
JK-CSM	$Cs_{0.5}Sr_{0.25}Zr_2(PO_4)_3$	$CsZr_2(PO_4)_3 + SrZr_4(PO_4)_6$
JK-CBM	$Cs_{0.5}Ba_{0.25}Zr_2(PO_4)_3$	$CsZr_2(PO_4)_3 + BaZr_4(PO_4)_6$
JK-CNM	$Ca_{0.25}Na_{0.5}Zr_2(PO_4)_3$	$(Ca_{0.25}Na_{0.5})Zr_2(PO_4)_3$
JK-CKM	$Ca_{0.25}K_{0.5}Zr_2(PO_4)_3$	$CaZr_4(PO_4)_6 + KZr_2(PO_4)_3$
JK-MNM	$Mg_{0.25}Na_{0.5}Zr_2(PO_4)_3$	$MgZr_4(PO_4)_6 + NaZr_2(PO_4)_3$
JK-MKM	$Mg_{0.25}K_{0.5}Zr_2(PO_4)_3$	$MgZr_4(PO_4)_6 + KZr_2(PO_4)_3$
JK-BNM	$Ba_{0.25}Na_{0.5}Zr_2(PO_4)_3$	$(Ba_{0.25}Na_{0.5})Zr_2(PO_4)_3$
JK-BKM	$Ba_{0.25}K_{0.5}Zr_2(PO_4)_3$	$(Ba_{0.25}K_{0.5})Zr_2(PO_4)_3$
JK-SNM	$Sr_{0.25}Na_{0.5}Zr_2(PO_4)_3$	$(Sr_{0.25}Na_{0.5})Zr_2(PO_4)_3$
JK-SKM	$Sr_{0.25}K_{0.5}Zr_2(PO_4)_3$	$SrZr_4(PO_4)_6 + KZr_2(PO_4)_3$

Table 23. Phase present for the system of $CaO\text{-}Na_2O\text{-}ZrO_2\text{-}P_2O_5$

Sample No	Composition(Moles)	Phase
JK-CNM4	$(1/8Ca3/4Na)Zr_2(PO_4)_3$	$(1/8Ca3/4Na)Zr_2(PO_4)_3$
JK-CNM	$(1/4Ca1/2Na)Zr_2(PO_4)_3$	$(1/4Ca1/2Na)Zr_2(PO_4)_3$
JK-CNMC	$(3/8Ca1/4Na)Zr_2(PO_4)_3$	$(3/8Ca1/4Na)Zr_2(PO_4)_3$

Table 24. Ionic radii of the alkali and alkaline earth elements (taken from Ref.116)

Element	Na	K	Rb	Cs	Mg	Ca	Sr	Ba
Ionic Radius(Å)	0.98	1.33	1.49	1.69	0.74	1.04	1.20	1.38

ferent combinations of alkali-alkaline earth elements, complete solubility was also verified by XRD analysis.

The substitution of alkaline earth elements into the NZP skeletal framework creates 50% vacancies in the Na positions compared with substitution of alkali elements only. Combinations of large alkaline earth ions with small alkali ions are more desirable than the opposite combination. Previous reports[4,62] for the compounds $Ca_{0.25}Na_{0.5}Zr_2(PO_4)_3$ and compound $Cs_{0.5}Sr_{0.25}Zr_2(PO_4)_3$, which show these two compounds have single phase, are well supported by this study.

4.2.1.3 $Y^{+2}O$-$Y'^{+2}O$-ZrO_2-P_2O_5(Y^{+2},Y'^{+2} = Mg, Ca, Sr, Ba)

Compounds substituted with 0.25:0.25 alkaline earth cations only were investigated for possible solid solubility. The structural formula for these substitutions can be expressed as $Y^{II}_{0.25}Y'^{II}_{0.25}Zr_2(PO_4)_3$ or $Y^{II}_{0.5}Y'^{II}_{0.5}Zr_4(PO_4)_6$, where Y^{II}, Y'^{II} = Mg,Ca,Sr,Ba and $Y^{II} \neq Y'^{II}$. Solid solubility resulted irrespective of ionic size differences of the two elements. The tendency for complete solid-solution by modification with alkaline earth-alkaline earth element combinations is possibly related to the resulting vacancy formation by substitution of elements with cation valence of +2. This tendency appears related to the ease of replacing half of the Na positions in the NZP structure with alkaline earth elements. Phase analysis for these substitutions is shown in Table 25. A previous study[59] reported that compound $Ca_{0.5}Sr_{0.5}Zr_4(PO_4)_6$ which corresponds to sample JK-CSC, is a single phase.

Additional elemental combinations have been synthesized for the CaO-MgO-ZrO_2-P_2O_5 system[$(\frac{1}{8}Ca\frac{3}{8}Mg)Zr_2(PO_4)_3$ and $(\frac{3}{8}Ca\frac{1}{8}Mg)Zr_2(PO_4)_3$]. The resulting phases identified are presented in Table 26 along with the sample JK-MCC[$Mg_{0.25}Ca_{0.25}Zr_2(PO_4)_3$]. XRD analysis indicated that the compound

Table 25. Phase analysis of the systems substituted by combinations of two one-quarter mole of alkaline earth elements

Sample No	Composition(Moles)	Phase
JK-MCC	$Mg_{0.25}Ca_{0.25}Zr_2(PO_4)_3$	$(Mg_{0.25}Ca_{0.25})Zr_2(PO_4)_3$
JK-MSC	$Mg_{0.25}Sr_{0.25}Zr_2(PO_4)_3$	$(Mg_{0.25}Sr_{0.25})Zr_2(PO_4)_3$
JK-MBC	$Mg_{0.25}Ba_{0.25}Zr_2(PO_4)_3$	$(Mg_{0.25}Ba_{0.25})Zr_2(PO_4)_3$
JK-CSC	$Ca_{0.25}Sr_{0.25}Zr_2(PO_4)_3$	$(Ca_{0.25}Sr_{0.25})Zr_2(PO_4)_3$
JK-CBC	$Ca_{0.25}Ba_{0.25}Zr_2(PO_4)_3$	$(Ca_{0.25}Ba_{0.25})Zr_2(PO_4)_3$
JK-BSC	$Ba_{0.25}Sr_{0.25}Zr_2(PO_4)_3$	$(Ba_{0.25}Sr_{0.25})Zr_2(PO_4)_3$

Table 26. Phase present for the system of $CaO-MgO-ZrO_2-P_2O_5$

Sample No	Composition(Moles)	Phases
JK-CMC4	$(1/8Ca3/8Mg)Zr_2(PO_4)_3$	$CaZr_4(PO_4)_6 + MgZr_4(PO_4)_6$
JK-MCC	$(1/4Ca1/4Mg)Zr_2(PO_4)_3$	$(1/4Ca1/4Mg)Zr_2(PO_4)_3$
JK-CMCC	$(3/8Ca1/8Mg)Zr_2(PO_4)_3$	$(3/8Ca1/8Mg)Zr_2(PO_4)_3$

($\frac{1}{8}$Ca$\frac{3}{8}$Mg)$Zr_2(PO_4)_3$, in which the mole percent of Mg is higher than the Ca, contained two NZP phases, $CaZr_4(PO_4)_6$ and $MgZr_4(PO_4)_6$. On the other hand, the compound ($\frac{3}{8}$Ca$\frac{1}{8}$Mg)$Zr_2(PO_4)_3$, in which the mole percent of Ca is higher than the Mg, showed complete solubility.

Considering the solid solubility behavior of the $Y^{III}_{0.25}Y'^{III}_{0.25}Zr_2(PO_4)_3$ system irrespective of ionic size differences, complete solubility was expected for both ($\frac{1}{8}$Ca$\frac{3}{8}$Mg)$Zr_2(PO_4)_3$ and ($\frac{3}{8}$Ca$\frac{1}{8}$Mg)$Zr_2(PO_4)_3$. However, the compound ($\frac{1}{8}$Ca$\frac{3}{8}$Mg)$Zr_2(PO_4)_3$ did not show the expected solubility. The reason might be related with unit cell equilibrium which will be presented in the Discussion section.

4.2.2 Linear thermal expansion

4.2.2.1 Rb_2O-$Q^{+1}{}_2O$-ZrO_2-P_2O_5(Q^{+1}=K, Cs)

Among the systems which were substituted with mixed combinations of alkali elements in the NZP structure, four compounds JK-RC1[$Rb_{0.25}Cs_{0.75}Zr_2(PO_4)_3$], JK-RC2 [$Rb_{0.5}Cs_{0.5}Zr_2(PO_4)_3$], JK-RC3[$Rb_{0.75}Cs_{0.25}Zr_2(PO_4)_3$], and JK-RK2[$Rb_{0.5}K_{0.5}Zr_2(PO_4)_3$], were selected for linear α measurements. Table 27 lists the linear α results for these compounds and Figure 22 shows the linear thermal expansion behavior up to 1000°C.

Samples JK-RC1 through RC3, substituted with Rb^+-Cs^+, showed very low linear thermal expansion. The linear thermal expansion values for $RbZr_2(PO_4)_3$ and $CsZr_2(PO_4)_3$ were $2x10^{-7}$/°C and $5x10^{-7}$/°C, respectively. The solid-solution of these two phases likely led to the decreased thermal expansion, which was suggested by other studies in which thermal expansion value was reduced by solid solution formation[120-121]. The linear α values for these compounds ranged from $-2x10^{-7}$/°C

Table 27. Linear thermal expansion results for (Rb-Cs) & (Rb-K) modified systems

Sample No	Phase	Stoichiometric Compound with Integer Value	Linear CTE α_1 ($\times 10^{-7}/^{\circ}C$)	Linear CTE Temp.Range ($^{\circ}C$)
JK-RC1	$Rb_{0.25}Cs_{0.75}Zr_2(PO_4)_3$	$RbCs_3Zr_8(PO_4)_{12}$	2	R.T.-1000
JK-RC2	$Rb_{0.5}Cs_{0.5}Zr_2(PO_4)_3$	$RbCsZr_4(PO_4)_6$	-0.3	R.T.-1000
JK-RC3	$Rb_{0.75}Cs_{0.25}Zr_2(PO_4)_3$	$Rb_3CsZr_8(PO_4)_{12}$	-2	R.T.-1000
JK-RK2	$Rb_{0.5}K_{0.5}Zr_2(PO_4)_3$	$RbKZr_4(PO_4)_6$	-15	R.T.-1000

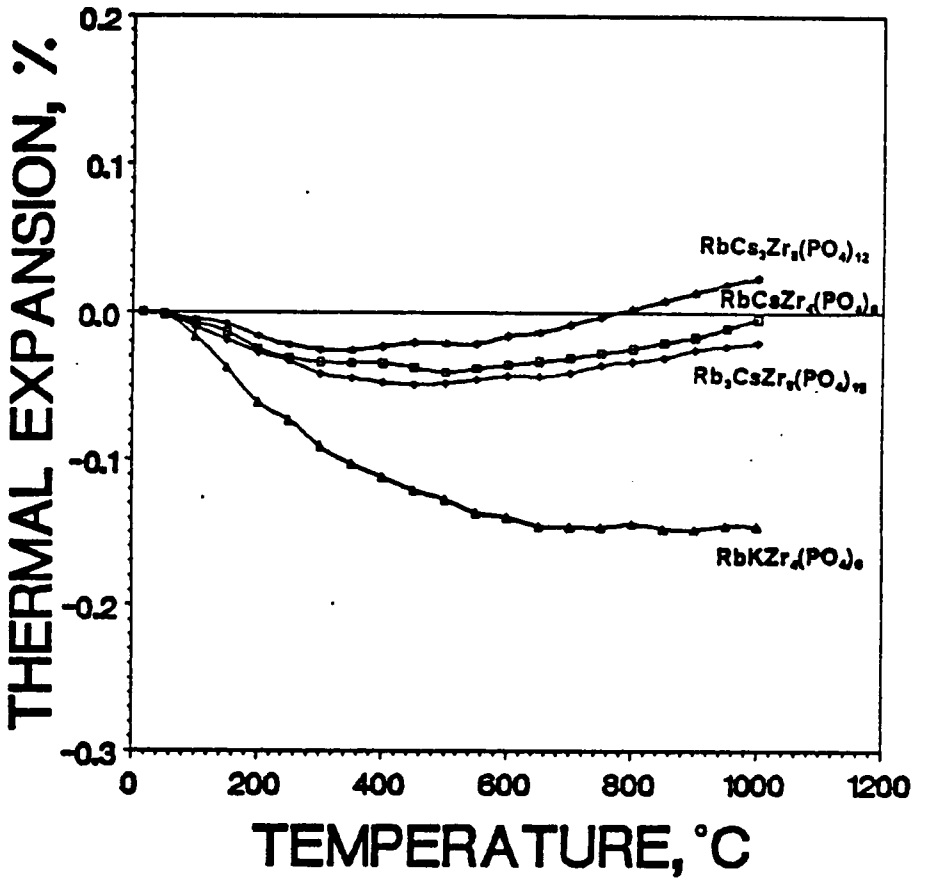

Figure 22. Linear thermal expansion behavior of (Rb-Cs) & (Rb-K) modified systems: $RbCs_2Zr_3(PO_4)_{12}$, $RbCsZr_4(PO_4)_6$, $Rb_3CsZr_6(PO_4)_{12}$, and $RbKZr_4(PO_4)_6$

to. $2x10^{-7}$/°C. The reduction of α values by the solid solution formation of $(Rb\text{-}Cs)Zr_2(PO_4)_3$ is related to the increase of Rb content which has a smaller ionic radius than Cs. The reason that Rb-rich $Rb_{0.75}Cs_{0.25}Zr_2(PO_4)_3$ has a smaller CTE than the Cs-rich $Rb_{0.25}Cs_{0.75}Zr_2(PO_4)_3$ is related to the increase in bond strength resulting from substitution by higher mole of smaller ions[122].

The thermal expansion of $Rb_{0.5}K_{0.5}Zr_2(PO_4)_3$ was $-15x10^{-7}$/°C. Considering the linear α values of $RbZr_2(PO_4)_3$ ($2x10^{-7}$/°C) and $KZr_2(PO_4)_3$ ($-22x10^{-7}$/°C), the change of α in the compound $Rb_{0.5}K_{0.5}Zr_2(PO_4)_3$ may be treated from the basic theory of thermal expansion behavior for composites[123-124] and also from the reduction of thermal expansion by solid solution formation.

4.2.2.2 $Q^{+}{}_2O$-$Q^{+2}O$-ZrO_2-P_2O_5 (Q^{+} = Na, K; Q^{+2} = Ca, Ba)

Linear thermal expansion results for the systems substituted with a Na:Ca ratio of 0.5:0.25, a K:Ba ratio of 0.5:0.25, and a Na:Ba ratio of 0.5:0.25 are listed in Table 28 and detailed expansion behavior is shown in Figure 23. The results for the systems modified by Ca:Na ratios of 0.125:0.75 and 0.375:0.25 are given in Table 29, and their linear expansion behavior is shown in Figure 24.

The compound $CaNa_2Zr_8(PO_4)_{12}$(JK-CNM) showed negative expansion behavior up to 600°C, but above 600°C expanded positively up to 900°C. The average expansion value from R.T. to 900°C was calculated as $1x10^{-7}$/°C. The systems showing single phase which were substituted with ¼ Ba-½ K($BaK_2Zr_8(PO_4)_{12}$) and ¼ Ba-½ Na($BaNa_2Zr_8(PO_4)_{12}$) had linear α values of $-7x10^{-7}$/°C up to 950°C and $-17x10^{-7}$/°C up to 900°C, respectively. Compounds substituted with ⅛ Ca-¾ Na($CaNa_6Zr_{16}(PO_4)_{24}$) and ⅜ Ca-¼ Na($Ca_3Na_2Zr_{16}(PO_4)_{24}$) had average thermal expansion values of $-51x10^{-7}$/°C and $-23x10^{-7}$/°C, respectively, up to 900°C.

Table 28. Linear thermal expansion results for (Ba-K), (Ca-Na), and (Ba-Na) modified systems

Sample No	Phase	Stoichiometric Compound with Integer Value	Linear CTE α_1 ($\times 10^{-7}/^{\circ}C$)	Linear CTE Temp.Range ($^{\circ}C$)
JK-BKM	$Ba_{0.25}K_{0.5}Zr_2(PO_4)_3$	$BaK_2Zr_8(PO_4)_{12}$	-7	R.T.-950
JK-CNM	$Ca_{0.25}Na_{0.5}Zr_2(PO_4)_3$	$CaNa_2Zr_8(PO_4)_{12}$	1	R.T.-900
JK-BNM	$Ba_{0.25}Na_{0.5}Zr_2(PO_4)_3$	$BaNa_2Zr_8(PO_4)_{12}$	-17	R.T.-900

Table 29. Linear thermal expansion results for (Ca-Na) modified systems

Sample No	Phase	Stoichiometric Compound with Integer Value	Linear CTE α_1 ($\times 10^{-7}/^{\circ}C$)	Linear CTE Temp.Range ($^{\circ}C$)
JK-CNM4	$(1/8Ca3/4Na)Zr_2(PO_4)_3$	$CaNa_6Zr_{16}(PO_4)_{24}$	-51	R.T.-900
JK-CNMC	$(3/8Ca1/4Na)Zr_2(PO_4)_3$	$Ca_3Na_2Zr_{16}(PO_4)_{24}$	-23	R.T.-900

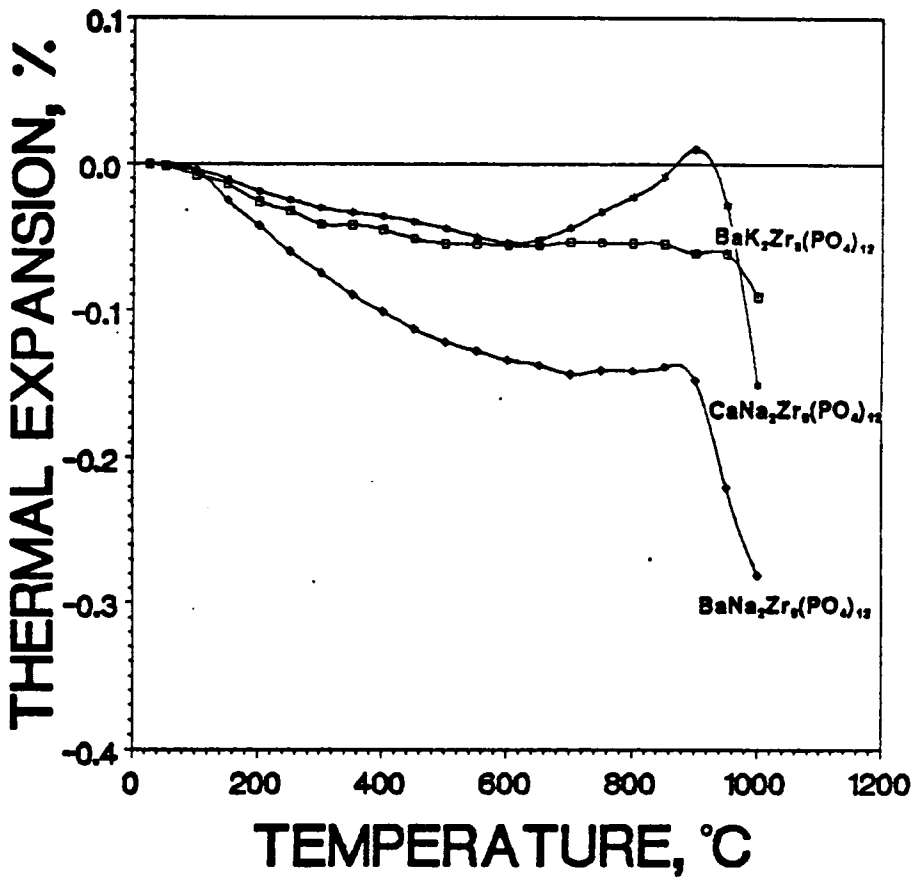

Figure 23. Linear thermal expansion behavior of (Ba-K), (Ca-Na), and (Ba-Na) modified systems: $BaK_2Zr_8(PO_4)_{12}$, $CaNa_2Zr_8(PO_4)_{12}$, and $BaNa_2Zr_8(PO_4)_{12}$

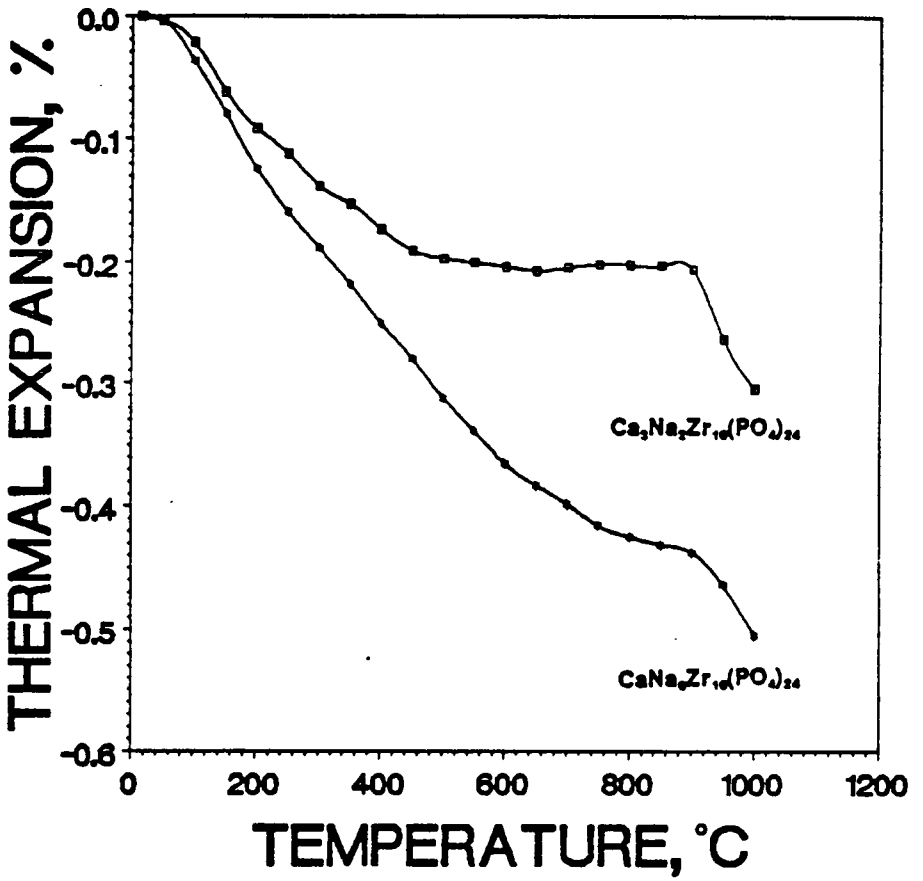

Figure 24. Linear thermal expansion behavior of (Ca-Na) modified systems: $Ca_3Na_2Zr_{16}(PO_4)_{24}$ and $CaNa_8Zr_{16}(PO_4)_{24}$

From Figure 23, two compounds $CaNa_2Zr_8(PO_4)_{12}$(JK-CNM) and $BaK_2Zr_8(PO_4)_{12}$(JK-BKM), having similar ionic size difference between the substituted cations, showed similar expansion behavior up to 600°C. However, the compound $BaNa_2Zr_8(PO_4)_{12}$ with a substituted cation size difference of 0.40Å, showed larger negative expansion values than the compounds having a smaller size difference.

The linear expansion behavior of the compounds substituted with alkali and alkaline earth elements is characterized by a sudden α decrease around 925°C. However, XRD analysis indicated that the thermal expansion transition which occurred around 925°C was a reversible reaction.

4.2.2.3 $Q^{+2}O$-$Q'^{+2}O$-ZrO_2-P_2O_5(Q^{+2},Q'^{+2} = Mg, Ca, Sr, Ba)

Linear thermal expansion was measured for the systems substituted with alkaline earth-alkaline earth elements. The results for these compounds are listed in Table 30 and Table 31. Detailed expansion behavior is shown in Figure 25 for the Ca-substituted compounds and in Figure 26 for other alkaline earth compounds.

$Ca_3MgZr_{16}(PO_4)_{24}$ showed more negative expansion characteristic than $MgCaZr_8(PO_4)_{12}$ ($-5x10^{-7}$/°C for $MgCaZr_8(PO_4)_{12}$ and $-10x10^{-7}$/°C for $Ca_3MgZr_{16}(PO_4)_{24}$). This result is expected due to the α values of ternary end member compounds $CaZr_4(PO_4)_6$($-18x10^{-7}$/°C) and $MgZr_4(PO_4)_6$($16x10^{-7}$/°C).

$CaSrZr_8(PO_4)_{12}$ showed a very small linear expansion, $5x10^{-7}$/°C up to 500°C, which agreed well with previous studies[59]. The average linear expansion value up to 1000°C for $CaSrZr_8(PO_4)_{12}$ is calculated as $13x10^{-7}$/°C. The compounds substituted with Ca and Ba combinations had a linear α of $37x10^{-7}$/°C up to 900°C. Again, we find compounds substituted with cation pairs with a small ionic size

Table 30. Linear thermal expansion results for (Ca-Mg), (Ca-Sr), and (Ca-Ba) modified systems

Sample No	Phase	Stoichiometric Compound with Integer Value	Linear CTE α_1 ($\times 10^{-7}/^{\circ}C$)	Temp.Range ($^{\circ}C$)
JK-MCC	$Mg_{0.25}Ca_{0.25}Zr_2(PO_4)_3$	$MgCaZr_8(PO_4)_{12}$	-5	R.T.-1000
JK-CSC	$Ca_{0.25}Sr_{0.25}Zr_2(PO_4)_3$	$CaSrZr_8(PO_4)_{12}$	13	R.T.-1000
JK-CBC	$Ca_{0.25}Ba_{0.25}Zr_2(PO_4)_3$	$CaBaZr_8(PO_4)_{12}$	37	R.T.-1000
JK-CMCC	$(3/8Ca1/8Mg)Zr_2(PO_4)_3$	$Ca_3MgZr_{16}(PO_4)_{24}$	-10	R.T.-1000

Table 31. Linear thermal expansion results for (Mg-Sr), (Mg-Ba), and (Ba-Sr) modified systems

Sample No	Phase	Stoichiometric Compound with Integer Value	Linear CTE α_1 ($\times 10^{-7}/^{\circ}C$)	Linear CTE Temp. Range ($^{\circ}C$)
JK-MSC	$Mg_{0.25}Sr_{0.25}Zr_2(PO_4)_3$	$MgSrZr_8(PO_4)_{12}$	18	R.T.-1000
JK-MBC	$Mg_{0.25}Ba_{0.25}Zr_2(PO_4)_3$	$MgBaZr_8(PO_4)_{12}$	20	R.T.-1000
JK-BSC	$Ba_{0.25}Sr_{0.25}Zr_2(PO_4)_3$	$BaSrZr_8(PO_4)_{12}$	32	R.T.-950

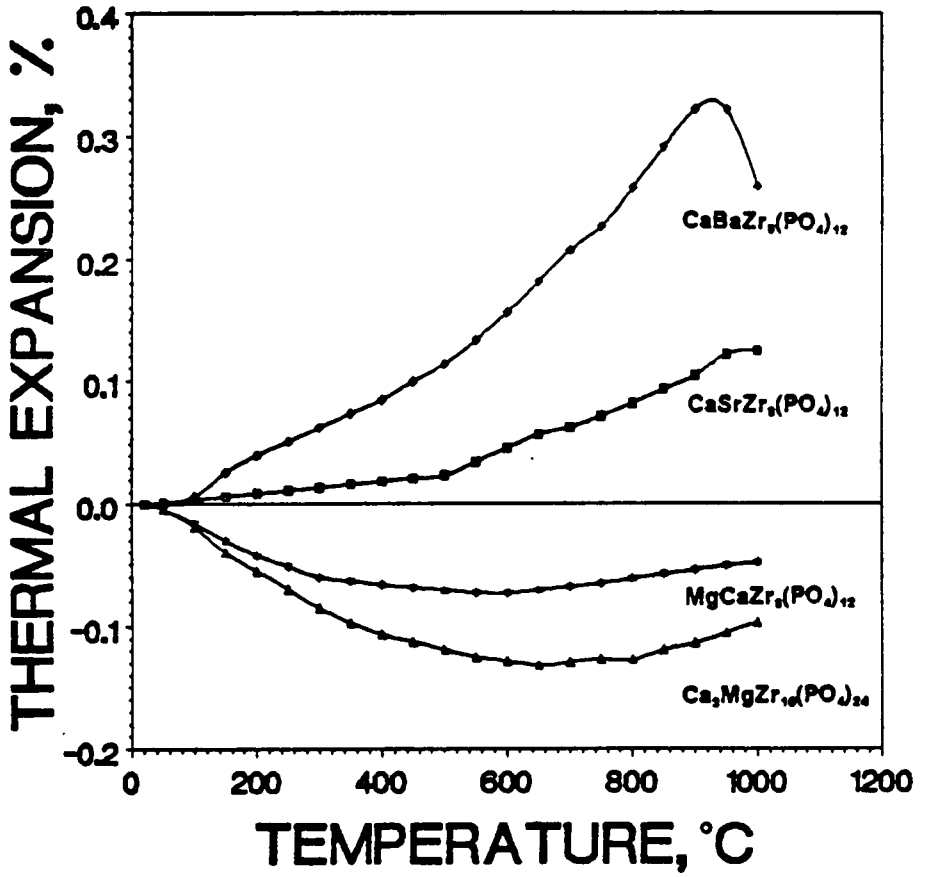

Figure 25. Linear thermal expansion behavior of (Ca-Ba), (Ca-Sr), and (Ca-Mg) modified systems: $CaBaZr_3(PO_4)_{12}$, $CaSrZr_3(PO_4)_{12}$, $MgCaZr_3(PO_4)_{12}$, and $Ca_3MgZr_{16}(PO_4)_{24}$

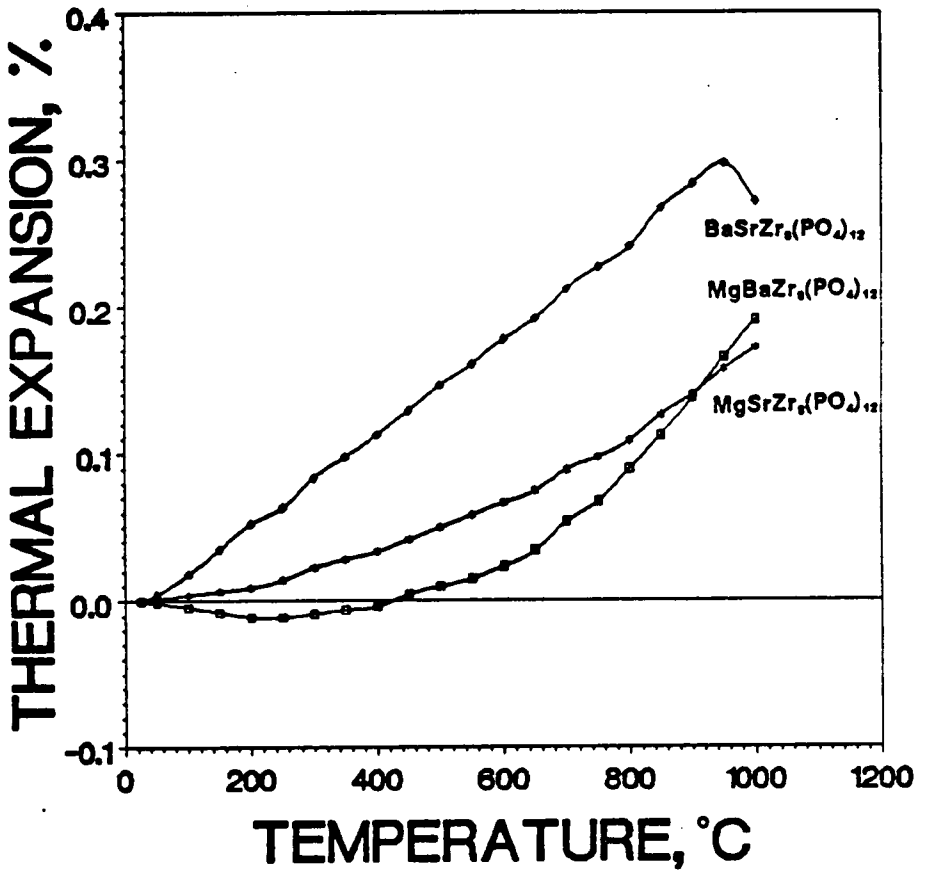

Figure 26. Linear thermal expansion behavior of (Ba-Sr), (Mg-Ba), and (Mg-Sr) modified systems: $BaSrZr_3(PO_4)_{12}$, $MgBaZr_3(PO_4)_{12}$, and $MgSrZr_3(PO_4)_{12}$

difference(0.16Å for Ca-Sr) to exhibit less expansion than the compounds substituted with a large ionic size difference(0.34Å for Ca-Ba)[116].

The systems substituted with Mg-Sr and Mg-Ba, $MgSrZr_8(PO_4)_{12}$ and $MgBaZr_8(PO_4)_{12}$, showed similar α values of $18x10^{-7}/°C$ and $20x10^{-7}/°C$, respectively. However for $MgBaZr_8(PO_4)_{12}$, the expansion rate above 600°C was much higher than for $MgSrZr_8(PO_4)_{12}$.

In compounds containing the Ba cation, $CaBaZr_8(PO_4)_{12}$ and $BaSrZr_8(PO_4)_{12}$, relatively high α values of $37x10^{-7}/°C$ and $32x10^{-7}/°C$, respectively, were measured for the sintered bar. However above 900°C, the length of bar started to decrease.

4.2.3 Axial thermal expansion

4.2.3.1 Rb_2O-Cs_2O-ZrO_2-P_2O_5

Lattice parameters from R.T. to 1400°C, in 200°C intervals, were measured for the compound $Rb_{0.5}Cs_{0.5}Zr_2(PO_4)_3$. Its mean axial α values are calculated and tabulated in Table 32 and detailed axial thermal expansion behavior is shown in Figure 27.

Compound $Rb_{0.5}Cs_{0.5}Zr_2(PO_4)_3$ had axial α values of $-11x10^{-7}/°C$ for the a-axis and $21x10^{-7}/°C$ for the c-axis. The calculated average linear α, $-0.3x10^{-7}/°C$, agrees well with the measured value of $-0.3x10^{-7}/°C$. The difference in axial thermal expansion($\alpha_c - \alpha_a$) was $32x10^{-7}/°C$, and was the same as that of $CsZr_2(PO_4)_3$ which turned out to be the system with the lowest anisotropy among ternary compounds.

Table 32. Lattice parameters and axial & linear CTE data for (½Rb½Cs)$Zr_2(PO_4)_3$ system

Sample Designation Phase		JK-RC2 $Rb_{0.5}Cs_{0.5}Zr_2(PO_4)_3$
Lattice parameter (Å at R.T.)	a-axis c-axis	8.62 24.69
Axial CTE ($x10^{-7}/°C$) (R.T.-1400°C)	α_a α_c $\alpha_c-\alpha_a$	-11 21 32
Calculated α_l Measured α_l	($x10^{-7}/°C$) ($x10^{-7}/°C$)	-0.3 -0.3

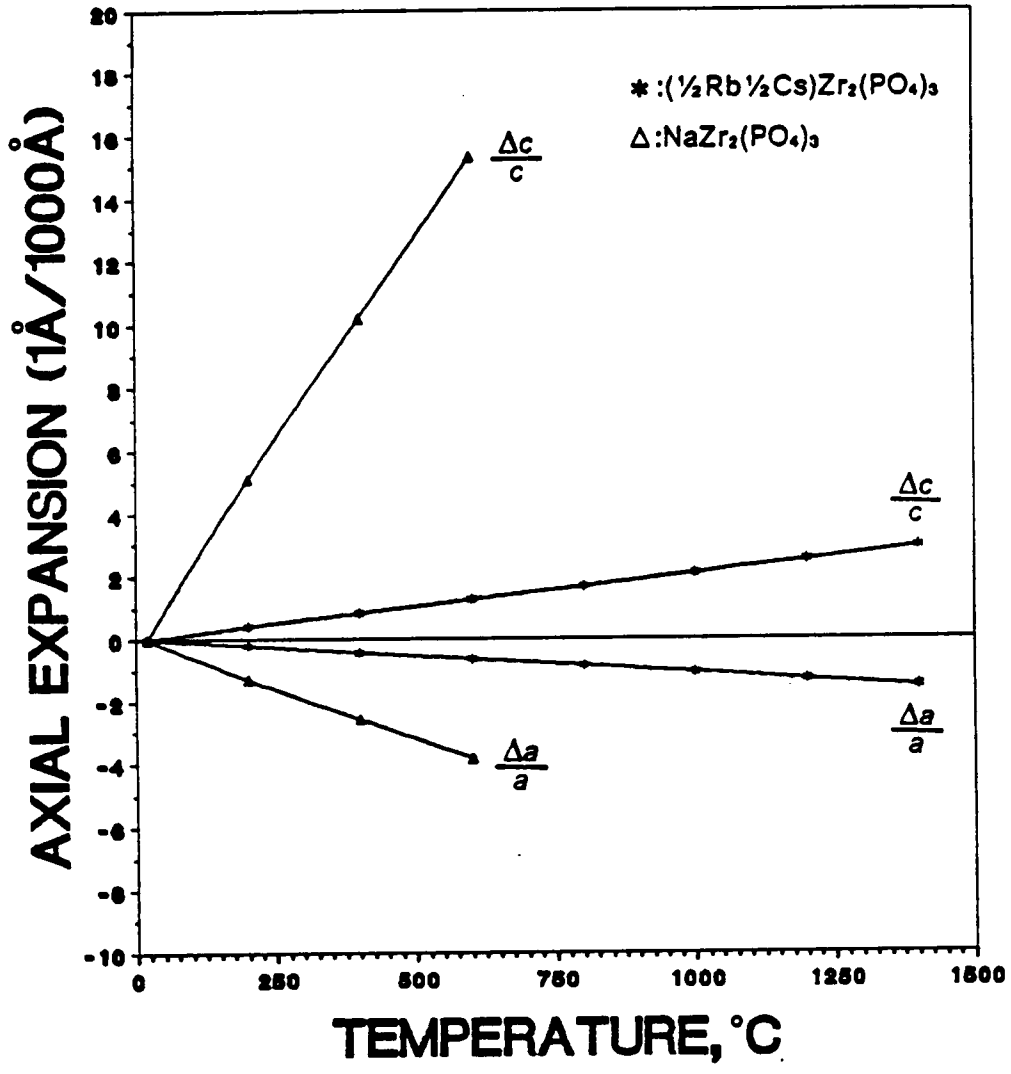

Figure 27. Axial thermal expansion behavior of $(\frac{1}{2}Rb\frac{1}{2}Cs)Zr_2(PO_4)_3$ system

4.2.3.2 MgO-CaO-ZrO_2-P_2O_5

For the two compounds $Ca_{0.5}Mg_{0.5}Zr_4(PO_4)_6$ and $(\frac{3}{8}Ca\frac{1}{8}Mg)Zr_2(PO_4)_3$, having linear α values of -5×10^{-7}/°C and -10×10^{-7}/°C, respectively, axial α values are summarized in Table 33 and their axial thermal expansion behavior is shown in Figures 28 and 29.

The axial thermal expansion behavior exhibited by these two systems were characterized by a transition at 600°C. $Ca_{0.5}Mg_{0.5}Zr_4(PO_4)_6$ showed a α value of -39×10^{-7}/°C(R.T.-600°C) and -14×10^{-7}/°C(600-1400°C) for the a-axis and 66×10^{-7}/°C(R.T.-600°C) and 47×10^{-7}/°C(600-1400°C) for the c-axis. $(\frac{3}{8}Ca\frac{1}{8}Mg)Zr_2(PO_4)_3$ had a α value of -47×10^{-7}/°C(R.T.-600°C) and -18×10^{-7}/°C(600-1400°C) for the a-axis and 81×10^{-7}/°C(R.T.-600°C) and 47×10^{-7}/°C(600-1400°C) for the c-axis.

From the relationship between axial α and linear α, the values of -4×10^{-7}/°C(R.T.-600°C) and 6×10^{-7}/°C(600-1400°C) were calculated for $Ca_{0.5}Mg_{0.5}Zr_4(PO_4)_6$. The compound $(\frac{3}{8}Ca\frac{1}{8}Mg)Zr_2(PO_4)_3$ had calculated average linear α values of -4×10^{-7}/°C(R.T.-600°C) and 10×10^{-7}/°C(600-1400°C). These axial expansion transitions correlate well with the linear thermal expansion behavior investigated in compounds $Ca_{0.5}Mg_{0.5}Zr_4(PO_4)_6$ and $(\frac{3}{8}Ca\frac{1}{8}Mg)Zr_2(PO_4)_3$.

The differences in axial thermal expansion$(\alpha_c - \alpha_a)$ was lower in the high temperature region(600-1400°C) than in the low temperature region(R.T.-600°C) for both compounds. The Ca-rich compound $(\frac{3}{8}Ca\frac{1}{8}Mg)Zr_2(PO_4)_3$ exhibited greater anisotropy than the compound $Ca_{0.5}Mg_{0.5}Zr_4(PO_4)_6$. $(\alpha_c - \alpha_a)$ values are 105×10^{-7}/°C(R.T.-600°C) and 61×10^{-7}/°C(600-1400°C) for compound $Ca_{0.5}Mg_{0.5}Zr_4(PO_4)_6$, and 128×10^{-7}/°C(R.T.-600°C) and 85×10^{-7}/°C(600-1400°C) for compound $(\frac{3}{8}Ca\frac{1}{8}Mg)Zr_2(PO_4)_3$.

Table 33. Lattice parameters and axial & linear CTE data for (Ca-Mg) modified systems

Sample Designation / Phase			JK-MCC $Ca_{0.5}Mg_{0.5}Zr_4(PO_4)_6$	JK-CMCC $(3/8Ca1/8Mg)Zr_2(PO_4)_3$
Lattice parameter (Å at R.T.)	a-axis		8.79	8.79
	c-axis		22.65	22.64
Axial CTE ($x10^{-7}/°C$)	R.T.-600°C	α_a	-39	-47
		α_c	66	81
		$\alpha_c-\alpha_a$	105	128
	600-1400°C	α_a	-14	-18
		α_c	47	67
		$\alpha_c-\alpha_a$	61	85
Calculated α_l ($x10^{-7}/°C$)	R.T.-600°C		-4	-4
	600-1400°C		6	10
Measured α_l ($x10^{-7}/°C$)			-5	-10

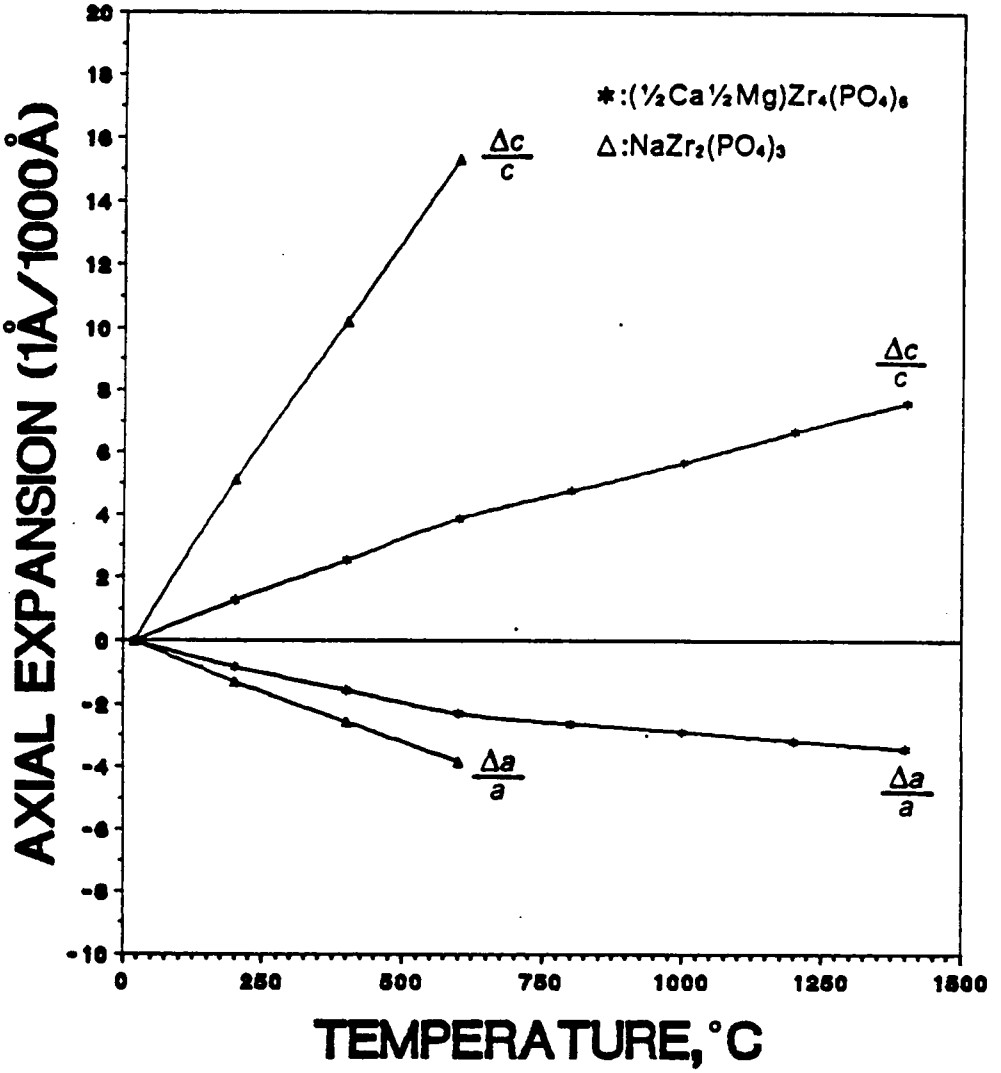

Figure 28. Axial thermal expansion behavior of $(\frac{1}{2}Ca\frac{1}{2}Mg)Zr_4(PO_4)_6$ system

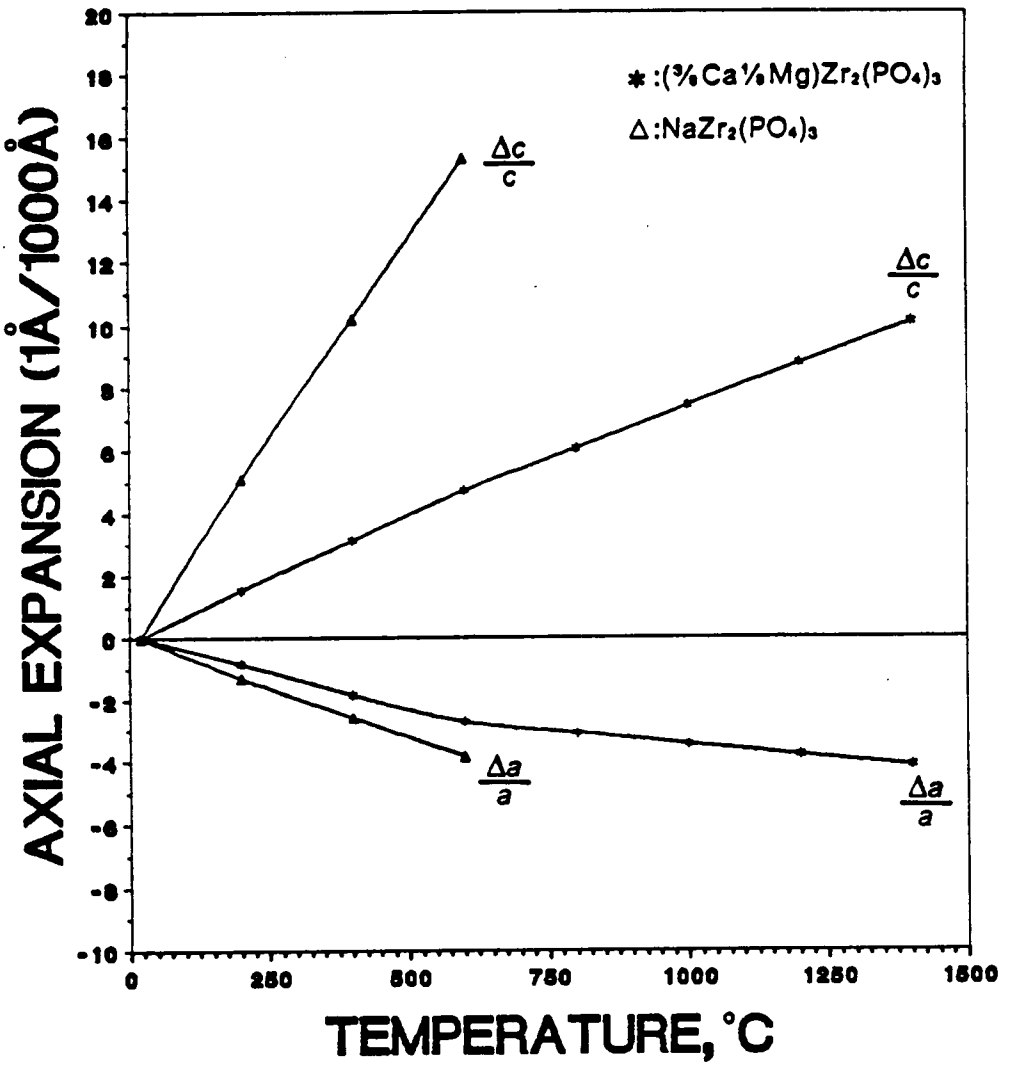

Figure 29. Axial thermal expansion behavior of (¾Ca¼Mg)$Zr_2(PO_4)_3$ system

4.2.4 Secondary material properties for the selected compounds

This section provides the secondary material properties of the compounds $Rb_{0.5}Cs_{0.5}Zr_2(PO_4)_3$ and $Ca_{0.5}Mg_{0.5}Zr_4(PO_4)_6$.

4.2.4.1 Structural attributes

Resulting structural attributes for these two compounds which were processed by solid-state reaction are summarized in Table 34. The percent theoretical density for both compounds exceeded 94%, which was in close agreement to values reported(92-99%) in previous studies[41,56].

Open porosities were measured as 4.5% and 3.4% for $Ca_{0.5}Mg_{0.5}Zr_4(PO_4)_6$ and $Rb_{0.5}Cs_{0.5}Zr_2(PO_4)_3$, respectively. Sample shrinkage was bigger in $Rb_{0.5}Cs_{0.5}Zr_2(PO_4)_3$ (12.5%) than in $Ca_{0.5}Mg_{0.5}Zr_4(PO_4)_6$ (10.6%). Meanwhile, more water was absorbed in $Ca_{0.5}Mg_{0.5}Zr_4(PO_4)_6$ (1.41%) than in $Rb_{0.5}Cs_{0.5}Zr_2(PO_4)_3$ (1.03%).

4.2.4.2 Thermal shock resistance

Thermal shock resistance was conducted for the sintered bars using the water quench method which involves the maximum quench temperature difference(ΔT_m) without observable cracking and the number of repeated quenchings from 1200°C. These results are tabulated in Table 35.

The maximum quench temperature difference was 1475°C for the compound $Ca_{0.5}Mg_{0.5}Zr_4(PO_4)_6$, however, the compound $Rb_{0.5}Cs_{0.5}Zr_2(PO_4)_3$ resisted fracture up to

Table 34. Structural attributes of (½Ca½Mg)$Zr_4(PO_4)_6$ and (½Rb½Cs)$Zr_2(PO_4)_3$

Compound	%Shrinkage	Bulk Density(g/cm^3)	%TD	%Open Porosity	%Water Absorption
$Ca_{0.5}Mg_{0.5}Zr_4(PO_4)_6$	10.6	3.101	94.1	4.5	1.41
$Rb_{0.5}Cs_{0.5}Zr_2(PO_4)_3$	12.5	3.202	95.9	3.4	1.03

Table 35. Thermal shock resistance of (½Ca½Mg)$Zr_4(PO_4)_6$ and (½Rb½Cs)$Zr_2(PO_4)_3$

Compound	ΔT_m (°C)	Allowable Repeated Quench with ΔT=1200°C
$Ca_{0.5}Mg_{0.5}Zr_4(PO_4)_6$	1475	5 times
$Rb_{0.5}Cs_{0.5}Zr_2(PO_4)_3$	>1625*	>20 times**

*No cracking was observed up to the maximum temperature difference of 1625°C used in the current experiments.

**No cracking was observed after 20 times of repeated quench.

1625°C. The sample $Ca_{0.5}Mg_{0.5}Zr_4(PO_4)_6$ cracked after 6 repeated quenches, while the specimen $Rb_{0.5}Cs_{0.5}Zr_2(PO_4)_3$ withstood 20 thermal cycles.

4.2.4.3 MOR test and fractography

MOR data were obtained from 3-point and 4-point bending tests, and their average values are summarized in Table 36. The average MOR of $Rb_{0.5}Cs_{0.5}Zr_2(PO_4)_3$ (49.14 and 52.71 MPa from 4-point&3-point, respectively) were almost 2½ times than that of $Ca_{0.5}Mg_{0.5}Zr_4(PO_4)_6$ (21.48 and 23.13 MPa from 4-point and 3-point, respectively). The trueness of the specimens used at 4-point bend testing are tabulated in Table 37. The maximum deviation from trueness along the height was measured as 0.007mm and 0.019mm, and the maximum face trueness was 0.010mm and 0.005mm for the $Ca_{0.5}Mg_{0.5}Zr_4(PO_4)_6$ and $Rb_{0.5}Cs_{0.5}Zr_2(PO_4)_3$, respectively.

Fractography of these two specimens were investigated by SEM and are shown in Figures 30 through 33. Figure 30 shows the fractography of $Rb_{0.5}Cs_{0.5}Zr_2(PO_4)_3$ at low magnification which shows relatively rough fracture surfaces. Figure 31 shows the overall fracture surfaces for $Ca_{0.5}Mg_{0.5}Zr_4(PO_4)_6$ to be relatively smooth compared with that of $Rb_{0.5}Cs_{0.5}Zr_2(PO_4)_3$. Figures 32 and 33, taken at higher magnification, show more prominent fracture features. Figure 32 shows that $Rb_{0.5}Cs_{0.5}Zr_2(PO_4)_3$ had a transgranular fracture path and hackle-type ridges[125]. Figure 33 showing the $Ca_{0.5}Mg_{0.5}Zr_4(PO_4)_6$ sample, the fracture features are characterized by intergranular fracture paths and rib-marks[125].

Table 36. MOR data for (½Ca½Mg)$Zr_4(PO_4)_6$ and (½Rb½Cs)$Zr_2(PO_4)_3$

$Ca_{0.5}Mg_{0.5}Zr_4(PO_4)_6$			$Rb_{0.5}Cs_{0.5}Zr_2(PO_4)_3$		
Sample	3-point (MPa)	4-point (MPa)	Sample	3-point (MPa)	4-point (MPa)
1	26.44	18.70	1	50.52	46.67
2	20.12	23.46	2	52.25	46.59
3	20.46	20.67	3	54.57	53.71
4	24.03	21.26	4	50.06	47.57
5	24.59	23.33	5	56.16	51.18
Average	23.13	21.48	Average	52.71	49.14

Table 37. Trueness for the samples used at 4-point bend testing

Compound	The Range of Height (mm)	Maximum Deviation from trueness (mm)	
		Along the Height	Along the Face
$Ca_{0.5}Mg_{0.5}Zr_4(PO_4)_6$	4.55-4.75	0.07	0.10
$Rb_{0.5}Cs_{0.5}Zr_2(PO_4)_3$	4.70-5.00	0.19	0.05

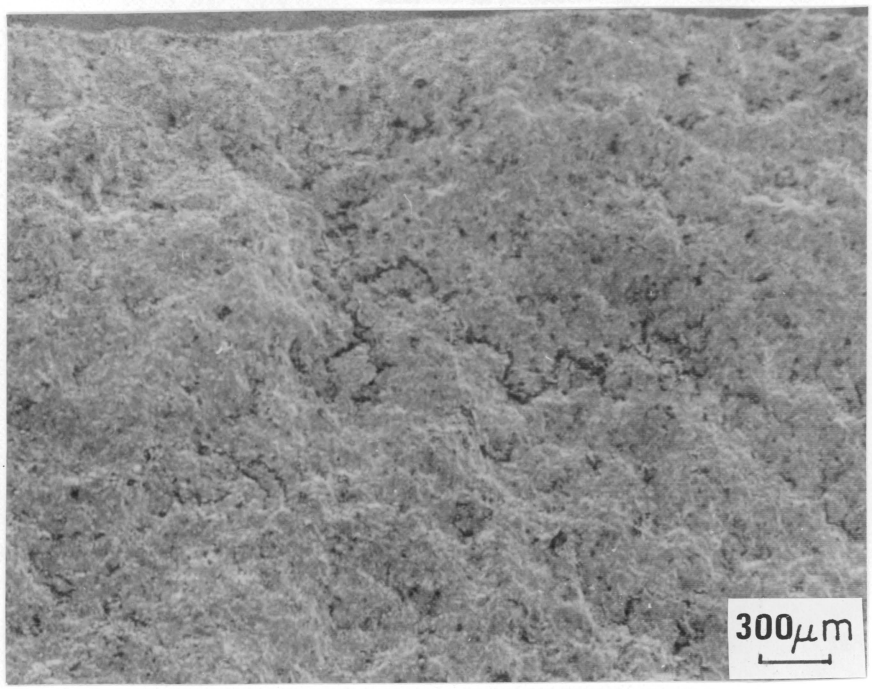

Figure 30. Scanning electron micrograph of fracture surface of $(\frac{1}{2}Rb\frac{1}{2}Cs)Zr_2(PO_4)_3$

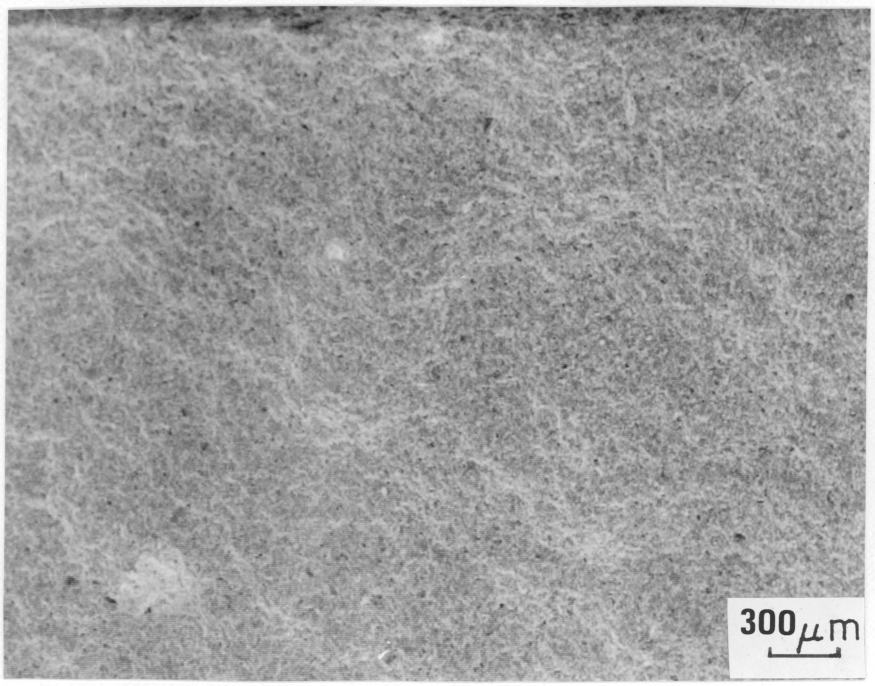

Figure 31. Scanning electron micrograph of fracture surface of $(\frac{1}{2}Ca\frac{1}{2}Mg)Zr_4(PO_4)_6$

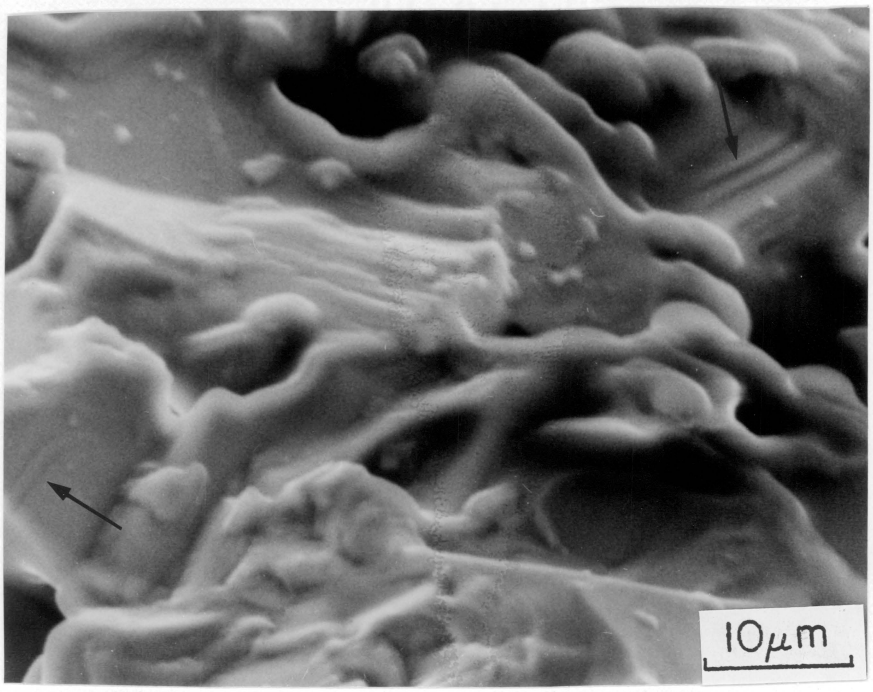

Figure 32. **Scanning electron micrograph of fracture surface of $(½Rb½Cs)Zr_2(PO_4)_3$:** Arrows represent the hackle-type mark.

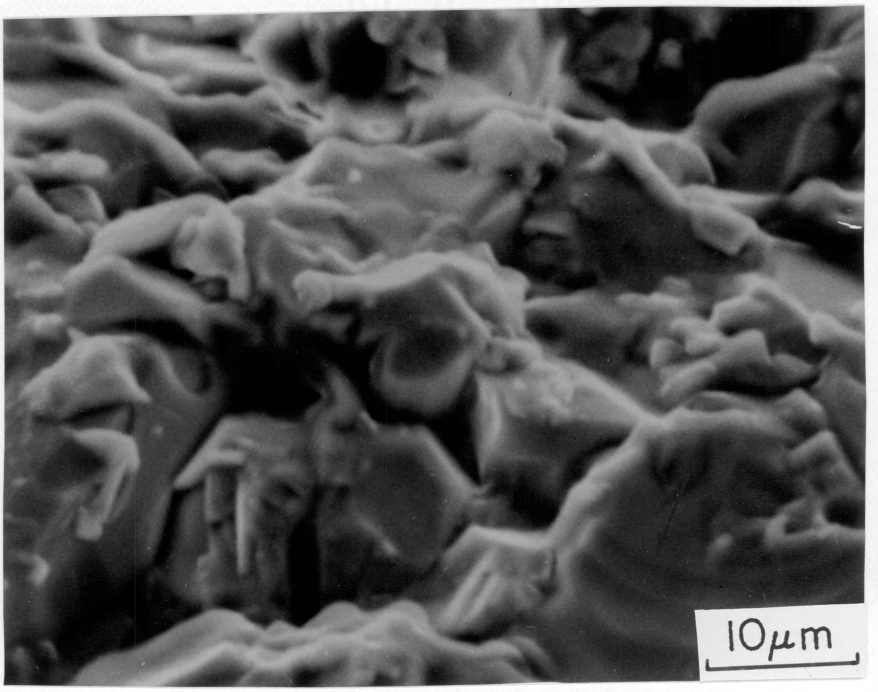

Figure 33. Scanning electron micrograph of fracture surface of $(\frac{1}{2}Ca\frac{1}{2}Mg)Zr_4(PO_4)_6$: Arrow represents the rib mark.

4.2.4.4 Microstructure

Microstructures for the both compounds were characterized by SEM and shown in Figures 34 and 35. The grains in the $Rb_{0.5}Cs_{0.5}Zr_2(PO_4)_3$ sample are finer and more spherical than those of $Ca_{0.5}Mg_{0.5}Zr_4(PO_4)_6$.

4.2.4.5 DTA analysis and long-term thermal stability

DTA runs were used to investigate phase stability for these two compounds. No phase instability was found up to 1500°C for both specimens. Long-term thermal stability was investigated by holding the samples at 1400°C for 96hrs. No changes were detected in $Ca_{0.5}Mg_{0.5}Zr_4(PO_4)_6$, but XRD phase identification results revealed the presence of ZrO_2, Rb_2O, and Cs_2O in compound $Rb_{0.5}Cs_{0.5}Zr_2(PO_4)_3$ following thermal exposure. This instability is likely due to the decomposition of P_2O_5.

4.2.5 Statistical analysis for (½Ca½Mg)$Zr_4(PO_4)_6$

4.2.5.1 Lot-to-lot variability and replicate test variability

Table 38 summarizes the statistical results for $Ca_{0.5}Mg_{0.5}Zr_4(PO_4)_6$. The mean α value from 10 lots was calculated as -5×10^{-7}/°C, while the average value from 10 replicate tests was -4.5×10^{-7}/°C.

Even though average values from two different analyses showed similar α values differing by 10 %, the differences in standard deviation and in coefficient of variation

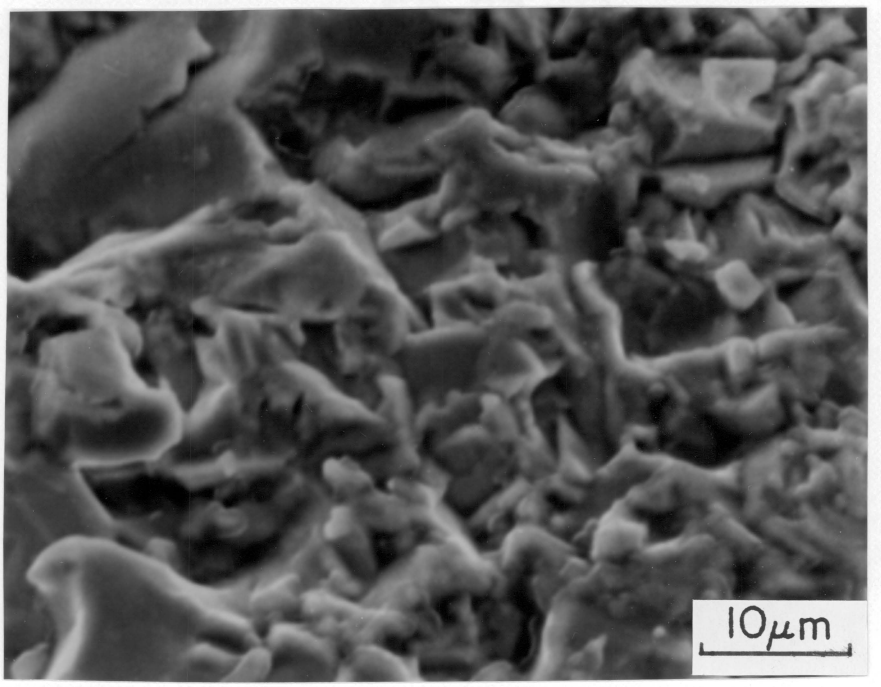

Figure 34. Scanning electron micrograph of as-polished $(\frac{1}{2}Ca\frac{1}{2}Mg)Zr_4(PO_4)_6$

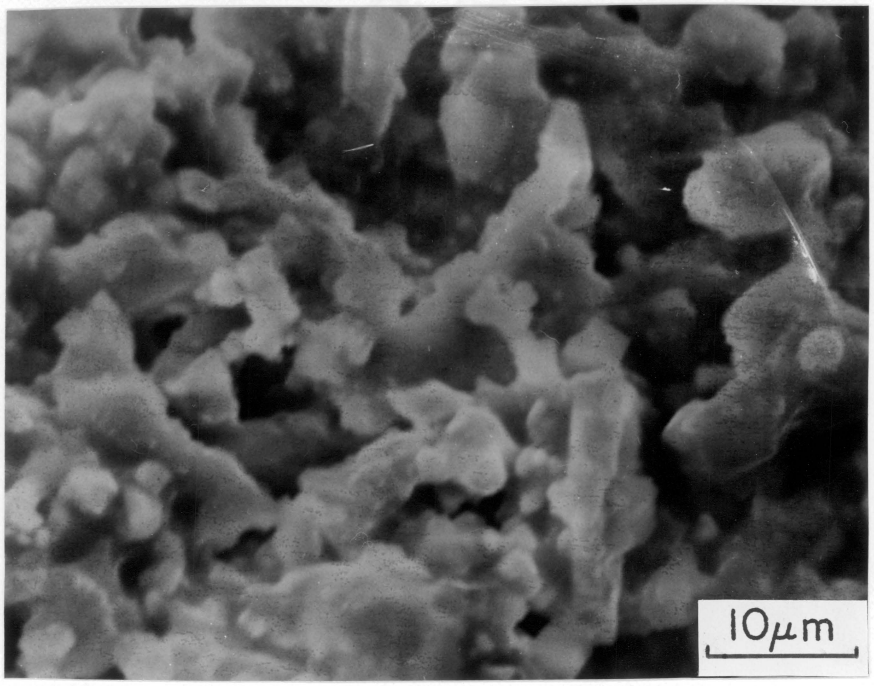

Figure 35. Scanning electron micrograph of polished and etched ($\frac{1}{2}Rb\frac{1}{2}Cs)Zr_2(PO_4)_3$

were 60 % & 80 %, respectively. Standard deviation for the lot-to-lot($0.72x10^{-7}$/°C) was much smaller than that for the replicate test($1.78x10^{-7}$/°C). In addition, the coefficient of variation for the lot-to-lot(-0.144) was closer to zero than that for the replicate test(-0.557). A t-value and an F-value[117] were calculated from the observed values for the lot-to-lot & the replicate test and resulted in -3.69 for the t-value and 0.027 for the F-value.

4.3 Quintenary(Na_2O-MgO-CaO-ZrO_2-P_2O_5) system

Three quinternary oxide compounds, based on the Na_2O-MgO-CaO-ZrO_2-P_2O_5 system, were synthesized and investigated for their solid-solubility using XRD. For any compound showing a single phase, the linear thermal expansion was measured. The following two sections, 4.3.1 and 4.3.2, present the results of solid-solubility and linear thermal expansion based on the quinternary(Na_2O-MgO-CaO-ZrO_2-P_2O_5) system.

4.3.1 Solid solubility

To investigate the solid solubility of quinternary(Na_2O-MgO-CaO-ZrO_2-P_2O_5) system, three different composites were selected. The resulting phases are summarized in Table 39.

As discussed in section 4.2.1.2, the quarternary system(CaO-Na_2O-ZrO_2-P_2O_5) showed complete solubility. However, in this quinternary system, only one sample,

Table 38. Statistical analysis for the $(\frac{1}{2}Ca\frac{1}{2}Mg)Zr_4(PO_4)_6$ compound

Statistical Value	Lot-to-lot variability	Replicate test variability
Average Value($\bar{x}$)	$-5.0 \times 10^{-7}/^{\circ}C$	$-4.5 \times 10^{-7}/^{\circ}C$
Standard Deviation(s)	$0.72 \times 10^{-7}/^{\circ}C$	$1.78 \times 10^{-7}/^{\circ}C$
Standard Error($s/\sqrt{n}$)	$0.228 \times 10^{-7}/^{\circ}C$	$0.74 \times 10^{-7}/^{\circ}C$
Coefficient of Variation($s/\bar{x}$)	-0.144	-0.557

Table 39. Phases present for Na-Mg-Ca & Na-Ca modified systems (*;from Table 23)

Sample No	Composition(Moles)	Phases
*JK-CNM4	$(1/8Ca3/4Na)Zr_2(PO_4)_3$	$(1/8Ca3/4Na)Zr_2(PO_4)_3$
JK-CMN22	$(1/16Ca1/16Mg3/4Na)Zr_2(PO_4)_3$	$(1/16Ca1/16Mg3/4Na)Zr_2(PO_4)_3$
*JK-CNM	$(1/4Ca1/2Na)Zr_2(PO_4)_3$	$(1/4Ca1/2Na)Zr_2(PO_4)_3$
JK-CMN44	$(1/8Ca1/8Mg1/2Na)Zr_2(PO_4)_3$	$CaZr_4(PO_4)_6 + NaZr_2(PO_4)_3$
*JK-CNMC	$(3/8Ca1/4Na)Zr_2(PO_4)_3$	$(3/8Ca1/4Na)Zr_2(PO_4)_3$
JK-CMN66	$(3/16Ca3/16Mg1/4Na)Zr_2(PO_4)_3$	$CaZr_4(PO_4)_6 + NaZr_2(PO_4)_3$

$Ca_{0.0625}Mg_{0.0625}Na_{0.75}Zr_2(PO_4)_3$, exhibited a single phase. The other two compounds, $Ca_{0.125}Mg_{0.125}Na_{0.5}\cdot Zr_2(PO_4)_3$ and $Ca_{0.1875}Mg_{0.1875}Na_{0.25}\cdot Zr_2(PO_4)_3$, resulted in two phases of $CaZr_4(PO_4)_6$ and $NaZr_2(PO_4)_3$. The reason that these two compounds consisted of two phases is associated with the amount of Mg. The ionic radii of Ca and Na are very similar(1.04Å and 0.98Å respectively[116]), whereas Mg has a much smaller ionic radius of 0.74Å[116]. This big difference in ionic size among these three elements resulted in the observed limited solid solubility.

For the $CaO\text{-}MgO\text{-}ZrO_2\text{-}P_2O_5$ quarternary system, compounds where the mole percent of Mg was higher than Ca also resulted in two phases of $CaZr_4(PO_4)_6$ and $MgZr_4(PO_4)_6$. However, for compounds equal in Mg and Ca or richer in Ca, $MgZr_4(PO_4)_6$ was not detected by X-ray diffraction. Therefore, samples $Ca_{0.125}Mg_{0.125}Na_{0.5}\cdot Zr_2(PO_4)_3$ and $Ca_{0.1875}Mg_{0.1875}Na_{0.25}\cdot Zr_2(PO_4)_3$ with equal mole percents of Ca and Mg did not show the $MgZr_4(PO_4)_6$ phase.

4.3.2 Linear thermal expansion

Linear thermal expansion measurement was conducted for $Ca_{0.0625}Mg_{0.0625}Na_{0.75}Zr_2(PO_4)_3$. The linear α was measured as $-25\times10^{-7}/°C$ up to 1000°C, and it is listed in Table 40 along with the value for $(1/8\,Ca\,3/4\,Na)Zr_2(PO_4)_3$. Detailed expansion behavior is shown in Figure 36.

The compound $Ca_{0.0625}Mg_{0.0625}Na_{0.75}Zr_2(PO_4)_3$ exhibited a large increase in thermal expansion compared with the system $(1/8\,Ca\,3/4\,Na)Zr_2(PO_4)_3$. This is probably due to the addition of Mg. The results for the ternary compounds, $CaZr_4(PO_4)_6$ and $NaZr_2(PO_4)_3$, showed negative expansion values of $-18\times10^{-7}/°C$ and $-33\times10^{-7}/°C$, respectively. On the other hand, $MgZr_4(PO_4)_6$ expanded positively, $16\times10^{-7}/°C$.

Table 40. Linear thermal expansion results for (Ca-Na) and (Ca-Mg-Na) modified systems (*;from Table 29)

Sample No	Phase	Stoichiometric Compound with Integer Value	Linear CTE α_1 ($\times 10^{-7}/^{\circ}C$)	Temp.Range ($^{\circ}C$)
*JK-CNM4	$(1/8Ca3/4Na)Zr_2(PO_4)_3$	$CaNa_6Zr_{16}(PO_4)_{24}$	-51	R.T.-1000
JK-CMN22	$(1/16Ca1/16Mg3/4Na)\cdot Zr_2(PO_4)_3$	$CaMgNa_{12}Zr_{32}(PO_4)_{48}$	-25	R.T.-1000

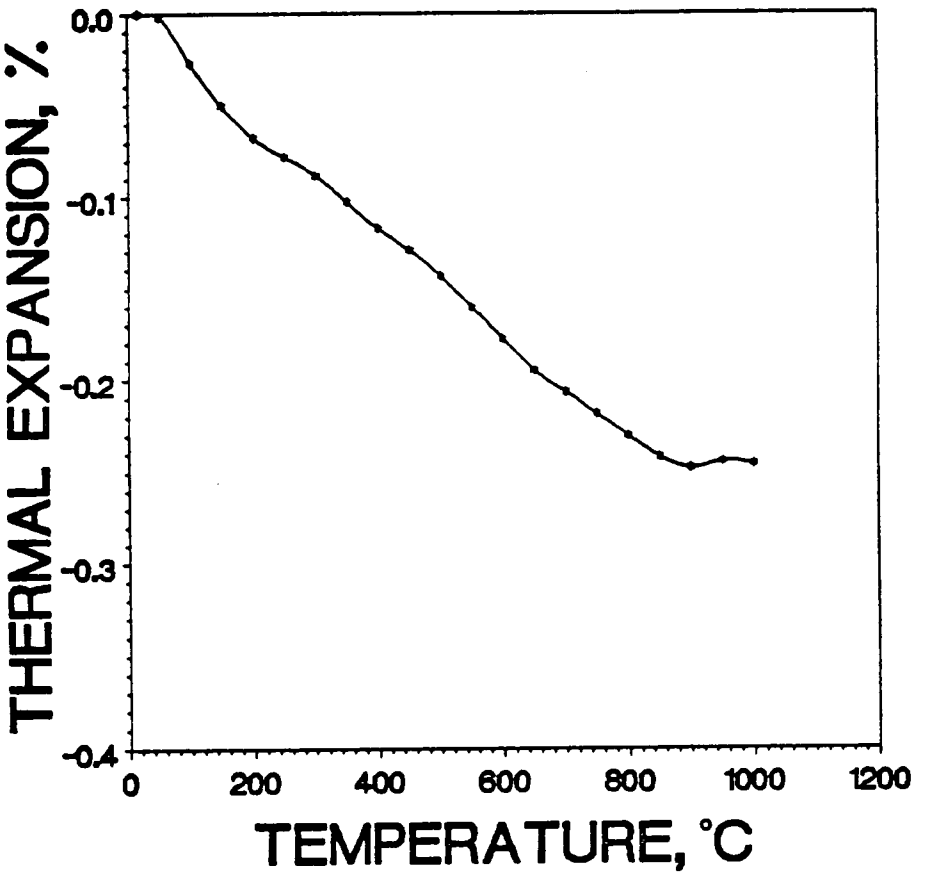

Figure 36. Linear thermal expansion behavior of $CaMgNa_{12}Zr_{32}(PO_4)_{48}$

Therefore, the compound replaced by Ca and Mg and Na($Ca_{0.0625}Mg_{0.0625}Na_{0.75}Zr_2(PO_4)_3$) versus just Ca and Na(($\frac{1}{8}Ca\frac{3}{4}Na$)$Zr_2(PO_4)_3$) showed a negative expansion value much closer to zero.

4.4 Summary of experimental evidence

All of the compounds considered in this study were synthesized by solid-state reaction. P_2O_5 was used directly to make NZP compounds, with acetone serving as a mineralizer as well as an aid to homogenizing mixtures. Heat treatments were conducted at 1100°C for 24h and at 1300°C for 4h, followed by furnace cooling to room temperature. Linear thermal expansion was measured up to 1000°C, while axial thermal expansion was measured up to 1400°C. This section provides the summary of experimental results presented in previous sections.

4.4.1 Ternary system

4.4.1.1 Linear thermal expansion

Five alkali elements with valence of +1 have been used to modify NZP structures. A Li-modified compound has shown a transition from positive to negative expansion at about 150°C. This transition is apparently related to the phase transition from monoclinic to hexagonal structure. Negative average linear thermal expansion values for the $NaZr_2(PO_4)_3$ and $KZr_2(PO_4)_3$ compounds have been obtained, and their

values are $-33x10^{-7}/°C$ and $-22x10^{-7}/°C$, respectively. The mean linear thermal expansion values for $RbZr_2(PO_4)_3$ was $2x10^{-7}/°C$ and for $CsZr_2(PO_4)_3$ was $5x10^{-7}/°C$.

Four alkaline earth elements have been used to modify the NZP structure. $CaZr_4(PO_4)_6$ has exhibited negative thermal expansion with a value of $-18x10^{-7}/°C$. Three other compounds modified by Mg, Sr, Ba have shown positive expansion. $MgZr_4(PO_4)_6$ and $BaZr_4(PO_4)_6$ have exhibited low α values of $16x10^{-7}/°C$ and $15x10^{-7}/°C$, respectively. The linear α value for the $SrZr_4(PO_4)_6$ compound was found to be $22x10^{-7}/°C$.

Four transition elements with a valence of +2 were selected to modify the NZP structure. $MnZr_4(PO_4)_6$ and $NiZr_4(PO_4)_6$ have shown the low linear thermal expansion values of $7x10^{-7}/°C$ and $10x10^{-7}/°C$, respectively. Modification with Cu has shown the value of $40x10^{-7}/°C$. The specimen $ZnZr_4(PO_4)_6$ has exhibited a low α value of $5x10^{-7}/°C$ up to 900°C, but the thermal expansion decreased suddenly above 900°C.

Four oxides containing cations with a +3 charge have been selected to investigate the possibility of synthesizing a modified NZP structure. For the substituted systems having +3 cation valence, only $YZr_6(PO_4)_9$($14x10^{-7}/°C$) has been included in the low thermal expansion group. Thermal expansion data for other compounds ($LaZr_6(PO_4)_9$, $AlZr_6(PO_4)_9$, and $CrZr_6(PO_4)_9$) ranged from $24x10^{-7}/°C$ to $29x10^{-7}/°C$.

Among the compounds substituted with a tetravalent ion to replace the Na cation in the NZP structure, compounds modified by Ti, Zr, and Hf from Group IV A have exhibited a thermal expansion transition from positive to negative at around 950°C. Before this expansion transition, $TiZr_8(PO_4)_{12}$ has shown the lowest α value($20x10^{-7}/°C$), but other two compounds, $Zr_3(PO_4)_4$ and $HfZr_8(PO_4)_{12}$, have shown α values of $42x10^{-7}/°C$ & $39x10^{-7}/°C$, respectively. Two other substitutions have also been evaluated, and their expansion values have been measured as $23x10^{-7}/°C$ for $SiZr_8(PO_4)_{12}$ and $11x10^{-7}/°C$ for $CeZr_8(PO_4)_{12}$.

The substitution of elements with +5 valence into the NZP structure has been considered; the selected elements were V, Nb, and Ta from Group V A. A compound substituted with V_2O_5 has shown two thermal expansion transitions, one around 300°C and again around 850°C. Low linear thermal expansion values have been obtained for samples of $NbZr(PO_4)_3$ and $TaZr(PO_4)_3$, and their thermal expansion values are $4x10^{-7}$/°C for $NbZr(PO_4)_3$ and $11x10^{-7}$/°C for $TaZr(PO_4)_3$. Table 41 shows the experimentally determined linear aggregate α values for the ternary compounds.

4.4.1.2 Axial thermal expansion

Among the alkali-modified systems, two compounds, $RbZr_2(PO_4)_3$ and $CsZr_2(PO_4)_3$ showing low α have been selected for the investigation of the change of lattice parameters from room temperature to 1400°C. $RbZr_2(PO_4)_3$ has shown axial α values of $12x10^{-7}$/°C for the a-axis and $30x10^{-7}$/°C for the c-axis. Axial α values of $CsZr_2(PO_4)_3$ have been evaluated as $-9x10^{-7}$/°C for the a-axis and $23x10^{-7}$/°C for the c-axis, and its axial thermal expansion difference($\Delta\alpha = 32x10^{-7}$/°C) is the lowest among the compounds considered.

$MgZr_4(PO_4)_6$ has shown the axial α values of $-22x10^{-7}$/°C for the a-axis and $58x10^{-7}$/°C for the c-axis. Meanwhile, $CaZr_4(PO_4)_6$ has exhibited large anisotropy compared with that of $MgZr_4(PO_4)_6$, i.e. $-38x10^{-7}$/°C for the a-axis and $79x10^{-7}$/°C for the c-axis. $BaZr_4(PO_4)_6$ has shown the largest anisotropic characteristic among the compounds studied, as its axial α values are $-67x10^{-7}$/°C and $279x10^{-7}$/°C for the a- and c-axes, respectively. Two compounds substituted with transition elements with +2 have shown strong anisotropy ($\Delta\alpha$) of $346x10^{-7}$/°C and $277x10^{-7}$/°C.

Among the systems substituted with cation valence of +3 or +4, three compounds, $YZr_6(PO_4)_9$, $TiZr_8(PO_4)_{12}$, and $CeZr_8(PO_4)_{12}$, showing low α have been selected

Table 41. Thermal expansion results for the modified ternary NZP systems

Sample No	Phase	Linear CTE	
		α_1 ($\times 10^{-7}/^{\circ}C$)	Temp.Range($^{\circ}C$)
JK-111	$LiZr_2(PO_4)_3$	-22	150-1000
JK-112	$NaZr_2(PO_4)_3$	-33	R.T.-1000
JK-113	$KZr_2(PO_4)_3$	-22	R.T.-1000
JK-114	$RbZr_2(PO_4)_3$	2	R.T.-1000
JK-115	$CsZr_2(PO_4)_3$	5	R.T.-1000
JK-121	$MgZr_4(PO_4)_6$	16	R.T.-1000
JK-122	$CaZr_4(PO_4)_6$	-18	R.T.-1000
JK-123	$SrZr_4(PO_4)_6$	22	R.T.-1000
JK-124	$BaZr_4(PO_4)_6$	15	R.T.-1000
JK-125	$MnZr_4(PO_4)_6$	7	R.T.-1000
JK-126	$NiZr_4(PO_4)_6$	10	R.T.-1000
JK-127	$CuZr_4(PO_4)_6$	40	R.T.-1000
JK-128	$ZnZr_4(PO_4)_6$	5	R.T.-900
JK-131	$YZr_6(PO_4)_9$	14	R.T.-1000
JK-132	$LaZr_6(PO_4)_9$	25	R.T.-1000
JK-133	$AlZr_6(PO_4)_9$	24	R.T.-1000
JK-134	$CrZr_6(PO_4)_9$	29	R.T.-1000
JK-141	$TiZr_8(PO_4)_{12}$	20	R.T.-980
JK-142	$Zr_3(PO_4)_4$	39	R.T.-980
JK-143	$HfZr_8(PO_4)_{12}$	42	R.T.-950
JK-144	$SiZr_8(PO_4)_{12}$	23	R.T.-1000
JK-145	$CeZr_8(PO_4)_{12}$	11	R.T.-1000
JK-151	$VZr(PO_4)_3$	20	400-800
JK-152	$NbZr(PO_4)_3$	4	R.T.-1000
JK-153	$TaZr(PO_4)_3$	11	R.T.-1000

to evaluate their axial α values. Their average axial α values ranged from -31 to $-29x10^{-7}/°C$ for the a-axis, and 39 to $46x10^{-7}/°C$ for the c-axis.

Axial thermal expansion behavior of compounds modified by Nb and Ta with +5 valence are characterized by a transition of lattice parameter at 600°C. The a-lattice parameters for both $NbZr(PO_4)_3$ and $TaZr(PO_4)_3$ compounds increase up to 600°C, but decrease above 600°C. Conversely, the c-axis decreases up to 600°C, but increases at temperatures above 600°C. Detailed axial thermal expansion values for the ternary modified compounds are summarized in Table 42.

4.4.2 Quarternary system

4.4.2.1 Solid solubility

To substitute for the Na^+ in the NZP structure, combinations of alkali-alkali, alkali-alkaline earth, and alkaline earth-alkaline earth elements have been considered. Among various combinations of alkali-alkali ions, two cases that of Rb^+-Cs^+ and that of Na^+-K^+ have shown complete solubility. In compounds substituted with Rb^+-K^+, only the composition $½Rb^+$-$½K^+$ has shown solubility, and other compositions $¾Rb^+$-$¼K^+$ and $¼Rb^+$-$¾K^+$ have not exhibited complete solubility.

Compounds substituted with a combination of one-half mole of alkali with one-quarter mole of alkaline earth ions have shown complete solubility for the case of combining large alkaline earth ions with small alkali ions; these are Ca^{2+}(1.04Å)-Na^+(0.98Å), Ba^{2+}(1.38Å)-Na^+(0.98Å), Ba^{2+}(1.38Å)-K^+(1.33Å), and Sr^{2+}(1.20Å)-Na^+(0.98Å)[116]. Compounds substituted with mixed alkaline earth ions

Table 42. Lattice parameters and axial thermal expansion coefficients for the systems with low CTE

Compound	Lattice parameter (Å at 25°C)		Axial CTE ($\times 10^{-7}$/°C)		$\Delta\alpha$ ($\lvert\alpha_c - \alpha_a\rvert$)	Temperature Range
	a_0	c_0	α_a	α_c	($\times 10^{-7}$/°C)	(°C)
$RbZr_2(PO_4)_3$	8.65	24.43	-12	30	42	R.T.-1400
$CsZr_2(PO_4)_3$	8.58	24.96	-9	23	32	R.T.-1400
$MgZr_4(PO_4)_6$	8.90	21.84	-22	58	80	R.T.-1400
$CaZr_4(PO_4)_6$	8.78	22.69	-38	79	117	R.T.-1400
$BaZr_4(PO_4)_6$	8.59	23.89	-67	279	346	R.T.-1400
$MnZr_4(PO_4)_6$	8.88	21.81	-96	250	346	R.T.-1400
$NiZr_4(PO_4)_6$	8.42	23.15	-89	188	277	R.T.-1400
$YZr_6(PO_4)_9$	8.29	24.75	-31	46	77	R.T.-1400
$TiZr_8(PO_4)_{12}$	8.25	24.69	-30	44	74	R.T.-1400
$CeZr_8(PO_4)_{12}$	8.31	24.75	-29	39	68	R.T.-1400
$NbZr(PO_4)_3$	8.25	23.92	24	-61	85	R.T.-600
			-25	79	104	600-1400
$TaZr(PO_4)_3$	8.39	23.85	38	-36	74	R.T.-600
			-35	78	113	600-1400

have shown solubility irrespective of the ionic size differences of the two elements selected.

4.4.2.2 Linear thermal expansion

Linear thermal expansion measurements have been conducted for the systems showing a single phase. Systems modified by Rb-Cs have shown very low linear α values ranging from -2 to $2x10^{-7}/°C$, and the $Rb_{0.5}Cs_{0.5}Zr_2(PO_4)_3$ compound has exhibited an average linear α value very close to zero; i.e. $-0.3x10^{-7}/°C$. That has turned out to be the closest value to zero among all the compounds studied.

The linear thermal expansion behavior of systems modified by alkali with alkaline earth elements has been characterized by a sudden decrease above 900°C or 950°C. In the systems substituted by mixed alkaline earth ions, that with smaller ionic size difference(0.16Å for Ca-Sr) exhibited a lower expansion value than the system with larger ionic size difference(0.34Å for Ca-Ba). Except for the Rb-Cs modified system, $Mg_{0.5}Ca_{0.5}Zr_4(PO_4)_6$ has shown the closest value to zero among the compounds having negative expansion, i.e. $-5x10^{-7}/°C$. Detailed linear thermal expansion results for the quarternary NZP compounds are summarized in Table 43.

4.4.2.3 Axial thermal expansion

$Rb_{0.5}Cs_{0.5}Zr_2(PO_4)_3$ has shown axial α values of $-11x10^{-7}/°C$ for the a-axis and $21x10^{-7}/°C$ for the c-axis, and the difference of two($\Delta\alpha$) is the same as that of $CsZr_2(PO_4)_3$, which has the lowest $\Delta\alpha$ value. Axial thermal expansion behavior of

Table 43. Linear thermal expansion results for the quarternary NZP-modified compounds

Sample No	Phase	Linear CTE	
		$\alpha(x10^{-7}/^{\circ}C)$	Temp.Range($^{\circ}C$)
JK-RC1	$RbCs_3Zr_8(PO_4)_{12}$	2	R.T.-1000
JK-RC2	$RbCsZr_4(PO_4)_6$	-0.3	R.T.-1000
JK-RC3	$Rb_3CsZr_8(PO_4)_{12}$	-2	R.T.-1000
JK-RK2	$RbKZr_4(PO_4)_6$	-15	R.T.-1000
JK-BKM	$BaK_2Zr_8(PO_4)_{12}$	-7	R.T.-950
JK-CNM	$CaNa_2Zr_8(PO_4)_{12}$	1	R.T.-900
JK-BNM	$BaNa_2Zr_8(PO_4)_{12}$	-17	R.T.-900
JK-CNM4	$CaNa_6Zr_{16}(PO_4)_{24}$	-51	R.T.-900
JK-CNMC	$Ca_3Na_2Zr_{16}(PO_4)_{24}$	-23	R.T.-900
JK-MCC	$CaMgZr_8(PO_4)_{12}$	-5	R.T.-1000
JK-CSC	$CaSrZr_8(PO_4)_{12}$	13	R.T.-1000
JK-CBC	$CaBaZr_8(PO_4)_{12}$	37	R.T.-900
JK-CMCC	$Ca_3MgZr_{16}(PO_4)_{24}$	-10	R.T.-1000
JK-MSC	$MgSrZr_8(PO_4)_{12}$	18	R.T.-1000
JK-MBC	$MgBaZr_8(PO_4)_{12}$	20	R.T.-1000
JK-BSC	$BaSrZr_8(PO_4)_{12}$	32	R.T.-950

Ca-Mg modified NZP-type quarternary compounds have been characterized by a transition at 600°C. Detailed values are summarized in Table 44.

4.4.2.4 Secondary material property characterization and statistical analysis

Secondary material properties for the compounds $Rb_{0.5}Cs_{0.5}Zr_2(PO_4)_3$ and $Ca_{0.5}Mg_{0.5}Zr_4(PO_4)_6$ with the linear α values of -0.3×10^{-7}/°C and -5×10^{-7}/°C, respectively, have been characterized and are summarized in Table 45. High %TD and MOR, low %open porosity, and better thermal shock resistance have been obtained for $Rb_{0.5}Cs_{0.5}Zr_2(PO_4)_3$. Meanwhile, $Ca_{0.5}Mg_{0.5}Zr_4(PO_4)_6$ has shown long-term thermal stability after 96hrs at 1400°C.

Lot-to-lot variability and replicate-test variability for the $Ca_{0.5}Mg_{0.5}Zr_4(PO_4)_6$ compound have been calculated, and the values of standard deviation have been obtained as follows: 0.72×10^{-7}/°C for the lot-to-lot, and 1.78×10^{-7}/°C for the replicate test. A t-value and an F-value have been calculated from the observed values for the lot-to-lot & the replicate test and are resulted in -3.69 for the t-value and 0.027 for the F-value.

4.4.3 Quinternary system

4.4.3.1 Solid solubility and linear thermal expansion

Three compositions with different mole ratios based on Na_2O-MgO-CaO-ZrO_2-P_2O_5 system have been considered, and only one compound

Table 44. Lattice parameters and axial thermal expansion coefficients for the quarternary compounds

Compound	Lattice parameter (Å at 25°C)		Axial CTE ($\times 10^{-7}$/°C)			Temperature Range (°C)
	a_o	c_o	α_a	α_c	$\alpha_c - \alpha_a$	
$Rb_{0.5}Cs_{0.5}Zr_2(PO_4)_3$	8.62	24.69	-11	21	32	RT-1400
$Ca_{0.5}Mg_{0.5}Zr_4(PO_4)_6$	8.79	22.65	-39	66	105	RT-600
			-14	47	61	600-1400
$(3/8Ca1/8Mg)Zr_2(PO_4)_3$	8.79	22.64	-47	81	128	RT-600
			-18	67	85	600-1400

Table 45. Comparison between (½Ca½Mg)$Zr_4(PO_4)_6$ and (½Rb½Cs)$Zr_2(PO_4)_3$

Material Properties		$Ca_{0.5}Mg_{0.5}Zr_4(PO_4)_6$	$Rb_{0.5}Cs_{0.5}Zr_2(PO_4)_3$
Structural Attributes	Density(g/cm^3)	3.101	3.203
	%Shrinkage	10.6	12.5
	%TD	94.1	95.9
	%Open Porosity	4.5	3.4
	%Water Absorption	1.41	1.03
Maximum Temp. Difference($^\circ C$)		1475	>1625*
Allowable Repeated Quench with $\Delta T=1200^\circ C$		5 times	>20 times**
MOR (MPa)	3-point	23.13	52.71
	4-point	21.48	49.14
Fractography		Transgranular Relatively Rough Hackle-type mark	Intergranular Relatively Smooth Rib mark
Long-term thermal stability after 96hrs at $1400^\circ C$		Remained same structure	Decomposed to Raw materials
Microstructure		coarse	Finer&more spherical

*,**:Refer to Table 35.

$Ca_{0.0625}Mg_{0.0625}Na_{0.75}Zr_2(PO_4)_3$ has shown complete solubility. Linear thermal expansion of $Ca_{0.0625}Mg_{0.0625}Na_{0.75}Zr_2(PO_4)_3$ has been evaluated as $-25 \times 10^{-7}/°C$.

Chapter V

Discussion

Most of the conventional low thermal expansion materials have some deficiencies which limit their use and application[126]. Lithium-alumino-silicate(LAS) has a limited range of use, owing to its low melting temperature[5,6]. In the case of aluminum titanate, it exhibits structural instability(decomposition into rutile and corundum) below 1300°C[127]. Vitreous silica goes through devitrification when held at higher temperatures, resulting in cristobalite formation[2]. Recent work[21,22] has identified NZP and its crystal structural analogs as a family of materials with a potential for low thermal expansion.

The purpose of this study was to synthesize new low thermal expansion materials based on NZP-type structure. Their thermal expansion values have been measured, and the structural stability has been evaluated by room and high temperature XRD, and a thermal expansion run for the stable range of ionic substitution. Linear and axial thermal expansion behavior have been investigated and presented with the analysis of factors affecting thermal expansion. Secondary material property

characterization has been focused on two compounds, $Ca_{0.5}Mg_{0.5}Zr_4(PO_4)_6$ and $Rb_{0.5}Cs_{0.5}Zr_2(PO_4)_3$, with the linear α values of -5×10^{-7}/°C and -0.3×10^{-7}/°C, respectively.

5.1 Structural analysis of NZP-type compounds synthesized

This section provides the structural analysis of the various NZP-type compounds synthesized. It includes the range of ionic substitutions for ternary & quarternary compounds and the effect of substitution elements on lattice parameters.

5.1.1 The range of ionic substitution

5.1.1.1 Ternary compounds

Among twenty-five different ternary compounds substituted with elements with +1 to +5 electron valence, only one compound showed a monoclinic structure at room temperature. It was due to the lowering of symmetry to monoclinic by a small ionic substitution of Li(0.68Å). Except for $LiZr_2(PO_4)_3$, other systems showed an isostructure with $NaZr_2(PO_4)_3$, which has a $R\bar{3}C$(hexagonal) structure[96]. However, even in compounds showing a NZP structure at R.T., the instability of the structure was noted in many systems substituted by transition elements with +2(Mn, Ni, Cu,

and Zn), +3(Y, La, Al, and Cr), +4(Ti, Zr, Hf, Si, and Ce), and +5(V, Nb, and Ta) electron valences, as well as with Mg(from alkaline-earth group) with a very small radius of 0.74Å. The instability of the structure was confirmed by high temperature XRD analysis and by its linear thermal expansion behavior.

All of the systems with a phase instability exhibited a change of diffraction intensity during a high temperature XRD run which can be associated with the texturing[108] or order-disorder transition[123]. One example showing a phase instability at a high temperature, the $MnZr_4(PO_4)_6$ system, is shown in Figures 37 and 38 and given in Tables 46 and 47, in comparison with the $RbZr_2(PO_4)_3$ compound which is considered to be stable.

Figures 37 and 38 show the diffraction peaks of $RbZr_2(PO_4)_3$ & $MnZr_4(PO_4)_6$ at room temperature and 1400°C, respectively. Diffraction patterns of $RbZr_2(PO_4)_3$ at R.T. exhibited the five major peaks of (110), (113), (024), (116), and (300); however, at 1400°C one more diffraction peak of (205) was observed with other intensity-reduced diffraction peaks investigated at R.T., but still held almost the same relative intensity ratios. Detailed comparisons of the diffraction intensities for the five major peaks are summarized in Table 46.

Five major peaks and (212) with strong intensity were shown for $MnZr_4(PO_4)_6$ at R.T., but at 1400°C, the diffraction intensities of the peaks were lowered significantly, and relative intensity ratios changed; furthermore many other peaks appeared, including (111), (112), (114). Meanwhile, the (212) peak disappeared. Detailed diffraction intensities are compared in Table 47. Discussions will be presented based on the characteristic of $R\bar{3}C$ structure and size and valence of ions selected.

Looking over the $R\bar{3}C$ structure reviewed in section 2.2.1, there exist six general positions: 6(a) & (b), 12(c), 18(d) & (e), 36(f). It is known that $NaZr_2(PO_4)_3$ occupies 12(c), 18(e), 6(b) and 36(f) in the unit cell[98], leaving the two other general positions

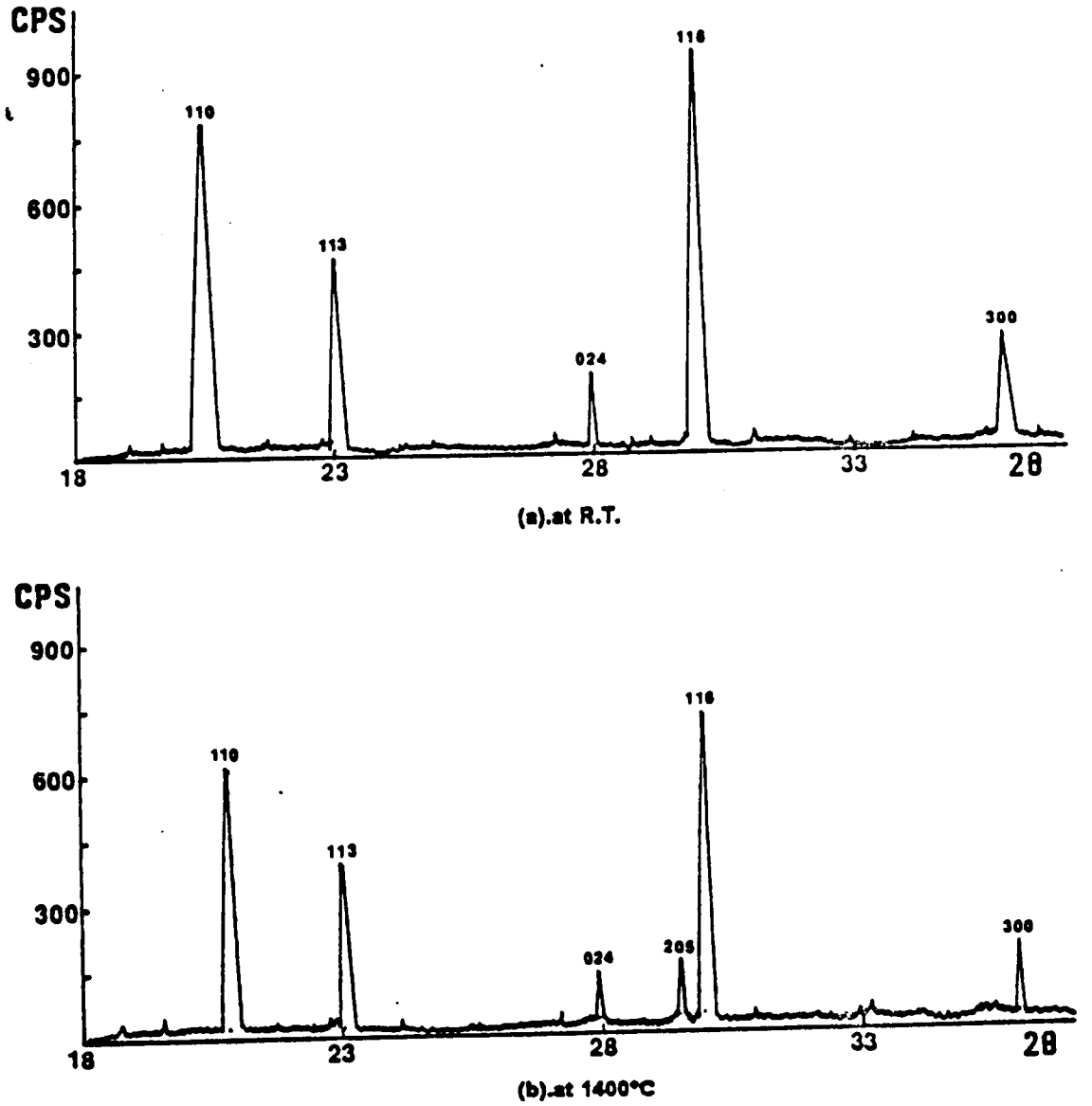

Figure 37. Diffraction pattern of $RbZr_2(PO_4)_3$ at R.T. and 1400°C

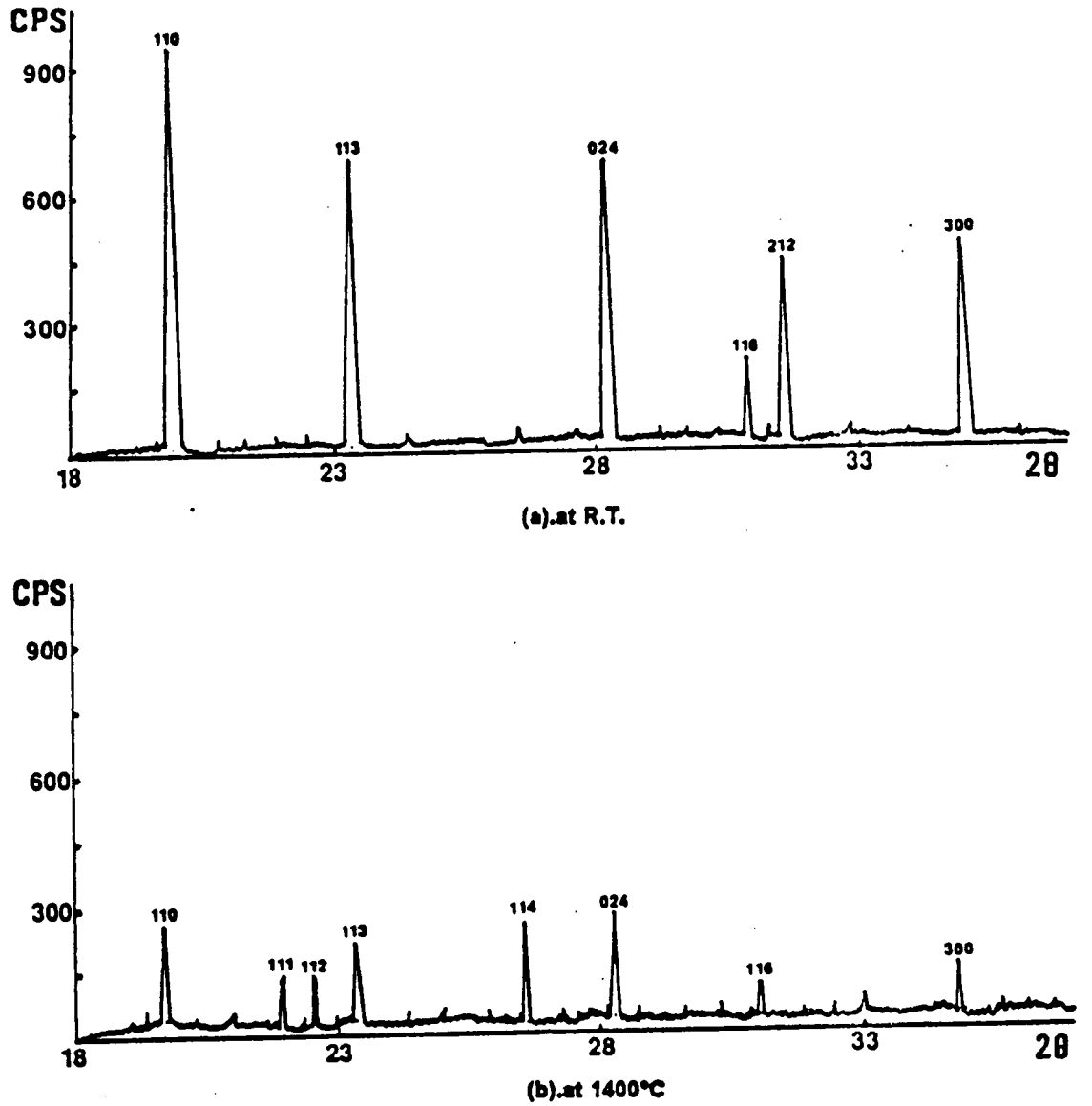

Figure 38. Diffraction pattern of $MnZr_4(PO_4)_6$ at R.T. and 1400°C

Table 46. Comparison of diffraction intensities of $RbZr_2(PO_4)_3$ for the selected planes at R.T. and 1400°C

Temperature (°C)	Diffraction Intensity[CPM(counts per minute)]					
	(110)	(113)	(024)	(205)	(116)	(300)
R.T.	42527	24517	9586	-	53538	15979
1400	39391	25100	7685	9091	45922	12988

Table 47. Comparison of diffraction intensities of $MnZr_4(PO_4)_6$ for the selected planes at R.T. and 1400°C

Temperature (°C)	Diffraction Intensity(CPM)								
	(110)	(111)	(112)	(113)	(114)	(024)	(116)	(212)	(300)
R.T.	52541	-	-	35021	-	29723	11544	25117	23116
1400	9665	7836	8302	9747	10487	15551	6004	-	7476

as vacancies. Other studies[22,36,37,43,48] show extra Na cations occupying the site of M_{II}(shown in Figure 2), which corresponds to the position of 18(e)[38]. Elements substituted by +2, +3, or +4 create vacancies of one-half, one-third, or one-quarter of the Na ion positions, respectively. Also, for the systems with +5 cation valence, elements with +5 valence substitute for Zr^{+4} randomly and create vacancies in place of Na ions. The complex and open structure of NZP might make it possible to locate elements with +2 or more valence in the M_{II} or other positions instead of Na position(6b). This explanation may clarify the change of diffraction intensity owing to the atomic movement investigated in some of the systems substituted with transition elements with +2 valence, elements with +3, +4, +5 valence, and Mg.

Ionic radii for the elements selected in this study to replace Na are summarized in Table 48, and those values are based on a coordination number of 6. According to the relation of structure to ionic radius suggested by Roy[128], the Gibbs free energy is expressed as follows:

$$G = U + PV + \frac{1}{2}hv - TS \quad (5.1)$$

Thus, free energy = lattice energy + terms which are very small at low P and T. Moreover, at low temperatures and pressures, G≃U; i.e., the lattice energy determines which structure will form. Lattice energy of an ionic crystal can be written from Born-Mayer's[129] treatment and Kapustinski's[128] approximations leading to a formulation of the type.

$$\textit{Lattice energy of an ionic crystal } U = \frac{constant}{r_{cation} + r_{anion}} \quad (5.2)$$

Therefore, ionic radius is the crucial factor to determine whether the structure is stable or not.

Table 48. Ionic radii of elements selected to modify NZP structure (summarized from Ref.116)

Elements with +1 valence	Ionic Radii (Å)	Elements with +2 valence	Ionic Radii (Å)	Elements with +3 valence	Ionic Radii (Å)	Elements with +4 valence	Ionic Radii (Å)	Elements with +5 valence	Ionic Radii (Å)
Li	0.68	Mg	0.74	Y	0.97	Ti	0.64	V	0.4
Na	0.98	Ca	1.04	La	1.04	Zr	0.82	Nb	0.66
K	1.33	Sr	1.20	Al	0.57	Hf	0.82	Ta	0.66
Rb	1.49	Ba	1.20	Cr	0.64	Si	0.39		
Cs	1.65	Mn	0.91			Ce	0.88		
		Ni	0.74						
		Cu	0.80						
		Zn	0.83						

Finally, it can be said that the range of ionic substitution to make ternary NZP-type compounds instead of Na are available for the elements selected from +1 to +5. However, only seven elements, Na,K,Rb,Cs,Ca,Sr,Ba, having ionic radius greater than 0.98Å but one exception for La(1.04Å), formed the stable structure without changing its skeletal framework and without changing the atomic positions, coming from the atomic movement of substituted elements up to a high temperature(1000°C for linear α and 1400°C for axial α measurements) applied in this study.

5.1.1.2 Quarternary and quinternary compounds

As for the basic ternary systems, seven compounds (modified by Na,K,Rb,Cs,Ca,Sr,Ba) showing stability have been selected, and their substitutional solid solution studies using alkali, alkaline earth elements with various combinations of moles, have been considered for the quarternary systems. Several combinations of Ca-Mg-Na have been selected for the quinternary compound formation. From the experimental results of the solid solubility for the quarternary and quinternary systems to modify the NZP-type structure, the following results are summarized and tabulated in Table 49.

For the systems substituted by alkali-alkali elements, Rb-Cs and Na-K combined systems showed complete solubility, exhibiting ionic size differences of 9.7% and 26.3%, respectively. However, in systems combined by Rb-K, only one combination of ½Rb-½K exhibited solubility, even though it had a smaller ionic difference(10.7%) than that of Na-K(26.3%).

Among the systems substituted with one-half mole of an alkali element and one-quarter mole of an alkaline earth element, the combinations of large alkaline

Table 49. Systems showing solid-solubility among quarternary & quinternary compounds considered

System	Ionic Size Difference of elements substituted	System	Ionic Size Difference of elements substituted
$Rb_{0.5}K_{0.5}Zr_2(PO_4)_3$	10.7%	$Ba_{0.25}K_{0.5}Zr_2(PO_4)_3$	3.6%
$Rb_{0.25}Cs_{0.75}Zr_2(PO_4)_3$	9.7%	$Sr_{0.25}Na_{0.5}Zr_2(PO_4)_3$	18.3%
$Rb_{0.5}Cs_{0.5}Zr_2(PO_4)_3$	9.7%	$Mg_{0.25}Ca_{0.25}Zr_2(PO_4)_3$	28.8%
$Rb_{0.75}Cs_{0.25}Zr_2(PO_4)_3$	9.7%	$Mg_{0.125}Ca_{0.375}Zr_2(PO_4)_3$	28.8%
$Na_{0.25}K_{0.75}Zr_2(PO_4)_3$	26.3%	$Mg_{0.25}Sr_{0.25}Zr_2(PO_4)_3$	38.3%
$Na_{0.5}K_{0.5}Zr_2(PO_4)_3$	26.3%	$Mg_{0.25}Ba_{0.25}Zr_2(PO_4)_3$	46.4%
$Na_{0.75}K_{0.25}Zr_2(PO_4)_3$	26.3%	$Ca_{0.25}Sr_{0.25}Zr_2(PO_4)_3$	13.3%
$Ca_{0.25}Na_{0.5}Zr_2(PO_4)_3$	5.8%	$Ca_{0.25}Ba_{0.25}Zr_2(PO_4)_3$	24.6%
$Ca_{0.125}Na_{0.75}Zr_2(PO_4)_3$	5.8%	$Ba_{0.25}Sr_{0.25}Zr_2(PO_4)_3$	13.0%
$Ca_{0.375}Na_{0.25}Zr_2(PO_4)_3$	5.8%	(1/16Ca1/16Mg3/4Na)· $Zr_2(PO_4)_3$	28.8%
$Ba_{0.25}Na_{0.5}Zr_2(PO_4)_3$	29.0%		

earth elements and small alkali elements showed complete solubility. Other mole combinations of ⅛Ca-¾Na and ⅜Ca-¼Na also supported the solubility trend observed in this finding.

Combinations of alkaline earth and other alkaline earth elements with one-quarter mole for each component showed solid solubility irrespective of ionic size difference, even with largest 46.4%(Mg-Ba). Meanwhile, the ⅜Ca-⅛Mg combination showed solubility, but ⅛Ca-⅜Mg(from Table 26) was not completely soluble. This might be explained from the instability of the ternary compound $MgZr_4(PO_4)_6$, because the combination of a higher concentration of Mg compared with the concentration of Ca showed a separation into two phases.

That result also can be extended to the quinternary system of $CaO\text{-}MgO\text{-}Na_2O\text{-}ZrO_2\text{-}P_2O_5$. For the system with a higher mole percent of Mg($\frac{1}{8}Mg, \frac{3}{16}Mg$) (from Table 39), two phases were obtained, but system with the smallest amount of Mg($\frac{1}{16}Mg$) showed complete solubility.

Generally solid solutions are stable when the mixed crystal has a lower free energy than the formation of two crystals of different composition or the formation of a new structure in which the foreign atoms are put on ordered sites[123]. The free energy is given by the relation

$$G = E + PV - TS \quad (5.3)$$

where E is largely determined by the structural energy and entropy is a measure of the randomness(probability) of the structure. If an atom added at random greatly increases the structural energy, the solid solution is unstable and two crystal structures result. On the other hand, if the addition of a foreign atom greatly lowers the structural energy, the system tends to form an ordered new phase.

The physical reason for ordering reactions is an interaction between atoms which constitute a solid solution[130]. When the typical value of the interaction energy is much larger than the thermal energy, the mutual positions of the atoms are determined from the internal energy minimum condition. The minimum of the internal energy in ordering alloys is attained if the periodical alternating of the different kinds of atoms arises, i.e., if an ordered phase is formed. For example, it takes place when the lowest energy corresponds to configurations in which each atom is surrounded by the other kinds of atoms.

Systems showing a single phase had extra diffraction peaks which might be coming from the ordering behavior. A relationship has already been developed between the static concentration waves generating the atomic distribution in an ordered phase and the X-ray diffraction pattern, showing more diffraction peaks due to superlattice reflections[130]. Therefore, it can be said that the trend approaching a solid solution in the NZP-type quarternary and quinternary systems is related to the ionic size difference as well as the tendency to make a more ordered structure.

5.1.2 The effect of substitution on lattice parameters

Lattice parameter measurements have been made for the selected systems using XRD with the maximum accuracy of 0.0005nm at room temperature. In Table 50, their lattice parameters for the systems considered are summarized with the value of ionic size of elements selected to substitute for the Na cation in the NZP-type structure.

Even though Na^+ is not included in its structure along the a-axis, as indicated by previous reports[22,25], the change in the lattice parameters by replacing other

Table 50. Lattice parameters & ionic radii of systems considered

System	Lattice Parameters(Å at R.T.)		Ionic Radius of Elements Substituted(Å)
	a-axis	c-axis	
$RbZr_2(PO_4)_3$	8.65	24.43	1.49
$CsZr_2(PO_4)_3$	8.58	24.96	1.65
$MgZr_4(PO_4)_6$	8.90	21.84	0.74
$CaZr_4(PO_4)_6$	8.78	22.69	1.04
$BaZr_4(PO_4)_6$	8.59	23.89	1.38
$MnZr_4(PO_4)_6$	8.88	21.81	0.91
$NiZr_4(PO_4)_6$	8.42	23.15	0.74
$YZr_6(PO_4)_9$	8.29	24.75	0.97
$TiZr_8(PO_4)_{12}$	8.25	23.92	0.66
$CeZr_8(PO_4)_{12}$	8.31	24.75	0.88
$NbZr(PO_4)_3$	8.25	23.92	0.66
$TaZr(PO_4)_3$	8.39	23.85	0.66
$Rb_{0.5}Cs_{0.5}Zr_2(PO_4)_3$	8.62	24.69	1.49(Rb) & 1.65(Cs)
$Ca_{0.5}Mg_{0.5}Zr_4(PO_4)_6$	8.79	22.65	0.74(Mg) & 1.04(Ca)
$(3/8Ca1/8Mg)\cdot Zr_2(PO_4)_3$	8.79	22.64	0.74(Mg) & 1.04(Ca)

cations instead of Na is known to be affected in the a-axis as well as the c-axis, experimentally[19,22,25,26,33,51]. In addition, the general trend[51] observed in alkali element modified systems is that the structure expands in the c-direction but contracts in the a-direction by the substitution of large cations.

In alkali(Rb,Cs) and alkaline earth(Mg,Ca,Ba) modified systems, the larger the cation substituted, the larger the c-axis but the smaller the a-axis. For the systems substituted with transition elements(Mn,Ni), the trend is opposite that of alkali and alkaline earth modified systems, i.e., the larger the cation, the smaller the c-axis but the larger the a-axis. Systems substituted with elements with +4 electron valence(Ti,Ce) tended to show that the big cation substitution contributes to the increase of both the a- and c-axes. For the systems substituted with Nb and Ta with the same ionic size and +5 electron valence, they showed a little difference in the lattice parameters of the a- and c-axes.

The lattice parameters for the quarternary compounds substituted with Rb-Cs and Ca-Mg were measured between the values of their ternary compounds. Ternary compounds $RbZr_2(PO_4)_3$ and $CsZr_2(PO_4)_3$ had lattice parameters of 8.65Å and 8.58Å for the a-axis, and 24.43Å and 24.96Å for the c-axis, respectively. Meanwhile, the lattice parameters of $Rb_{0.5}Cs_{0.5}Zr_2(PO_4)_3$ were calculated as 8.62Å and 24.69Å for the a- and c-axes, respectively. A similar tendency for the Ca-Mg modified quarternary compounds with the Rb-Cs modified compounds was investigated as well.

Figure 39 shows a plot of the c-axis versus the a-axis for the ternary systems considered. The dotted zone represents the systems having phase and structure stability discussed in section 5.2.1.1. Additionally, the lattice parameters for $NaZr_2(PO_4)_3$, $KZr_2(PO_4)_3$, and $SrZr_4(PO_4)_6$, known to be stable phases, are cited in other work[25,26,131], and the results are plotted in Figure 39 and summarized in Table 51 with other data. The lattice parameters of systems showing phase stability

in NZP-type ternary compounds range from 8.58Å to 8.80Å for the a-axis, and from 22.69Å to 24.96Å for the c-axis.

From Figure 39 and Table 51, the results of this study show a good correlation with other reported data, showing a decrease of the a-axis and an increase of the c-axis with large cation substitutions. Also the lattice parameter of the c-axis including octahedra, consisting of substitution elements and oxygen, turned out to be dependent on the ionic size of substituted elements irrespective of the electron valences of +1 and +2. Vacancies formed by the substitution of elements with +2 electron valence did not greatly affect the lattice parameter of the c-axis. This means that Ca, Sr, and Ba atoms easily replaced half of the position of the Na cation in the NZP structure without changing its skeletal framework, thereby maintaining the equilibrium state.

5.2 Thermal expansion behavior

5.2.1 Linear thermal expansion behavior investigated in NZP-type compounds

The linear thermal expansion behavior of NZP-type modified systems showed different trends with the different substitution elements. Excluding the systems showing sudden changes of thermal expansion, the linear aggregate thermal expansion behavior investigated in this study can be classified into three categories: neg-

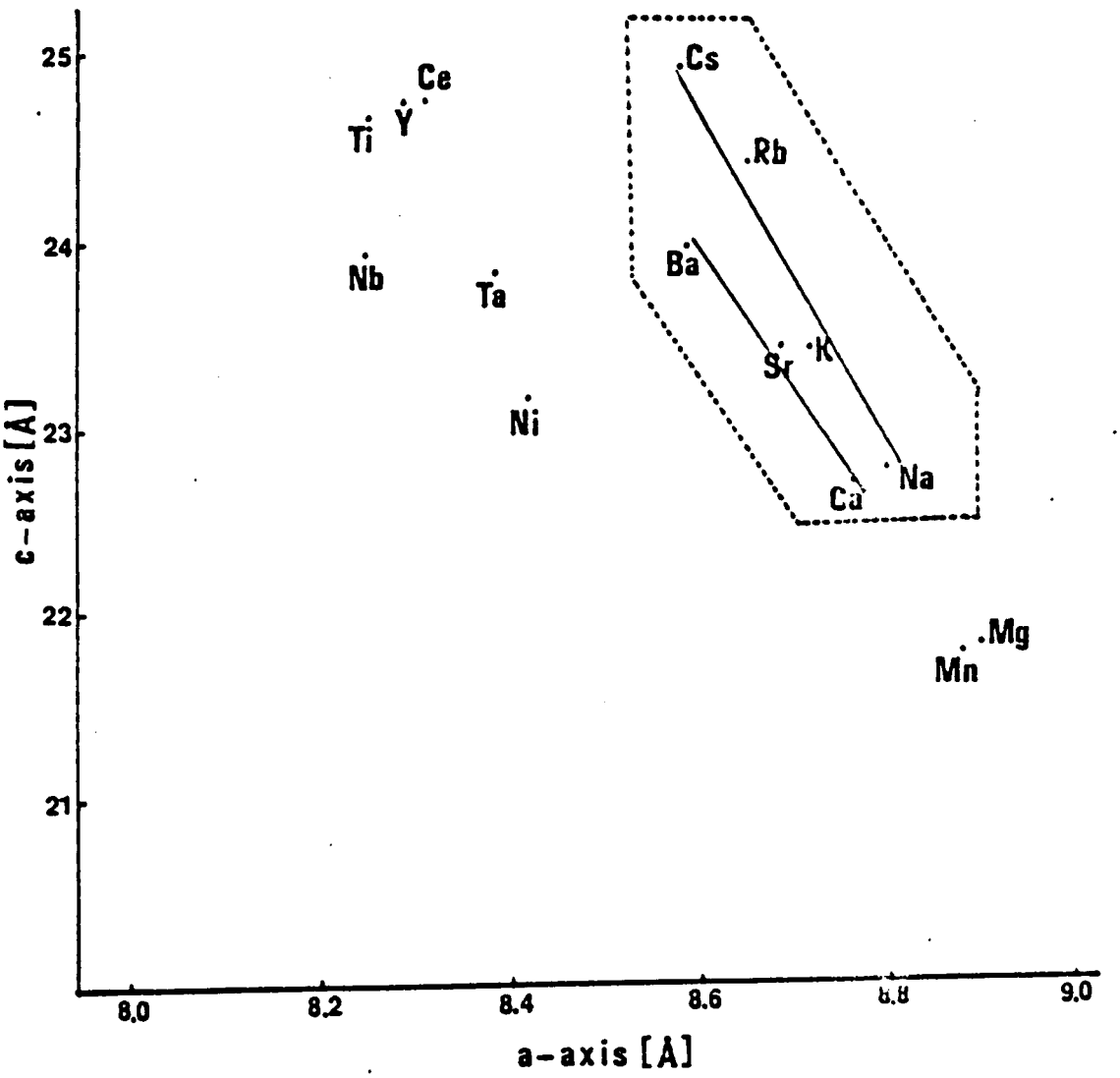

Figure 39. **Plot of lattice parameters c versus a for $MZr_2(PO_4)_3$:** where M = Li, K, Rb, Cs, ½Mg, ½Ca, ½Sr, and ½Ba [$KZr_2(PO_4)_3$; taken from Ref.26, $NaZr_2(PO_4)_3$; taken from Ref.25, and $SrZr_4(PO_4)_6$; taken from Ref.131]

Table 51. Lattice parameters for the systems showing phase stability in NZP-type ternary compounds

System	Lattice Parameters(Å at R.T.)		Ionic Radius of Elements substituted(Å)
	a-axis	c-axis	
*$NaZr_2(PO_4)_3$	8.80	22.76	0.98
**$KZr_2(PO_4)_3$	8.71	23.89	1.33
$RbZr_2(PO_4)_3$	8.65	24.43	1.49
$CsZr_2(PO_4)_3$	8.58	24.96	1.65
$CaZr_4(PO_4)_6$	8.78	22.69	1.04
+$SrZr_4(PO_4)_6$	8.69	23.39	1.20
$BaZr_4(PO_4)_6$	8.59	23.89	1.38

*:Referred from Ref.25

**:Referred from Ref.26

+:Referred from Ref.131

ative, positive, and transition(from negative to positive). Table 52 shows those categories classified by the substitution elements.

Most of the substitutional elements tended to promote positive thermal expansion. However, elements such as Li, Na, K, and Ca tended to contract their sintered bodies, and combinations of elements, including Na, K, or Ca also resulted in negative linear expansions.

Two exceptions combined by ¼Ca-¼Ba and ¼Ca-¼Sr including Ca were obtained to show positive behavior, which can be considered from the effect of Ba and Sr. Other exceptions were investigated for the systems combined by Ca-Mg(¼Ca-¼Mg and ⅜Ca-⅛Mg), exhibiting the transition at around 600°C.

Substitution of Rb, Cs, or combinations of Rb and Cs which led to low linear α values also resulted in the transition from negative to positive at around 500°C. Moreover, the transition elements of Ni and Zn showing low linear aggregate α values of 10×10^{-7}/°C and 5×10^{-7}/°C, respectively, exhibited the transition at about 500°C.

The expansion of a three-dimensional framework can be considered the sum of a bond-length expansion and a tilting effect[66]. The apparent thermal expansions of bonds between the individual atoms and oxygen resulted from both the stretching of the bond length[22], which is related to the strength of the chemical bond, and the changing of the bond angle with rising temperature: the apparent thermal expansion coefficients for several metal-oxygen bonds were empirically determined by Hazen et al[132]. Tilting of polyhedra is restricted to the direction of channels[133]. The more restricted the tilt is in the direction of the channel, the smaller the thermal expansion.

In the $NaZr_2(PO_4)_3$ system, the thermal expansions of sodium, zirconium, and phosphorus cation coordination polyhedra were observed by Hazen et al as 108, 0.0, and -2.3(all $\times10^{-7}$/°C), respectively[52]. They claim that the large thermal expansion

Table 52. Effect of substitution elements on thermal expansion

Linear CTE Behavior	Substitution Elements
Positive	1/2Mg, 1/2Ba, 1/2Sr, 1/2Cu, 1/2Mn, 1/3Cr, 1/3Y, 1/3Al, 1/4Zr, 1/4Si, 1/4Hf, 1/4Ce, 1/4Ti, Ta, Nb, V, (1/4Ca-1/4Ba), (1/4Ca-1/4Sr), (1/4Ba-1/4Sr), (1/4Mg-1/4Ba), (1/4Mg-1/4Sr)
Negative	Li, Na, K, 1/2Ca, (1/2K-1/2Rb), (1/2K-1/4Ba), (1/2Na-1/4Ba), (1/2Na-1/4Ca), (1/8Ca-3/4Na), (3/8Ca-1/4Na), (1/8Na-1/16Ca-1/16Mg)
Transition	Rb, Cs, (1/4Rb-3/4Cs), (1/2Rb-1/2Cs), (3/4Rb-1/4Cs), 1/2Ni, 1/2Zn, (1/4Ca-1/4Mg), (3/8Ca-1/8Mg)

of the sodium site is offset by rotations in the Zr-P polyhedral framework, thus yielding the low net expansion of NZP.

The findings of this study showing anomalous thermal expansion behavior are correlated with the different trends of substituted cation coordination polyhedra and rotations of polyhedra in the Zr-P framework with rising temperatures. In particular, systems showing negative expansion are also related to the compression mechanism of ceramic-type materials which can be described as bond compression and bond angle bending[67].

In crystalline solids, the unit-cell equilibrium theory, based on thermodynamics and lattice-dynamics, might be used as the general mechanism to interpret most of the trends occurring in thermal expansion behavior. As the temperature increases, the amplitude of the vibration of the individual atoms increases. The free energy of the crystal is no longer minimal for the vibrations around the assumed equilibrium configuration; hence the crystal will expand or contract until it reaches a volume where the free energy is minimized at a certain temperature.

5.2.2 Correlation between linear α & axial α

The axial α data and linear α values up to 1000°C are summarized in Table 53, and the ratios of axial α values along a- & c-axes are also included. Except for the $NbZr(PO_4)_3$ and $TaZr(PO_4)_3$ systems, the c-axis expanded with increasing temperature while the a-axis contracted. As reviewed earlier[22,52,58], the positive thermal expansion of the c-axis strains the PO_4 tetrahedra bridge linking the $O_3ZrO_3MO_3ZrO_3$ groups(where M represents the substituted cation) in the direction of the c-axis, so that the O-P-O bond angles spread in the direction of the c-axis. Consequently, the

PO_4 tetrahedra contracted in the direction normal to this spreading, and the α_a actually became negative, which affected the expansion of the c-axis.

Systems substituted by Rb and Cs having very low anisotropy showed good agreement between calculated average α from axial α values and linear measured α, considering the experimental error and the accuracy of equation $(\alpha_l = \frac{2}{3}\alpha_a + \frac{1}{3}\alpha_c)$ [19] for the hexagonal system.

Systems classified as having phase instability in sections 5.2.1.1 and 5.2.2, i.e., $MgZr_4(PO_4)_6$, $YZr_6(PO_4)_9$, $TiZr_8(PO_4)_{12}$, and $CeZr_8(PO_4)_{12}$, exhibited a great difference up to $29x10^{-7}/°C$ between the calculated and measured linear α. Evidently, the inconsistency of those data results from the atomic movement due to phase instability and the effect of ZnO added to aid sintering, because the powders investigated in high temperature XRD did not include the zinc oxide(ZnO).

However, in systems of $MnZr_4(PO_4)_6$ and $NiZr_4(PO_4)_6$, also confirmed as having an unstable phase, a relatively good correlation was obtained for the relationship between the calculated linear α and the measured linear α. Their phase instability became evident above 1000°C, as seen in Figures 15 and 16 showing the axial thermal expansion behavior of these systems.

System $BaZr_4(PO_4)_6$, showing the largest anisotropy $(\Delta\alpha(\alpha_c - \alpha_a) = 346x10^{-7}/°C)$ and the biggest anisotropy ratio(4.16), exhibited a large decrease in measured linear thermal expansion compared with that calculated. It may be attributed to the lowering of the thermal expansion due to the microcracking, which can result from the large thermal expansion anisotropy verified in many articles theoretically[117,118,134,135] and experimentally[22,94,95,136,137].

The linear thermal expansion of $CaZr_4(PO_4)_6$ system was measured as $-18x10^{-7}/°C$, reflecting a large decrease from the calculated linear thermal expansion. The only differences between the two different polycrystalline bodies of the measured

Table 53. Axial & linear CTE values for selected systems with low CTE

System	Axial CTE ($\times 10^{-7}/°C$)		Calculated	Measured	
	α_a	α_c	α_l ($\times 10^{-7}/°C$)	α_l ($\times 10^{-7}/°C$)	$\lvert\alpha_c/\alpha_a\rvert$
$RbZr_2(PO_4)_3$	-12	30	2	2	2.50
$CsZr_2(PO_4)_3$	-9	23	2	5	2.56
$MgZr_4(PO_4)_6$	-22	58	5	16	2.64
$CaZr_4(PO_4)_6$	-38	79	1	-18	2.08
$BaZr_4(PO_4)_6$	-67	279	45	15	4.16
$MnZr_4(PO_4)_6$	-51	112	3	7	2.20
$NiZr_4(PO_4)_6$	-70	172	10	10	2.46
$YZr_6(PO_4)_9$	-27	62	3	14	2.30
$TiZr_8(PO_4)_{12}$	-30	34	-9	20	1.13
$CeZr_8(PO_4)_{12}$	-35	57	-4	11	1.63
$NbZr(PO_4)_3$	24/-25	-61/79	-4/10	4	2.54/3.16
$TaZr(PO_4)_3$	38/-35	-35/78	13/1	11	0.92/2.23
$Rb_{0.5}Cs_{0.5}Zr_2(PO_4)_3$	-11	21	-0.3	-0.3	1.91
$Ca_{0.5}Mg_{0.5}Zr_4(PO_4)_6$	-39/-14	66/47	-4/6	-5	1.69/3.36
$(3/8Ca1/8Mg)Zr_2(PO_4)_3$	-47/-18	81/67	-4/10	-10	1.72/3.72

axial α and the linear α are the addition of ZnO and the sintering time applied. To explain this particular behavior, a close examination of crystallinity was done and will be presented in the subsequent section.

The systems substituted by +5 electron valence, i.e. $NbZr(PO_4)_3$ and $TaZr(PO_4)_3$, showed fairly good agreement between the calculated and measured linear α up to 1000°C, even though their axial thermal expansion behavior exhibited a transition characteristic at 600°C, which is shown in Figures 20 and 21. Their axial thermal expansion behavior might be explained by a order-disorder transition.

5.2.3 The effect of crystallinity on thermal expansion

Table 54 lists the measured linear α values for the sintered bar with ZnO and without ZnO, as well as the calculated linear thermal expansion value. The zinc oxide used to promote the sinterability, which is based on an ionic exchange mechanism[56] due to the similar ionic radius of Zn^{+2}(0.83Å)[116] and Zr^{+4}(0.82Å)[116], significantly affected thermal expansion of $CaZr_4(PO_4)_6$. Linear α for the sintered bar without ZnO was much closer to the calculated value. In addition, the difference($5x10^{-7}$/°C) between linear α without ZnO($-4x10^{-7}$/°C) and the calculated linear α($1x10^{-7}$/°C) is considered within the allowable range of experimental error.

The intensity of the peak/background for the sintered powders with/without ZnO are compared in Table 55, and X-ray diffraction patterns are shown in Figures 40(a) and (b). Five major peaks with above 1000 cps(counts per seconds) and one minor peak were selected to compare the diffracted intensity ratio of the peak/background; and those are (104), (110), (113), (024), (116) for the major peaks, and (015) for minor peak. The relative ratios of intensity for the powder with ZnO to that for the powder

Table 54. Measured & calculated linear CTE values for the $CaZr_4(PO_4)_6$ system

Linear CTE ($x10^{-7}/^{o}C$)	With ZnO	-18
	Without ZnO	-4
Calculated Linear CTE(from Table 53)		1

Table 55. Intensity ratio of peak/background for the sintered $CaZr_4(PO_4)_6$ with/without ZnO

Condition	Peak/ Background					
	(104)	(110)	(015)	(113)	(024)	(116)
With ZnO	2.419	2.703	1.534	3.036	2.749	3.173
Without ZnO	2.120	2.320	1.234	2.657	2.407	2.757

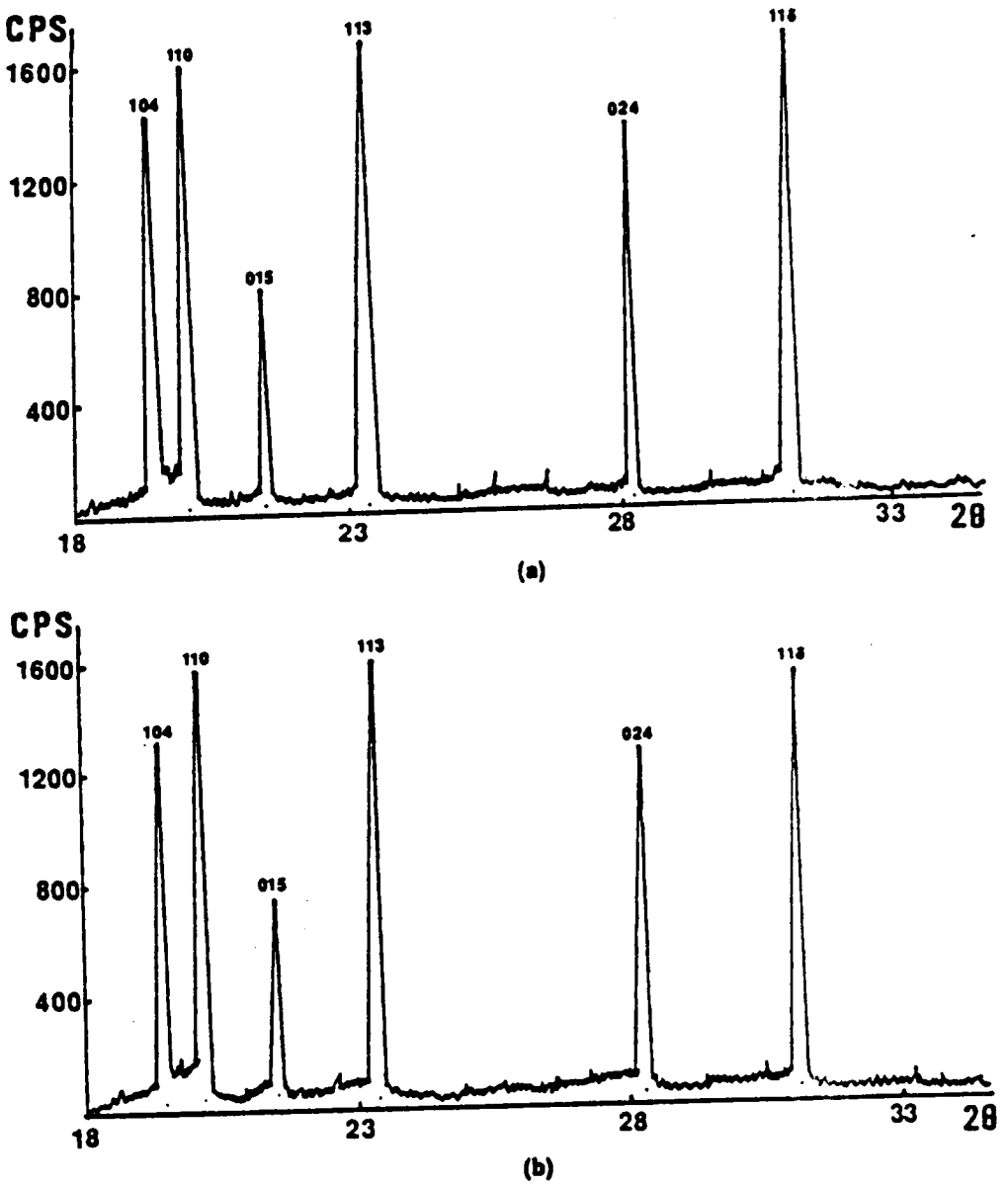

Figure 40. X-ray diffraction patterns for the sintered $CaZr_4(PO_4)_6$ with/without ZnO: (a).For the sintered powders without ZnO, (b).For the sintered powders with ZnO

without ZnO for the major peaks ranged from 0.858(for (110) plane) to 0.876(for (104) and (024) plane), with the average relative ratio being 0.871. It represents a decrease in crystallinity with the addition of ZnO in $CaZr_4(PO_4)_6$.

In powders without ZnO with better crystallinity, the minor peaks were found to be clearer than powders(with ZnO) with poorer crystallinity. The diffraction intensity of (015) for the powders with ZnO was decreased more than that of the expected value from the tendency observed in the major peaks; i.e., a 19.6% decrease compared with the reduction of 12.9% in the major peaks. Even for (202) and (205), which exist in samples without ZnO, diffracted peaks are not seen clearly in the powdered samples with ZnO.

From the above discussion, the crystallinity may be one of the factors affecting thermal expansion behavior, especially when considering complex systems like NZP structures. The finding of the effect of crystallinity on thermal expansion can be extended to explain the difference of linear thermal expansion results between this study and other reports.

Some of materials which used different processing methods in other articles[4,19,21,22,60] showed a large disparity of linear α values with this study, but most of the materials showed good agreement, as was described previously. $KZr_2(PO_4)_3$ is representatively included in the category which does not show a good correlation with the data determined in this study. Its thermal expansion was reported as $4x10^{-7}/°C$[22,60] by Oota et al. However, this study shows the linear α value for the $KZr_2(PO_4)_3$ as $-22x10^{-7}/°C$(from Table 9). The difference of the linear α value between this study and the previously reported value may be related to the change of crystallinity, which comes from the different processing techniques with the methods applied in other studies.

Finally, it can be said that the higher crystallinity enables polycrystalline bodies to have a thermal expansion close to the calculated linear thermal expansion from the axial α values, based on the analysis of $CaZr_4(PO_4)_6$ system.

5.3 Secondary material properties between (Ca-Mg) & (Rb-Cs) modified NZP-type systems

Secondary material properties have been characterized for the compounds of $Ca_{0.5}Mg_{0.5}Zr_4(PO_4)_6$ and $Rb_{0.5}Cs_{0.5}Zr_2(PO_4)_3$ with linear α values of $-5x10^{-7}$/°C and $-0.3x10^{-7}$/°C, respectively. The reason that these two compounds are selected lies in the negative thermal expansion coefficients being close to zero. If a ceramic body with negative expansion is subjected to a very rapid fall in its local temperature, it may be less dangerous because the outer skin of the body will be subjected to a compressive stress, which should have a smaller tendency to produce damage. Table 55 shows a comparison of the measured material properties between the two compounds.

The better thermal shock resistance obtained in $Rb_{0.5}Cs_{0.5}Zr_2(PO_4)_3$ can be considered due to the linear α value being closer to zero. The high MOR value of $Rb_{0.5}Cs_{0.5}Zr_2(PO_4)_3$ resulted from the small percentage open porosity, and the finer and more spherical grain distribution compared with that of $Ca_{0.5}Mg_{0.5}Zr_4(PO_4)_6$. However, being held at 1400°C for 96hrs, the $Rb_{0.5}Cs_{0.5}Zr_2(PO_4)_3$ compound decomposed to raw materials(Rb_2O, Cs_2O, and ZrO_2) which come from the dissociation of P_2O_5. On the other hand, even after the same treatment for $Ca_{0.5}Mg_{0.5}Zr_4(PO_4)_6$ it remained stable.

Therefore, for an application requiring a temperature close to 1400°C, it is recommended that $Ca_{0.5}Mg_{0.5}Zr_4(PO_4)_6$ be used.

Chapter VI

Conclusions

The purpose of this study was to develop new low thermal expansion materials by a novel method, expecting good thermal shock resistance for the application in ceramic diesel engines. The NZP structure was selected as the basic system and many possible modifications were conducted. The following findings can be summarized.

1. The use of P_2O_5 was helpful in synthesizing ZrO_2 free NZP-type compounds. Acetone served as a mineralizer as well as an aid in making homogeneous mixtures.

2. Even though the elements with electron valences from +1 to +5 were used to substitute for Na^+ in the NZP structure, only systems having lattice parameters from 8.58Å to 8.80Å for the a-axis/from 22.69Å to 24.96Å for the c-axis showed phase stability, possibly up to 1400°C in the ternary compounds.

3. It was found that solid solutions of NZP-type quarternary compounds could be readily formed from the following combinations: various combinations of Rb-Cs, Na-K, and ½Rb-½K for the alkali-alkali elements, large alkaline earth-small alkali elements, and various combinations of alkaline earth-alkaline earth elements.

4. Ultra-low linear thermal expansion values less than $10x10^{-7}$/°C up to 1000°C in absolute value were obtained in $RbZr_2(PO_4)_3$, $CsZr_2(PO_4)_3$, $(Rb\text{-}Cs)Zr_2(PO_4)_3$, $(Ca\text{-}Mg)Zr_4(PO_4)_6$ compounds, which result from the sum of negative expansion for the a-axis and positive expansion for the c-axis.

5. A change in crystallinity by the addition of ZnO to promote sinterability affected linear thermal expansion behavior; the higher the crystallinity, especially in $CaZr_4(PO_4)_6$, the closer the calculated linear α from the axial α values came to the measured linear α.

6. In crystalline solids, a unit-cell equilibrium based on thermodynamics and lattice-dynamics might be generally applied to interpret various thermal expansion behaviors such as positive and negative behavior, the transition of expansion, a sudden decrease and increase, and unusual behavior owing to the atomic movement.

7. Secondary material properties have been characterized for the compounds of $Ca_{0.5}Mg_{0.5}Zr_4(PO_4)_6$ and $Rb_{0.5}Cs_{0.5}Zr_2(PO_4)_3$ with the linear α values of $-5x10^{-7}$/°C and $-0.3x10^{-7}$/°C, respectively. High %TD & MOR, a low % open porosity, and better thermal shock resistance were obtained in the $Rb_{0.5}Cs_{0.5}Zr_2(PO_4)_3$ compound. Meanwhile, the $Ca_{0.5}Mg_{0.5}Zr_4(PO_4)_6$ compound showed long-term thermal stability.

Chapter VII

References

1. F.A.Hummel, "A Review of Thermal Expansion Data of Ceramic Materials, Especially Ultra-low Expansion Composites," *Interceram*, 33[6], 27-30(1984).

2. W.H.Dumbaugh,Jr., and J.W.Malmendier, "Refractory Glasses," *High Temperature Oxides, Part IV, Edited by A.M.Alper*, Academic Press, New York and London, 1-14(1971).

3. M.E.Milberg, and H.D.Blair, "Thermal Expansion of Cordierite," *J.Am.Ceram.Soc.*, 60[7-8], 372-373(1977).

4. R.Roy, D.K.Agrawal, J.Alamo, and R.A.Roy, "A New Structural Family of Near-Zero Expansion Ceramics," *Mat.Res.Bull.*, 19[4], 471-477(1984).

5. J.S.Moya, A.G.Verduch and M.Hortal, "Thermal Expansion of β-Eucryptite Solid Solutions," *Trans. & Journ. of British Ceram. Soc.*, 73[6], 177-178(1974).

6. H.Schulz, "Thermal Expansion of Beta Eucryptite," *J.Am.Ceram.Soc.*, 57[7], 313-318(1974).

7. A.Makishima, T.Ustugi, and T.Sakaino, "Grüneisen's Constant of Low Expansion Aluminosilicate Glass Containing Copper Oxide,"*ibid.*, 62[3-4], 224(1979).

8. K.Matusita and J.D.Mackenzie, "Low Expansion Copper Aluminosilicate Glasses," *J.Non-Cryst. Solids*, 30[3], 285-292(1979).

9. G.H.Beall and H.L.Rittler, "Glass-Ceramics Based on Pollucite," *Advances in Ceramics*, American Ceramic Society, 4, 301-312(1982).

10. K.Matusita, J.D.Mackenzie, K.Kamiya, and S.Sakka, "Low Expansion Glass-Ceramics Prepared from Cu_2O-Al_2O_3-SiO_2 Glasses," *ibid.*, 277-286.

11. W.R.Manning, O.Hunter,Jr., F.W.Calderwood, and D.W.Stacy, "Thermal Expansion of Nb_2O_5," *J.Am.Ceram.Soc.*, 55[7], 342-347(1972).

12. D.W.Richerson and F.A.Hummel, "Synthesis and Thermal Expansion of Polycrystalline Cesium Minerals," *ibid.*, 55[5], 269-273(1972).

13. C.E.Holcombe, Jr., "Thermal Expansion Coefficients for Low Expansion Oxides," *Am.Ceram.Soc.Bull.*, 59[12], 1219(1980).

14. H.P.Kirchner, K.M.Merz, and W.R.Brown, "Thermal Expansion of Uranium Pyrophosphate and of Ceramic Bodies in the System UO_2-UP_2O_7," *J.Am.Ceram.Soc.*, 46[3], 137-141(1963).

15. W.Ostertag, G.R.Fischer, and J.P.Williams, "Thermal Expansion of Synthetic β-Spodumene and β-Spodumene-Silica Solid Solutions," *ibid.*, 51[11], 651-654(1968).

16. G.F.Hawkins and E.G.Wolff, "Isotropic Zero CTE Materials," *Thermal Expansion, No.7, Edited by D.C.Larsen*, Plenum Press, New York and London, 103-118(1979).

17. K.R.Land, F.A.Hummel, "Subsolidus Relations in the System ZrO_2-ThO_2-P_2O_5," *J.Am.Ceram.Soc.*, 54[8], 407-409(1971).

18. I.Yamai and T.Oota, "Low Thermal Expansion Polycrystalline Zirconyl Phosphate Ceramic," *ibid.*, 68[5], 273-278(1985).

19. G.E.Lenain, H.A.Mckinstry, S.Y.Limaye, and A.Woodward, "Low Thermal Expansion of Alkali-Zirconium Phosphates," *Mat.Res.Bull.*, 19[11], 1451-1456(1984).

20. D.E.Harrison, H.A.Mckinstry, and F.A.Hummel, "High Temperature Zirconium Phosphates," *J.Am.Ceram.Soc.*, 37[6], 277-280(1954).

21. J.Alamo and R.Roy, "Ultralow Expansion Ceramics in the System Na_2O-ZrO_2-P_2O_5-SiO_2," *ibid.*, 67[5], c78-80(1984).

22. T.Oota and I.Yamai, "Thermal Expansion Behavior of $NaZr_2(PO_4)_3$-type Compounds," *ibid.*, 69[1], 1-6(1986).

23. E.Bruton, *Diamonds*, N.A.G.Press Ltd., London, 300-307(1970).

24. P.Predecki, J.Haas, J.Faber,Jr., and R.L.Hitterman, "Structural Aspects of the Lattice Thermal Expansion of Hexagonal Cordierite," *J.Am.Ceram.Soc.*, 70[3], 175-182(1987).

25. L.Hagman, and P.Kierkegaard, "The Crystal Structure of $NaMe^{IV}_2(PO_4)_3$; Me^{IV} = Ge, *Ti*, *Zr*, " *Acta Chem. Scan.*, 22[6], 1822-1832(1968).

26. M.Sljukic, B.Matkovic, and B.Prodic, "The Crystal Structure of $KZr_2(PO_4)_3$," *Z.Kristallographie*, 130, 148-161(1969).

27. M.Sljukic, B.Matkovic, B.Prodic, and S.Scarnicar, "Preparation and Crystallographic Data of Phosphates with Common Formula $M^IM^{IV}_2(PO_4)_3$(M^I = *Li*, *Na*, *K*, Rb, *Cs*; M^{IV} = *Zr*, *Hf*) ," *Croat. Chem. Acta*, 39, 145-148(1967).

28. B.Matkovic, B.Prodic, and M.Sljukic, "Preparation and Structural Studies of Phosphates with Common Formula $M^IM^{IV}_2(PO_4)_3$(M^I = *Li*, *Na*, *K*, Rb, *Cs*; M^{IV} = *Th*, *U*, *Zr*, *Hf*) ," *Bull. Soc. Chim. Fr.*, 1777-1779(1968).

29. R.Masse, A.Durif, J.C.Guitel, and I.Torjman, "Structure Cristalline du Monophosphate Lacunaire $KTi_2(PO_4)_3$, Monophosphates Lacunaires $NbGe(PO_4)_3$ et $M^{+5}Ti(PO_4)_3$ pour M^{+5} = Sb, Nb, Ta," *Bull.Soc.Fr.Min.Cristall.*, 95, 47-55(1972).

30. R.Masse, "Monophosphates $M^{III}BaTi(PO_4)_3$ pour M^{III} = Cr et Fe Monophosphates du Type Langbe'inite," *ibid.*, 95, 405-411(1972).

31. R.Masse, J.C.Guitel, and R.Perret, "Structure Cristalline de la Varie'te' Rhomboe'drique du Sulfate Ferrique $Fe_2(SO_4)_3$," *ibid.*, 96, 346-349(1973).

32. R.Perret, A.T.Sorel, J.P.Peter, and R.Masse, "Les Sulfates Triples $M^IM^{II}M^{III}(SO_4)_3$ I.Les Sulfates Rhomboe'driques $NaM^{II}M^{III}(SO_4)_3$(M^{II} = Mg, Mn, Co, Ni, Zn; M^{III} = Al, Ga, In, Cr, Fe)," *ibid.*, 98, 103-106(1975).

33. N.G.Chernorukov, I.A.Korshunov, and T.V.Prokof'eva, "Crystallographic Characteristics of Double Phosphates and Arsenates of Zirconium, $M^{II}Zr_4(PO_4)_6$, $M^IZr_2(AsO_4)_3$, and $M^{II}Zr_4(AsO_4)_6$, " *Sov.Phys.-Crystallogr.(Engl.Transl.)*, 23[4], 475(1978).

34. D.Petit, P.Colomban, G.Collin, and J.P.Boilot, "Fast Ion Transport in $LiZr_2(PO_4)_3$: Structure and Conductivity," *Mat.Res.Bull.*, 21, 365-371(1986).

35. H.Kohler, and H.Schulz, "Nasicon Solid Electrolytes, Part II- X-Ray Diffraction Experiments on Sodium-Zirconium-Phosphate Single Crystals at 295°K and at 993°K," *ibid.*, 21, 23-31(1986).

36. D.Tranquil, J.J.Capponi, and J.C.Joubert, "Crystal Structure and Ionic Conductivity in $Na_4Zr_2Si_3O_{12}$," *J.Solid State Chem.*, 39, 219-229(1981).

37. H.Y-P.Hong, "Crystal Structures and Crystal Chemistry in the $Na_{1+x}Zr_2Si_xP_{3-x}O_{12}$,"*Mat.Res.Bull.*, 11, 173-182(1976).

38. C.Delmas, R.Olazcuaga, G.Le Flem, P.Hagenmuller, F.Cherkaoui, and R.Brochu, "Crystal Chemistry of the $Na_{1+x}Zr_{2-x}L_x(PO_4)_3$ (L = Cr, In, Yb) Solid Solutions," *ibid.*, 16, 285-290(1981).

39. M.Nagai, S.Fujitsu, and T.Kanazawa, "Ionic Conductivity in the System $NaZr_2(PO_4)_3$-$Na_3Y_2(PO_4)_3$, " *J.Am.Ceram.Soc.*, 63[7-8], 476-477(1980).

40. T.Takahashi, K.Kuwabara, and M.Shibata, "Solid-State Ionics— Conductivities of Na^+ ion Conductors based on NASICON," *Solid State Ionics*, 1, 163-175(1980).

41. J.B.Goodenough, H.Y-P.Hong, and J.A.Kafalas, "Fast Na^+-ion Transport in Skeleton Structures," *Mat.Res.Bull.*, 11, 203-220(1976).

42. B.E.Taylor, A.D.English, and T.Berzins, "New Solid Ionic Conductors," *ibid.*, 12, 171-182(1977).

43. M.Nagai, S.Fujitsu, T.Kanazawa, and H.Yanagida, "The Dependence of Structure and Conductivity in Three-dimensional Phosphate Ionic Conductors on Composition," *J.Mat.Sci.*, 16, 1633-1642(1981).

44. R.J.Cava, E.M.Vogel, and D.W.Johnson, Jr., "Effect of Homovalent Framework Cation Substitutions on the Sodium Ion Conductivity in $Na_3Zr_2Si_2PO_{12}$," *J.Am.Ceram.Soc.*, 65[9], c157-159(1982).

45. K.D.Kreuer, and U.Warhus, "NASICON Solid Electrolytes, Part IV. Chemical Durability," *Mat.Res.Bull.*, 21, 357-363(1986).

46. G.Desplanches, M.Rigal, and A.Wicker, "Phase Transformation in an $Na_3Zr_2Si_2PO_{12}$ Ceramic," *Ceram.Bull.*, 59[5], 546-548(1980).

47. U.Alpen, M.F.Bell, and W.Wichelhaus, "Phase Transition in NASICON($Na_3Zr_2Si_2PO_{12}$)," *Mat.Res.Bull.*, 14, 1317-1322(1979).

48. J.P.Boilot, J.P.Salanie, G.Desplanches, and D.L.Potier, "Phase Transformation in $Na_{1+x}Si_xZr_2P_{3-x}O_{12}$ Compounds," *ibid.*, 14, 1469-1477(1979).

49. K.D.Kreuer, H.Kohler, U.Warnus, and H.Schulz, "NASICON Solid Electrolytes, Part III: Solid Conductivity Enhancement along Domain and Grain Boundaries," *ibid.*, 21, 149-159(1986).

50. A.Clearfield, and A.S.Medina, "On the Mechanism of Ion Exchange in Crystalline Zirconium Phosphates-III," *J.Inorg.Nucl.Chem.*, 32, 2775-2780(1980).

51. J.Alamo, and R.Roy, "Crystal Chemistry of the $NaZr_2(PO_4)_3$, NZP or CTP, Structure Family," *J.Mat.Sci.*, 21, 444-450(1986).

52. R.M.Hazen, L.W.Finger, D.K.Agrawal, and H.A.Mckinstry, " High-Temperature Crystal Chemistry of Sodium Zirconium Phosphate(NZP)", *J.Mat.Res.*, 2[3], 329-337(1987).

53. J.Alamo, R.Roy, and H.A.Mckinstry, "Crystal Chemical Parameters Correlation in the Sodium Zirconium Phosphate-type Structure," *Bull.Am.Ceram.Soc.*, 61, 333(1982).

54. G.E.Lenain, H.A.Mckinstry, and D.K.Agrawal, "Improvement of Crystallinity of $KZr_2P_3O_{12}$ by Sol-Gel Synthesis," *J.Am.Ceram.Soc.*, 68[9], c224-225(1985).

55. D.K.Agrawal, and R.Roy, "Composite Route to "Zero" Expansion Ceramics," *J.Mat.Sci.*, 20, 4617-4623(1985).

56. D.K.Agrawal, and V.S.Stubican, "Synthesis and Sintering of $Ca_{0.5}Zr_2P_3O_{12}$-Low Thermal Expansion Material," *Mat.Res.Bull.*, 20, 99-106(1985).

57. S.Komarneni, G.E.Lenain, and R.Roy, "Thermal Expansion of $NH_4Zr_2(PO_4)_3$," *J.Mat.Sci.Let.*, 5, 1-3(1986).

58. G.E.Lenain, H.A.Mckinstry, J.Alamo, and D.K.Agrawal, "Structural Model for Thermal Expansion in $MZr_2P_3O_{12}$(M = Li, Na, K, Rb, Cs)," *J.Mat.Sci.*, 6, 17-22(1987).

59. H.A.Mckinstry, D.K.Agrawal, G.E.Lenain, C.S.Vikram, S.Y.Limaye, and A.Patankar, "Ultra-Low Thermal Expansion Ceramics," Final scientific report submitted to Dept. of Air Force, AFOSR/NC Contract No.AFOSR-83-0291, August 1986.

60. T.Oota, and I.Yamai, "Low Thermal Expansion $KZr_2(PO_4)_3$ Ceramic," *Yogyo Kyokai Shi*, 95[5], 71-77(1987).

61. T.Oota, and I.Yamai, "Low Thermal Expansion Polycrystalline Zirconyl Phosphate Ceramic: Solid-Solution and Microcracking-Related Properties," *J.Am.Ceram.Soc.*, 70[8], 585-590(1987).

62. R.Roy, E.R.Vance, and J.Alamo, "[NZP], A New Radiophase for Ceramic Nuclear Waste Forms," *Mat.Res.Bull.*, 17, 585-589(1982).

63. C.Kittel, *Introduction to Solid State Physics*, John Wiley & Sons,Inc., 1976.

64. J.B.Austin, "Thermal Expansion of Nonmetallic Crystals," *J.Am.Cer.Soc.*, 35[10], 243-253(1952).

65. R.K.Kirby, "Thermal Expansion of Ceramics," *NBS 303*, 41-61(1969).

66. H.D.Megaw, "Crystal Structures and Thermal Expansion," *Mat.Res.Bull.*, 6[10], 1007-1018(1971).

67. R.M.Hazen, and L.W.Finger, *Comparative Crystal Chemistry*, John Wiley & Sons Ltd., 1982.

68. H.P.Kirchner, "Thermal Expansion Anisotropy of Oxides and Oxide Solid Solutions," *J.Am.Cer.Soc.*, 52[7], 379-386(1969).

69. V.J.Tennery, "High-Temperature Phase Transitions in $PbZrO_3$," *ibid.*, 483-486(1966).

70. O.M.Stansfield, "Thermal Expansion of Polycrystalline HfO_2-ZrO_2 Solid Solutions," *ibid.*, 48[8], 436-437(1965).

71. Y.Baskin, Y.Harada, and J.H.Handwerk, "Some Physical Properties of Thoria Reinforced by Metal Fibers," *ibid.*,43[9], 489-494(1960).

72. T.Takamori, M.Tomozawa, "Behavior of Interlayers of Glass-to-Tungsten Seals," *ibid.*, 48[8], 405-409(1965).

73. O.Hunter,Jr., and W.E.Browell, "Thermal Expansion and Elastic Properties of Two-Phase Ceramic Bodies," *ibid.*, 50[1], 19-22(1967).

74. R.J.Beals, and R.L.Cook, "Directional Dilatation of Crystal Lattices at Elevated Temperatures," *ibid.*, 40[8], 279-284(1957).

75. R.E.Fryxell, and B.A.Chandler, "Creep, Strength, Expansion, and Elastic Moduli of Sintered BeO as a Function of Grain Size, Porosity, and Grain Orientation," *ibid.*, 47[6], 283-291(1964).

76. K.M.Merz, W.R.Brown, and H.P.Kirchner, "Thermal-Expansion Anisotropy of Oxide Solid Solutions," *ibid.*, 45[11], 531-536(1962).

77. H.P.Kirchner, "Thermal Expansion Anisotropy of Oxides and Oxide Solid Solutions," *ibid.*, 52[7], 379-386(1969).

78. W.D.Kingery, "Factors Affecting Thermal Stress Resistance of Ceramic Materials," *ibid.*, 38[1], 3-15(1955).

79. P.K.Foster, and I.R.Hughes, "Internal Stress in Ceramics Containing Cristobalite," *ibid.*, 49[9], 515(1966).

80. A.Q.Tool, "Effect of Heat-Treatment on the Density and Constitution of High-Silica Glasses of the Borosilicate Type," *ibid.*, 31[7], 177-186(1948).

81. H.N.Ritland, "Limitations of the Fictive Temperature Concept," *ibid.*, 39[12], 403-406(1956).

82. T.Kakamori, "Effects of Thermomechanical History on Properties of Glasses," *ibid.*, 46[8], 366-370(1963).

83. E.A.Bush, and F.A.Hummel, "High-Temperature Mechanical Properties of Ceramic Materials: II.Beta-Eucryptite," *ibid.*, 42[8], 388-391(1959).

84. G.H.Beall, B.R.Karstetter, and H.L.Rittler, "Crystallization and Chemical Strengthening of β-Quartz Glass-Ceramics," *ibid.*, 50[4], 181-190(1967).

85. H.P.Kirchner, R.M.Gruver, and R.E.Walker, "Chemically Strengthened, Leached Alumina and Spinel," *ibid.*, 50[4], 169-173(1967).

86. B.R.Karstetter, and R.O.Voss, "Chemical Strengthening of Glass-Ceramics in the System Li_2O-Al_2O_3-SiO_2," *ibid.*, 50[3], 133-137(1967).

87. C.J.Koenig, "Influence of Particle-Size Distribution on the Properties of Nepheline Syenite," *ibid.*, 38[7], 231-241(1955).

88. M.D.Burdick, and H.S.Parker, "Effect of Particle Size on Bulk Density and Strength Properties of Uranium Dioxide Specimens," *ibid.*, 39[5], 181-187(1956).

89. R.L.Coble, and W.D.Kingery, "Effect of Porosity on Physical Properties of Sintered Alumina," *ibid.*, 39[11], 377-385(1956).

90. R.L.Coble, and W.D.Kingery, "Effect of Porosity on Thermal Stress Fracture," *ibid.*, 38[1], 33-37(1955).

91. S.Aronson, E.Cisney, and A.B.Auskern, "Thermal Expansion of Nonstoichiometric Zirconium Carbides," *ibid.*, 49[8], 456(1966).

92. E.M.Baroody, E.M.Simons, and W.H.Duckworth, "Effect of Shape on Thermal Fracture," *ibid.*, 38[1], 38-43(1955).

93. J.Wachtman, "Moving toward Tougher Ceramics," *Adv.Mat.& Proc.*, 133[1], 45-46(1988).

94. J.A.Kuszyk, and R.C.Bradt, "Influence of Grain Size on Effects of Thermal Expansion Anisotropy in $MgTi_2O_5$," *J.Am.Ceram.Soc.*, 56[8], 420-423(1973).

95. J.J.Cleveland, and R.C.Bradt, "Grain Size/Microcracking Relations for Pseudobrookite Oxides," *ibid.*, 61[11-12], 478-481(1978).

96. G.H.Stout, and L.H.Jensen, *X-ray Structure Determination*, The Macmillan Co., New York, 1968.

97. The International Union of Crystallography, *International Tables for X-Ray Crystallography*, The Kynoch Press, England, 1969.

98. M.J.Buerger, *Crystal Structure Analysis*, Wiley, New York, 1960.

99. J.Alamo, and R.Roy, "Revision of Crystalline Phases in the System ZrO_2-P_2O_5," *J.Am.Ceram.Soc.*, 67[5], c80-82(1984).

100. K.Robinson, G.V.Gibbs, and P.H.Ribbe, "Quadratic Elongation: A Quantitative Measure of Distortion in Coordination Polyhedra," *Science*, 172, 567-570(1971).

101. R.Roy, "Aids in Hydrothermal Experimentation: II.Methods of Making Mixtures for Both Dry and Wet Phase Equilibrium Studies," *J.Am.Ceram.Soc.*, 39[4], 144-146(1956).

102. R.F.Haaker, and R.C.Ewing, "Solution-Gelation Method for Preparing Polycrystalline Zircon," *ibid.*, 64[11], c149(1981).

103. S.Sakka, "Sol-Gel Synthesis of Glasses: Present and Future," *Am.Ceram.Soc.Bull.*, 64[11], 1463-1466(1985).

104. D.W.Johnson, Jr., "Sol-Gel Processing of Ceramics and Glass," *ibid.*, 64[12], 1597-1602(1985).

105. B.H.Davis, "Effect of pH on Crystal Phase of ZrO_2 Precipitated from Solution and Calcined at 600°C," *J.Am.Ceram.Soc.*, 67[8], c168(1984).

106. W.D.Bond, G.D.Davis, P.Angeli, P.F.Becher, and T.N.Tiegs, "Status of Experimental Studies on the Sol-Gel Synthesis of Ceramic Powders for High-Strength Ceramic Materials Applications," ORNL/TM-9835, Oak Ridge National Laboratory, 1987.

107. L.M.Sheppard, "Low Temperature Synthesis of Ceramics," *Adv.Mat.Prog.*, 130[5], 47-51(1986).

108. B.D.Cullity, *Elements of X-Ray Diffraction*, Addison-Wesley Pub. Co., Inc., 1978.

109. T.A.Hahn, and R.K.Kirby, "Thermal Expansion of Platinum from 293 to 1900°K," *AIP Conf. Proc., No.3*, 87-95(1972).

110. ASTM, "Standard Methods for Apparent Porosity, Water Absorption, Apparent Specific Gravity, and Bulk Density of Burned Refractory Brick and Shapes by Boiling Water," *ASTM C20-83*, 1984.

111. J.T.Jones and M.F.Berard, *Ceramics: Industrial Processing and Testing*, The Iowa State Univ. Press, Ames, Iowa, 1972.

112. ASTM, "Standard Test Method for True Specific Gravity of Refractory Materials by Water Immersion," *ASTM C135-66*, 1984.

113. D.Lewis III, "Thermal Shock and Thermal Shock Fatigue Testing of Ceramics with the Water Quench Test," *Fracture Mechanics of Ceramics*, Vol.6, edited by R.C.Bradt, A.G.Evans, D.P.H.Hasselman, and F.F.Lange, Plenum Press, New York, 1983.

114. W.E.C.Creyke, I.E.J.Sainsbury, and R.Morrell, *Design with Non-Ductile Materials*, Applied Science Publishers, Ltd., 1982.

115. ASTM, "Standard Practice for Measuring Trueness and Squareness of Rigid Block Thermal Insulation," *ASTM C550-81*,1984.

116. F.D.Bloss, *Crystallography and Crystal Chemistry*, Holt, Reinhart and Winston, Inc., 1971.

117. H.Sahai and J.Berriostchinson, *A Dictionary of Statistical, Scientific, and Technical Terms*, Wadworth Pub. Co., 1981.

118. J.Neter, W.Wasserman, and G.A.Whitmore, *Applied Statistics*, Allyn and Bacon, 1982.

119. L.F.Lynch, C.G.Ruderer, and W.H.Duckworth, *Engineering Properties of Selected Ceramic Materials*, Table 5.4.7-1, Am.Ceram.Soc.,Inc., Columbus, OH(1966).

120. J.J.Brown, R.E.Swanson, and F.A.Hummel, "Low Expansion Ceramics for Diesel Engine Applications," in Ceramic Technology for Advanced Heat Engines Project Semiannual Progress Report for October 1987 through March 1988, Oak Ridge National Laboratory, Oak Ridge, Tenn.,(to be published).

121. W.F.Horn, and F.A.Hummel, "The System $AlPO_4$-SiO_2," *Cen.Glass.Cer.Bull.*, 26(1-4), 47-59(1979).

122. C.S.Barrett, W.D.Nix, and A.S.Tetelman, *The Principles of Engineering Materials*, Prentice-Hall, Inc., New Jersey, 1973.

123. W.D.Kingery, H.K.Bowen, and D.R.Uhlmann, *Introduction to Ceramics*, John Wiley & Sons, 1976.

124. P.S.Turner, "Thermal-Expansion Stresses in Reinforced Plastics," *J.Res.NBS*, 37, 239-250(1946).

125. V.D.Frechette, "Markings on Crack Surfaces of Brittle Materials: A Suggested Unified Nomenclature," *Fractography of Ceramic and Metal Failures, ASTM STP 827*, J.J.Mecholsky, Jr., and S.R.Powell, Jr., Eds., ASTM, 104-109(1984).

126. S.Y.Limaye, W.C.Morgan, and T.B.Jackson, "New Low Thermal Expansion Structural Ceramics," First Quarterly Report(Dec.1.1987-Feb.29.1988), DOE Report No.DOE/ER/80502-1.

127. E.Kato, K.Daimon, and J.Takahashi, "Decomposition Temperature of β-Al_2TiO_5," *J.Am.Cer.Soc.*, 63[5-6], 355-356(1980).

128. O.Muller, and R.Roy, *The Major Ternary Structural Families*, Springer-Verlag, 1974.

129. M.D.Karkhanavala, and F.A.Hummel, "The Polymorphism of Cordierite," *J.Am.Cer.Soc.*, 36[12], 389-392(1953).

130. A.G.Khachaturyan, "Ordering in Substitutional and Interstitial Solid Solutions," *Prog.Mat.Sci.*, 22, 1-150(1978).

131. JCPDS X-ray Diffraction File No.33-1360.

132. R.M.Hazen, C.T.Prewitt, "Effects of Temperature and Pressure on Interatomic Distances in Oxygen-based Minerals," *Am.Min.*, 62, 309-315(1977).

133. C.E.Holcombe,Jr., "Observations on Very Low Expansion Oxides," *J.Less-Com. Met.*, 60, 135-136(1978).

134. M.Ortiz, "A Continuum Theory of Crack Shielding in Ceramics," *Trans.ASME*, 54, 54-58(1987).

135. Y.Fu, and A.G.Evans, "Some Effects of Microcracks on the Mechanical Properties of Brittle Solids-I.Stress, Strain Relations," *Acta Metall.*, 33[8], 1515-1523(1985).

136. E.A.Bush, and F.A.Hummel, "High-Temperature Mechanical Properties of Ceramic Materials: I.Magnesium Dititanate," *J.Am.Cer.Soc.*, 41[6], 189-195(1958).

137. R.W.Rice, and R.C.Pohanka, "Grain-Size Dependence of Spontaneous Cracking in Ceramics," *ibid.*, 62[11-12], 559-563(1973).

The vita has been removed from the scanned document